Energy, economic and safety evaluation of blue hydrogen production through modelling and simulation

Yiming Li

Supervisor: Dr. Alasdair N Campbell

A thesis submitted in partial fulfilment of the requirement for the degree of

Doctor of Philosophy

School of Chemical, Materials & Biological Engineering

Faculty of Engineering

The University of Sheffield

January 2025

Declaration

I, the author, confirm that the Thesis is my own work. I am aware of the University's Guidance on the Use of Unfair Means (*www.sheffield.ac.uk/ssid/unfair-means*). This work has not been previously been presented for an award at this, or any other, university.

Acknowledgement

My PhD journey began on February 6, 2021. It feels like it was only yesterday. That year, I was 23 years old. As I write this, I am 27 years old. Over the past four years, I have transformed from a recipient of knowledge to a contributor.

In the first year of my PhD study, the COVID was spreading around the world. It was not an easy time. I would like to thank my family first, especially my parents, brothers and sisters. My parents provided financial support for my PhD research. Although they did not receive a university education, their simple wisdom, rooted in traditional Chinese culture, motivated them to provide unwavering support and encouragement, especially when I faced moments of hesitation and difficulty. I am also deeply grateful to my cousin, an esteemed professor at Hefei University of Technology. Although our research fields are different, his extensive research experience offered me invaluable practical advice.

Throughout my PhD journey, I owe a special thanks to my supervisor, Dr Alasdair N Campbell, who guided me through some of the most challenging moments. His kindness, integrity, and exceptional expertise helped me navigate confusion and uncertainty. His professional insight sharpened my critical thinking, and without his constructive feedback, this thesis would not have reached the standard of quality it holds today.

Abstract

Driven by net-zero emissions scenarios, global demand for hydrogen (H_2) is growing rapidly and expected to exceed 200 million tonnes/year by 2030. Currently, steam methane reforming (SMR) remains the primary hydrogen production method but it generates significant carbon dioxide (CO_2) emissions. Blue hydrogen production (BHP) aims to mitigate this impact, though challenges in energy efficiency, cost, and safety remain. Through optimizing processes, modifying configurations and developing risk assessment systems, these challenges can be addressed.

A rate-based model of post-combustion carbon capture (PCC) process was developed at pilot scale and scaled up to commercial scale for capturing CO_2 from SMR process. The energy performance of this PCC process using piperazine (PZ) and advanced flash stripper (AFS) configuration was investigated and compared with the standard PCC process using Monoethanolamine (MEA). The results indicated that the energy consumption of PZ was lower than that of MEA, and that can be further reduced by using AFS configuration.

The detailed models of the commercial-scale SMR process was developed and integrated with PCC process. A novel configuration was proposed to lower both costs and energy consumption. Compared to the standard BHP process, the proposed energy and cost-saving blue hydrogen production (ECSB) process using 30 wt.% PZ reduced energy penalty by 36 % and levelized cost of blue hydrogen (LCBH) by 20 %.

An integrated model is developed based on the ECSB process to investigate the relationship between potential process safety improvements and economic benefits. In addition, a weighted risk index (WRI) method is proposed to assess the overall process risk of BHP process. The results of integrating risk and economics analysis showed that the recommended operating temperature should be between 800-1000 °C. The operating pressures above 30 bar should be avoided.

Keywords: Blue hydrogen production; Steam methane reforming; Post-combustion carbon capture; Process modelling and simulation; Energy and cost-saving configuration; Technical and economic assessment; Integrated safety and economic assessment.

List of peer-reviewed Publications and Presentations

Li Y, Ren J, Ma H, Campbell AN. Technical and economic performance assessment of blue hydrogen production using new configuration through modelling and simulation. International Journal of Greenhouse Gas Control. 2024;134:104112.

Li Y, Tian C, Campbell AN. Integrated safety and economic assessment of BHP through modelling and simulation. Applied Energy. 2025. (submitted)

Table of Contents

List of Figures

List of Tables

Nomenclature

A	Cross sectional area (m^2)
a	Attraction parameter related to intermolecular forces
a_i	The stoichiometric coefficient of component i in the reaction equation
b	Repulsion parameter related to molecular size
C_i	Concentration of component i
C_i^j	The severity of the consequences for scenario j that classified in node i
D	Diameter of packed columns (m)
E_a	activation energies (kJ/mol)
F_{CO_2}	CO_2 mass fraction
F_{LV}	Flow parameters
F_p	Packing factor (m^{-1})
f_i	The frequency for node i
f_i^j	The frequency for the scenario j that classified in node i
G	Flue gas mass flowrate (kg/s)
i	Interest rate
K_{eq}	Equilibrium constants
k	Pre-exponential factor
k_2	Second-order CO_2 absorption rate constants (m_3/kmol·s)
k_4	Modified gas load
L	Solvent mass flowrate (kg/s)

M_{CO_2}	CO_2 molar mass (kg/kmol)
M_{MEA}	MEA molar mass (kg/kmol)
n	Project life (year)
Q	The annual production of hydrogen
R	Universal gas constant
r	reaction rate (m^3/kmol·s)
r_d	The discount factor
S_{H_2}	Selling price of hydrogen
T	Temperature (K)
V_W	Gas mass flow rate per unit cross-sectional area (kg/m^2s)
W_{MEA}	MEA concentration (wt.%)
w_i	The weight for node i

Greek letters

α_P	Pressure correction factor for the risk of nodes
α_T	Temperature correction factor for the risk of nodes
μ_L	Viscosity (Pa·s)
ρ_L	Liquid density (kg/m^3)
ρ_V	Vapour density (kg/m^3)
ΔH	Standard enthalpy of reaction (kJ/mol)
$\Delta\alpha$	MEA absorption capacity (mol_{CO_2}/ mol_{MEA})

Abbreviations

AC	Additional costs
ACC	Annual capital cost
AFS	Advanced flash stripper
APEA	Aspen Economic Process Analyzer®
ATR	Auto-thermal reforming
AWE	Alkaline water electrolysis
BHP	Blue hydrogen production
CAC	CO_2 avoidance cost
CAPEX	Capital expenditure
CCS	Carbon capture and storage
CF	Net cash flow
DEC	Direct equipment cost
DFC	Direct field cost
ECSB	Energy and cost-saving blue hydrogen production
Elec-NRTL	Electrolyte Non-Random-Two-Liquid
EPC	Engineering procurement and construction
F&EI	Dow's fire and explosion index
GPDC	Generalised pressure drop correlation
HTS	High-temperature water gas shift
IC	Installation cost
IEA	International Energy Agency

IPCC	Intergovernmental Panel on Climate Change
I2SI	Integrated inherent safety index
KGly	Aqueous potassium glycinate
LCBH	Levelized cost of blue hydrogen
LCH	Levelized cost of hydrogen
L/G	Liquid to gas
LTS	Low-temperature shift
MEA	Monoethanolamine
MF	Material Factor
NaGly	Aqueous sodium glycinate
NPV	Net present value
O&M	Operating and maintenance
OC	Owner's cost
OPEX	Operational expenditure
PC	Project contingency
PCC	Post-combustion capture
PEM	Proton exchange membrane electrolysis
PR	Peng-Robinson
PO_X	Partial oxidation
PSA	Pressure swing adsorption
PSI	Process stream index
PZ	Piperazine
QRA	Quantitative risk assessment

RK	Redich-Kwong
RVPSA	Rapid vacuum pressure swing adsorption
S/C	steam to carbon
SMR	Steam methane reforming
SOEC	Solid oxide electrolysis cells
TAC	Total annual costs
TEC	Total equipment cost
TIC	Total indirect cost
TPC	Total plant cost
TSA	Temperature swing adsorption
UHF	Unit Hazard Factor
WGS	Water-gas shift
WRI	Weighted risk index

Chapter 1. Introduction

1.1 Overview

This chapter establishes the foundation of this PhD dissertation. Section 1.2 gives the overview of the background. Section 1.3 reveals the motivations driving the research. The aims and objectives are discussed in Section 1.4, followed by an outline of the predicted novel contributions. The scope of the research is explained in Section 1.6, and the research methodology is provided in Section 1.7. Finally, Section 1.8 presents the outline of the dissertation.

1.2 Background

1.2.1 Current CO_2 emissions and hydrogen demand

The global hydrogen (H_2) demand was around 100 million tonnes in 2022 with about 57.9 % coming from industry and 42.1 % from oil refining (IEA, 2023). Figure 1.1 shows the H_2 demand in a net-zero scenario from 2020 to 2030. According to International Energy Agency (IEA) predictions, the global H_2 demand is expected to double by 2030. More sectors are considering using H_2 as an alternative energy carrier (IEA, 2021). However, traditional hydrogen production methods are accompanied by substantial carbon dioxide (CO_2) emissions. In 2023, the CO_2 emissions from H_2 production was over 900 million tonnes (IEA, 2023).

Currently, the issue of greenhouse gas emissions has attracted unprecedented attention worldwide. According to the report from the Intergovernmental Panel on Climate Change (IPCC), the CO_2 concentration in the atmosphere is forecasted to rise to 570 ppm by 2100. Limiting global temperature increases within 1.5 °C and achieving net-zero CO_2 emissions by 2050 are critical goals (IPCC, 2019). With the growing demand for hydrogen worldwide,

reducing carbon emissions from hydrogen production becomes essential for meeting net-zero emissions targets by 2050.

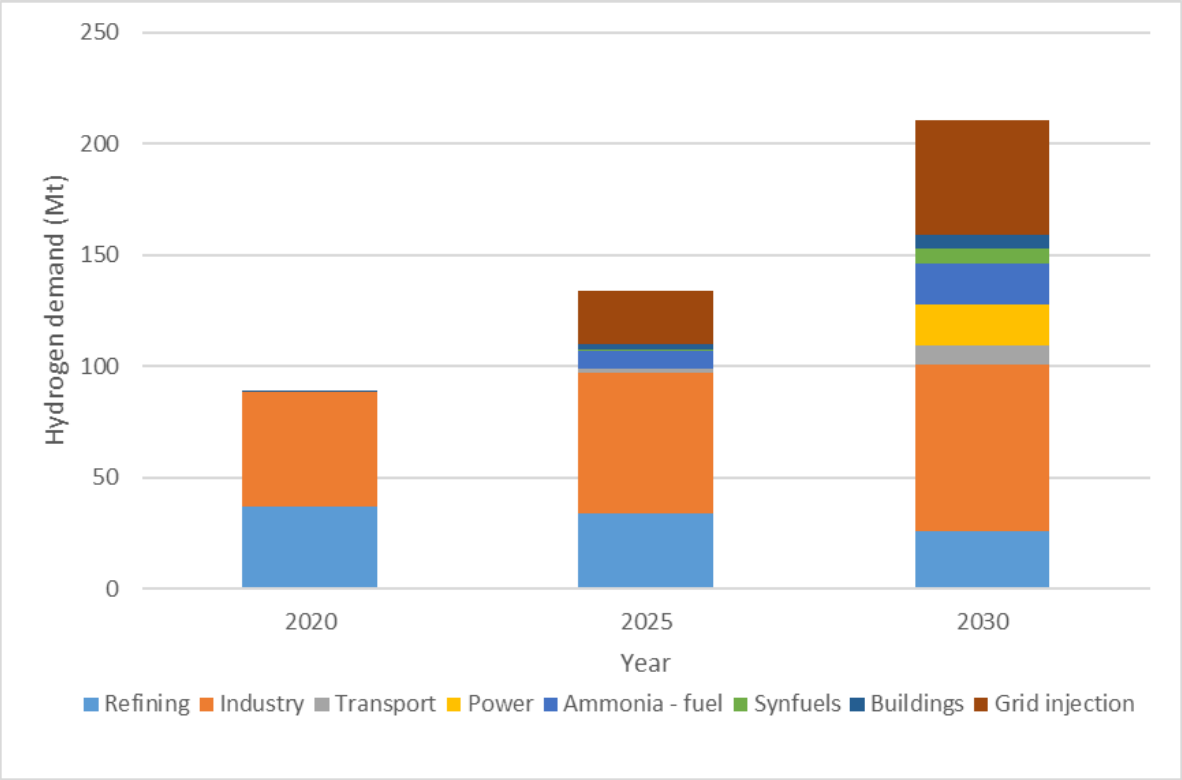

Figure 1.1 Global H_2 demand for achieving the net-zero target (IEA, 2021).

1.2.2 Overview of H_2 production technologies

1.2.2.1 Hydrogen cleanness

According to the specifics of the carbon emission and the production technologies, hydrogen cleanness is usually described in terms of colour, including grey, blue and green hydrogen (Dawood et al., 2020). Figure 1.2 shows the difference between them.

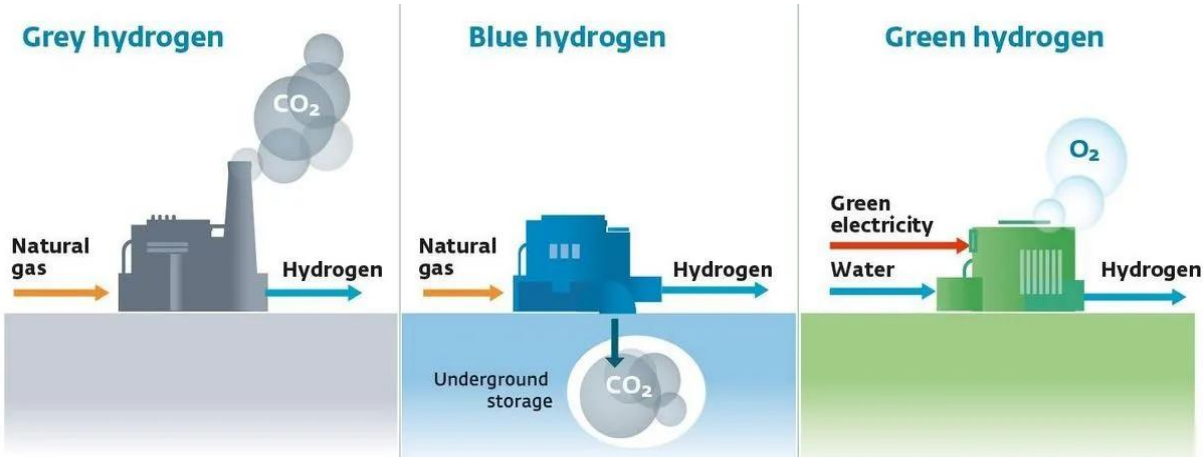

Figure 1.2 Depiction of grey, blue and green hydrogen production (TWH, 2021).

Grey hydrogen refers to H_2 produced through the reforming of fossil fuels and without carbon capture. Steam methane reforming (SMR) is the predominant method for grey hydrogen production (IEA, 2021). However, it emits 7-10 tonnes of CO_2 to the atmosphere for every tonne of grey hydrogen produced (Soltani et al., 2014).

Blue hydrogen involves the production of grey hydrogen, which is then processed with carbon capture and storage (CCS) technology, thereby reducing its impact on environment through separating CO_2 from the H_2 production plant (Khan et al., 2021).

Green hydrogen is generated from water electrolysis. The entire process is powered by renewable energy and only produces H_2 and O_2. Therefore, it will not cause any negative impact on the environment (Van-de-Graaf et al., 2020).

Beyond grey, blue, and green hydrogen, several other colours are used in industry and academia to describe different hydrogen production methods:

Pink hydrogen represents hydrogen produced through electrolysis powered by nuclear energy. It shares the zero-emissions benefit of green hydrogen but relies on nuclear power rather than renewables (Shirizadeh and Quirion, 2023).

White Hydrogen refers to naturally occurring geological hydrogen found underground. This

hydrogen is not produced but extracted directly from natural reservoirs (Aimikhe and Eyankware., 2023).

Black (or brown) hydrogen is derived from gasification of black or brown coal (i.e., lignite), while the co-product CO_2 is released into the atmosphere (Gür, 2021).

1.2.2.2 Different methods of hydrogen production

Currently, commercially available hydrogen production methods include SMR, auto-thermal reforming (ATR), gasification, partial oxidation (PO_X), and water electrolysis. Among them, SMR is the most used hydrogen production method. Over 50 % of hydrogen is produced through the SMR process (IEA, 2021). Thus, the SMR process is investigated in this study as the hydrogen production method.

Steam methane reforming

In the SMR process, natural gas (mostly methane) and steam are converted to carbon monoxide and hydrogen over a Ni-based catalyst. This kind of catalyst has high activity and a low price, but it is sensitive to H_2S poisoning. Thus, a desulfurization unit is necessary, where H_2S is adsorbed to prevent catalyst poisoning (IEAGHG, 2017). After desulfurization, heavier hydrocarbons are broken down to methane in the pre-reformer, which reduces the coking and sintering in the subsequent steps. The reactions (1.1) and (1.2) in the main reformer are equilibrium-limited and highly endothermic.

$$CH_4 + H_2O \leftrightarrow CO + 3H_2, \Delta H^0_{298} = 206\, kJ/mol \quad (1.1)$$

$$CH_4 + 2H_2O \leftrightarrow CO_2 + 4H_2, \Delta H^0_{298} = 164.9\, kJ/mol \quad (1.2)$$

These reactions are normally carried out at 700-1100 °C and 20-35 bar (Soltani et al., 2014). Figure 1.3 provides the details of the SMR process (Faheem et al., 2021). The main reforming is usually followed by a water-gas shift (WGS) process. The reaction (1.3) is equilibrium-limited and slightly exothermic:

$$CO + H_2O \leftrightarrow CO_2 + H_2, \Delta H^0_{298} = -41.1\, kJ/mol \quad (1.3)$$

The high pressure and temperature results in high reaction rate, while the CO conversion is favoured at low temperatures. Thus, WGS usually includes two stages. The first stage is high-temperature shift (HTS) at 320-380 °C and 30 bar; the second stage is low-temperature shift (LTS) at around 200 °C and 20 bar. Catalysts in HTS are primarily Fe_2O_3 promoted with Cr_2O_3 and in LTS the catalyst is composed of zinc oxide and aluminium oxide (Iruretagoyena et al., 2018).

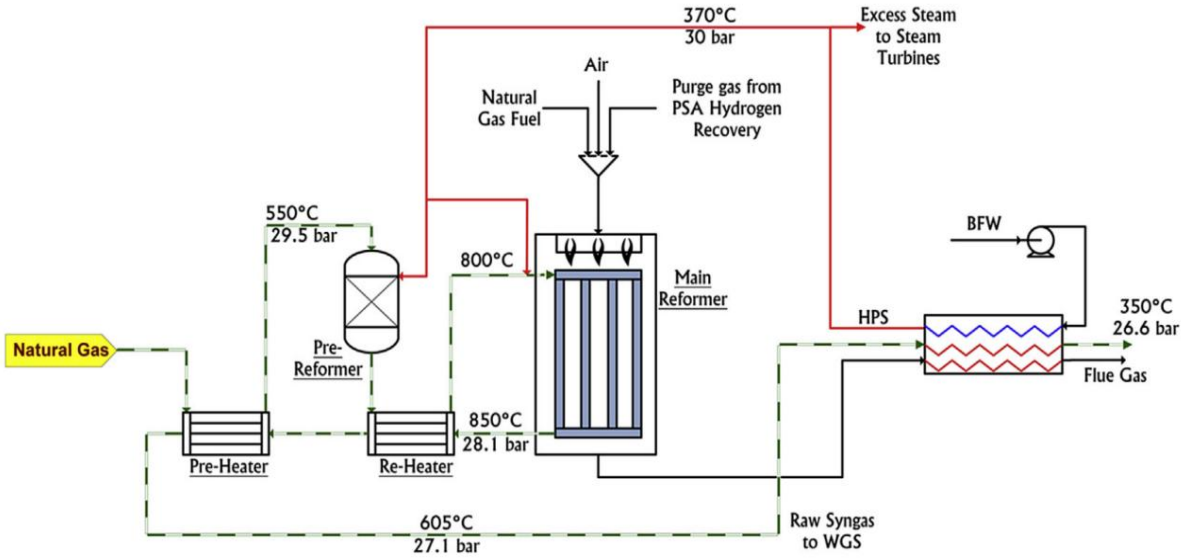

Figure 1.3 The flowsheet of the SMR process (Salkuyeh et al., 2017)

Auto-thermal reforming

In the ATR process, natural gas is blended with steam and oxygen. Therefore, natural gas is partially combusted in the reactor to supply the heat required in the reforming process. The main reactions (1.4 and 1.5) normally occur at temperatures between 900-1150 °C and the pressure over 70 bar (Noh et al., 2024).

$$CH_4 + 1/2H_2O + 1/4O_2 \leftrightarrow 5/2H_2 + CO, \Delta H^0_{298} = 84\, kJ/mol \quad (1.4)$$

$$CH_4 + 2O_2 \leftrightarrow 2H_2O + CO_2, \Delta H^0_{298} = -802.7\, kJ/mol \quad (1.5)$$

It also followed by a WGS reaction to increase the H_2 yield. The flowsheet of ATR process is shown in Figure 1.4 (Salkuyeh et al., 2017). In this process, the O_2 can also be replaced by air, depending on the syngas requirements of the downstream process (Voldsund et al., 2016).

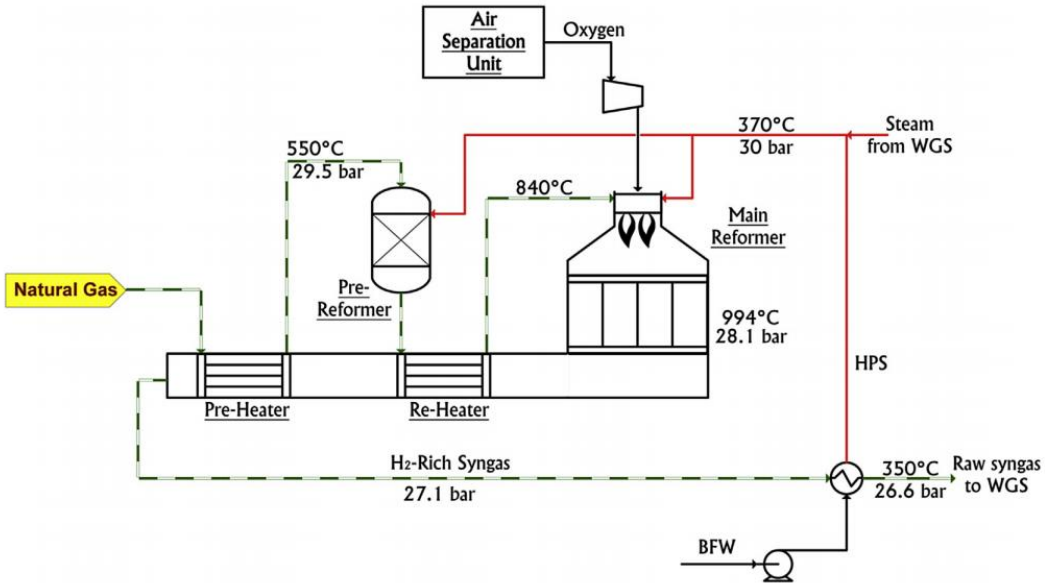

Figure 1.4 The flowsheet of the ATR process (Salkuyeh et al., 2017).

The H_2 concentration of the syngas is controlled by varying the proportion of oxygen and steam in the feed. However, high temperature and pressure reforming conditions require a high quality of reactor materials, which limits their use in industrial applications.

Pyrolysis/gasification

Pyrolysis/gasification referred to the processes of converting solid fuels to syngas. The feed is first pyrolyzed to produce solid char, liquid tar, and light gases including: H_2, CH_4, CO, CO_2, etc. Then, the intermediate is mixed with steam and oxygen/air in gasifiers, and some of them are combusted with oxygen to meet the heat requirement for the reactions (Voldsund et al., 2016). The main reactions in pyrolysis/gasification process are as follows:

$$C + O_2 \leftrightarrow CO_2, \Delta H^0_{298} = -394\, kJ/mol \quad (1.6)$$

$$C + 1/2\, O_2 \leftrightarrow CO, \Delta H^0_{298} = -111\, kJ/mol \quad (1.7)$$

$$C + H_2O \leftrightarrow H_2 + CO, \Delta H_{298}^0 = 131\ kJ/mol \quad (1.8)$$

$$C + CO_2 \leftrightarrow 2CO, \Delta H_{298}^0 = 172\ kJ/mol \quad (1.9)$$

These reactions normally occur under high temperatures (1350-1600 °C) and high pressures (40-85 bar). High temperatures shift the reaction equilibrium toward the production of more syngas. It is sometimes necessary to integrate an additional WGS process to increase yields by converting CO to H_2 (Liu et al., 2010a).

Partial oxidation

PO_X produces syngas from hydrocarbons. The feed is blended with a sub-stoichiometric amount of oxygen and partially burnt in a reactor to provide heat. The main reaction (1.10) is exothermic and can be carried out with or without a catalyst (Voldsund et al., 2016).

$$CH_4 + 1/2O_2 \leftrightarrow 2H_2 + CO, \Delta H_{298}^0 = -36\ kJ/mol \quad (1.10)$$

The typical temperature range for the PO_X process is 900-1150 °C and the pressure ranges is 35-80 bar. The feedstock for a large-scale PO_X process can be any hydrocarbons. It is usually followed by WGS and H_2 separation unit in hydrogen production (Liu et al., 2010a).

Water electrolysis

Water electrolysis refers to the process of the decomposition of water into H_2 and O_2 by electricity. During water electrolysis, electrons are captured or released by ions on the electrode's surface. The reduction half-reaction produces H_2 at the cathode and the oxidation half-reaction produces O_2 at the anode (Santos et al., 2013). The overall reaction is:

$$2H_2O \rightarrow 2H_2 + O_2, \Delta H_{298}^0 = 571.6\ kJ/mol \quad (1.11)$$

The primary challenge of water electrolysis is the high capital cost compared to fossil-based hydrogen production methods. Currently, the main technologies for water electrolysis include alkaline water electrolysis (AWE), proton exchange membrane electrolysis (PEM)

and solid oxide electrolysis cells (SOEC). Among these, both AWE and PEM electrolysers are already commercially available, with AWE being the more mature and cost-effective technology, while PEM is gaining popularity due to its rapid response and compatibility with intermittent renewable energy sources. SOEC is still in the early stages of commercial deployment, primarily demonstrated in pilot-scale projects (IEA., 2022).

1.2.3 Introduction to carbon capture process

1.2.3.1 Carbon capture approaches

The CCS process involves the separation, transportation, and storage of CO_2. The three primary methods for capturing CO_2 are post-combustion carbon capture (PCC), pre-combustion carbon capture and oxy-fuel combustion processes (Wang et al., 2011).

The principle of PCC is to separate CO_2 after fuel combustion has taken place. Currently, PCC has been widely studied and applied because it can be integrated with existing fossil fuel power plants without significant modifications (Wang et al., 2011).

Pre-combustion capture is the process to separate CO_2 from fossil fuels before they are combusted. The pre-combustion capture technologies are mostly applied in gasification and reforming processes (Jansen et al., 2015).

In oxy-fuel combustion, pure O_2 is used to replace air as the oxidation for fuel combustion. This process would generate CO_2-rich flue gas and thus the flue gas can be directly sent for CO_2 compression (Wang et al., 2011).

1.2.3.2 Different carbon capture methods

The separation technologies for CCS include chemical absorption, physical absorption, adsorption, cryogenics separation and membrane separation (Rao and Rubin, 2002). The most suitable technology is selected based on the CO_2 partial pressure and the required capture level. The following subsections briefly discuss these technology options.

Chemical absorption

Chemical absorption involves a reaction between CO_2 and a specified solvent, producing a weakly bonded intermediate compound. The solvent is then regenerated in a high-temperature stripping process to release pure CO_2 (Li et al., 2016). Figure 1.5 shows a typical chemical absorption process (Ma et al., 2021). This method is often used to capture CO_2 under low CO_2 partial pressure due to its high selectivity.

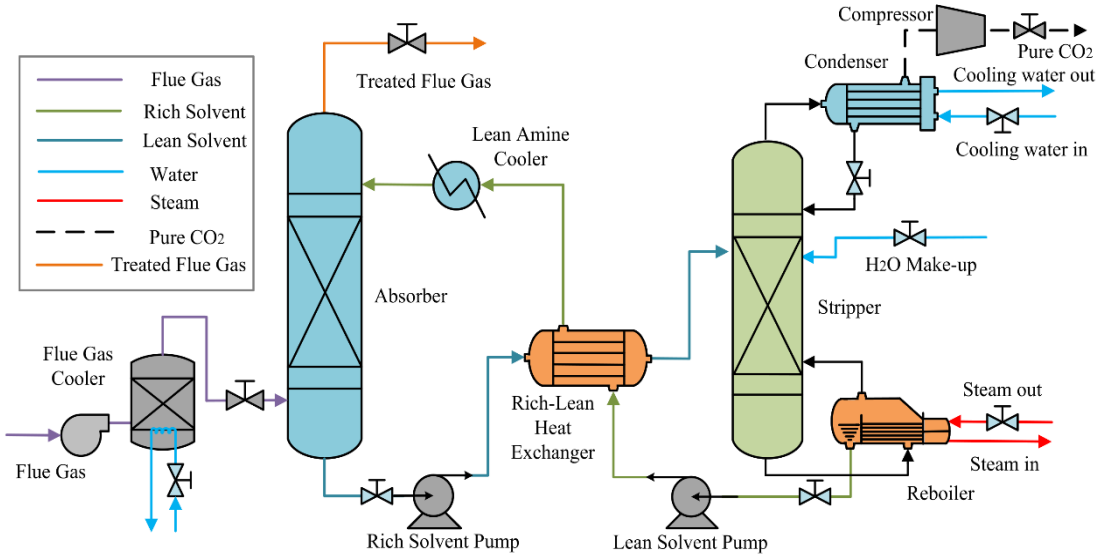

Figure 1.5 Flowsheet diagram of a PCC process with chemical solvent (Ma et al., 2021).

Physical absorption

Physical absorption operates according to Henry's law, where CO_2 is absorbed into solvents such as Selexol (dimethyl ethers of polyethylene glycol) and Rectisol (methanol). This method is usually used under conditions of high CO_2 partial pressure and low temperatures. (Wang et al., 2011).

Adsorption

Adsorption is a process where molecules from a gas or liquid attach to the surface of a solid material. Activated carbon and zeolites are popular adsorbents used in adsorption process. The temperature swing adsorption (TSA) and pressure swing adsorption (PSA) are most

widely used approaches for adsorbent regeneration (Pérez-Botella et al., 2022).

Cryogenic separation

Cryogenic separation is condensation process, where CO_2 is condensed at -57 °C under atmospheric pressure. It is particularly effective for flue gases with a high CO_2 concentration. Therefore, it is well-suited for oxy-fuel CO_2 capture (Song et al., 2019). While the process generates a liquid CO_2 stream, eliminating the need for additional compression, the high energy demands for refrigeration can significantly raise the overall capture costs.

Membrane separation

Membrane separation is performed based on CO_2 selectivity. It can be divided into organic membranes (not suitable for high temperature applications) and inorganic membranes (suitable for high temperature applications). The separation efficiency is influenced by the partial pressure of CO_2. The advantage of this method is that it is not prone to operational problems, while the disadvantage is that it is expensive and has a low capture level.

1.3 Research motivations

Currently, the global hydrogen demand is rapidly increasing under the net-zero emission scenarios (IEA, 2023). According to the IEA predictions, the global hydrogen demand may exceed 200 million tonnes/year by 2030. The contributions of blue hydrogen and green hydrogen to this demand increase are significant (IEA, 2021). In comparison to green hydrogen production, BHP currently holds a commercial deployment advantage (Li et al., 2024). This advantage stems from it being an improvement upon existing hydrogen production technologies rather than reconstruction. Thus, the existing hydrogen plants can continue to operate without the need for radical changes. In the long term, green hydrogen has the potential to serve as the final solution for achieving net-zero emissions. Nonetheless, given its current high costs, the deployment of BHP could play a crucial role as a more viable

short-term alternative.

A standard BHP process consists of hydrogen production and carbon capture processes. The SMR is the predominant technology for hydrogen production process. The CO_2 emissions in the SMR process can be captured from three main sources: (I) the syngas stream before the H_2 separation unit; (II) the tail gas following the H_2 separation unit; and (III) the flue gas from the furnace (Soltani et al., 2014). Physical adsorption is frequently employed to capture CO_2 from the syngas or tail gas stream due to the high CO_2 partial pressure in these streams. Conversely, chemical absorption is better suited for capturing CO_2 from flue gas, which are at low pressure. Most current research on BHP focuses on CO_2 capture from the syngas or tail gas stream (Antonini et al., 2021b, Papalas et al., 2020, Pellegrini et al., 2020). However, a notable limitation of these studies is that only 38-62 % of total carbon emissions are captured, since the CO_2 from the flue gas is emitted into the atmosphere (Roussanaly et al., 2020, Howarth and Jacobson, 2021). To fully decarbonize the SMR process, it is crucial to consider the capture of CO_2 from the flue gas.

In contrast to the growing demand for blue hydrogen, the commercial deployment of BHP remains challenging. Firstly, the integration of carbon capture process significantly increases costs and energy consumption (Khan et al., 2021, Li et al., 2024). The addition of a solvent-based PCC plant to a standalone SMR plant (with a capacity of 200 $tonne_{H_2}$/day) is estimated to increase capital costs by $ 117 million and operating costs by $ 28 million per year (Khan et al., 2021). In addition, the energy consumption when adding large-scale CCS units using Monoethanolamine (MEA) is around 4.5-5.5 $GJ/tonne_{CO_2}$ (Otitoju et al., 2021). Secondly, potential safety concerns raise apprehensions (Ade et al., 2022). Numerous safety incidents associated with hydrogen production demonstrates these safety concerns (PNNL, 2023). One recent hydrogen explosion incident happened in the Styrian town of Leibnitz, Austria, on 10 August 2023 (Collins, 2023). A storage tank containing hundreds of litres of hydrogen exploded. The dull bang and huge pressure wave were felt several kilometres away and caused injuries to one employee. These incidents remind us to revisit the hydrogen

production from a safety perspective.

Currently, the primary approaches for reducing the cost and energy consumption in carbon capture processes involve implementing new process configurations and new solvents (Otitoju et al., 2021). Different configurations and solvents of PCC process were evaluated in previous studies (Rinker et al., 1996, Zhang et al., 2002, Derks et al., 2006, Edali et al., 2009, Rayer et al., 2012, Van Wagener et al., 2013, Li et al., 2016, Rezazadeh et al., 2017, Diego et al., 2018, Gao et al., 2019). Among them, the use of the advanced flash stripper (AFS) configuration and piperazine (PZ) solvent in the PCC process has been shown to lower both energy consumption and costs (Otitoju et al., 2021, Li et al., 2024). However, research on BHP remains fragmented, with most studies focusing separately on either hydrogen production process or carbon capture process. There is a notable gap in process design and integration due to the lack of research with a holistic perspective. Exergy analysis of the SMR process have reported the exergy efficiencies ranging from 60 % to 78 % (Chen et al., 2012, Živković et al., 2016, Rahman et al., 2019). The wasted exergy from SMR process presents an opportunity to enhance the efficiency of the PCC process.

Although risk assessment of SMR processes has been covered by a large amount of literature, there is a gap in risk assessment of BHP. Primarily, in contrast to existing studies that only focus on the risk assessments of hydrogen production process, risk assessments for BHP need also to consider the potential economic effects. While proposing process improvements to reduce associated risks, there is also a need to investigate any economic repercussions that may occur. Secondly, a new risk assessment method is required to evaluate the impact of changes in operating parameters on the overall process risk of commercial-scale BHP. Currently, many studies have investigated process risks for specific scenarios. However, risk assessment methods for the overall process risk are very limited. Since the risk and economic assessments are equally important in commercial-scale BHP, a method for evaluating the overall process risk from a holistic perspective is needed. In addition, this method should also consider the potential impact of operating parameters on

process risk to provide help for decision makers in economic risk trade-offs.

1.4 Aim and objectives

This PhD study aims to reduce the cost and energy consumption of the commercial-scale BHP process through modelling, simulation and performance evaluation of process using different solvents and configurations. In addition, an integrated model was developed to investigate the relationship between potential process safety improvements and economic benefits. To achieve this aim, the following objectives are proposed:

- A comprehensive literature review of BHP.
- Model development, validation and scale-up of PCC process in Aspen Plus® V11.
- Energy performance assessment and process optimisation of PCC process with different solvents and configurations.
- Model development and validation of SMR process in Aspen Plus® V11.
- Model integration of commercial-scale SMR and PCC processes.
- Technical and economic performance assessment of BHP process with different configurations.
- Risk assessment of BHP process using the proposed new risk assessment method.
- Integrated safety and economic assessment of BHP through modelling and simulation.

1.5 Novel contributions

Based on the literature review in Chapter 2, the novel contributions to this study are summarized as follows:

(a) The PCC process using different solvents has been extensively studied. Most of these

studies were based on flue gases from power plants. Considering that the energy performance of a PCC plant is greatly affected by the flue gas properties, an accurate model is needed to predict the performance of the PCC process for capturing CO_2 from flue gases of SMR plants. In this study, the energy performance of the PCC process with PZ and the AFS configuration was investigated and compared with a standard PCC process using MEA. Subsequently, the PZ-based PCC process was optimized to determine the best operating parameters with the lowest energy consumption.

(b) An energy and cost-saving configuration is developed to reduce the cost and energy consumption of BHP process. This configuration is characterized by: (I) the application of PZ as a solvent in PCC process, known for its high CO_2 absorption efficiency; (II) an optimized heat exchange system that recovers the waste exergy from flue gas; and (III) the implementation of AFS which simplifies the stripper design and reduces capital cost.

(c) The technical and economic evaluation of the commercial-scale BHP process with different solvents and configurations is demonstrated in this PhD dissertation for the first time.

(d) A new risk assessment method is proposed to evaluate the overall process risk of commercial-scale BHP. This method based on the index approach. It classifies different scenarios into four nodes and defines the severity of different nodes by weighting. In addition, this method considers the impact of changes in operating parameters on overall process risk.

(e) An integrated model was developed to investigate the relationship between potential process safety improvements and economic benefits. The interaction between the process, economic and safety variables is investigated through modelling and simulation. The impact of operating parameters on overall process risk and economic benefits was investigated.

1.6 Scope of this study

This study is focused on the economic, energy and safety performance assessment of commercial-scale BHP process.

- The hydrogen production method in this study is limited to fixed-bed SMR process.
- The carbon capture method in this study is limited to solvent-based PCC process.
- Modelling of downstream processes behind the carbon capture process, such as CO_2 compression, transportation, and storage, is not covered in this study.
- All simulation performed in this thesis are based on steady-state models.

1.7 Research methodology

1.7.1 Overview of the research methodology

A diagram of the research methodology is provided in Figure 1.6. The first step involves a literature review of BHP to outline the aim and objectives of this study. Then, the study of modelling and simulation for SMR and PCC processes will be carried out. After that, process integration and design will be performed for BHP process. Finally, the energy, economic and risk assessment will be performed.

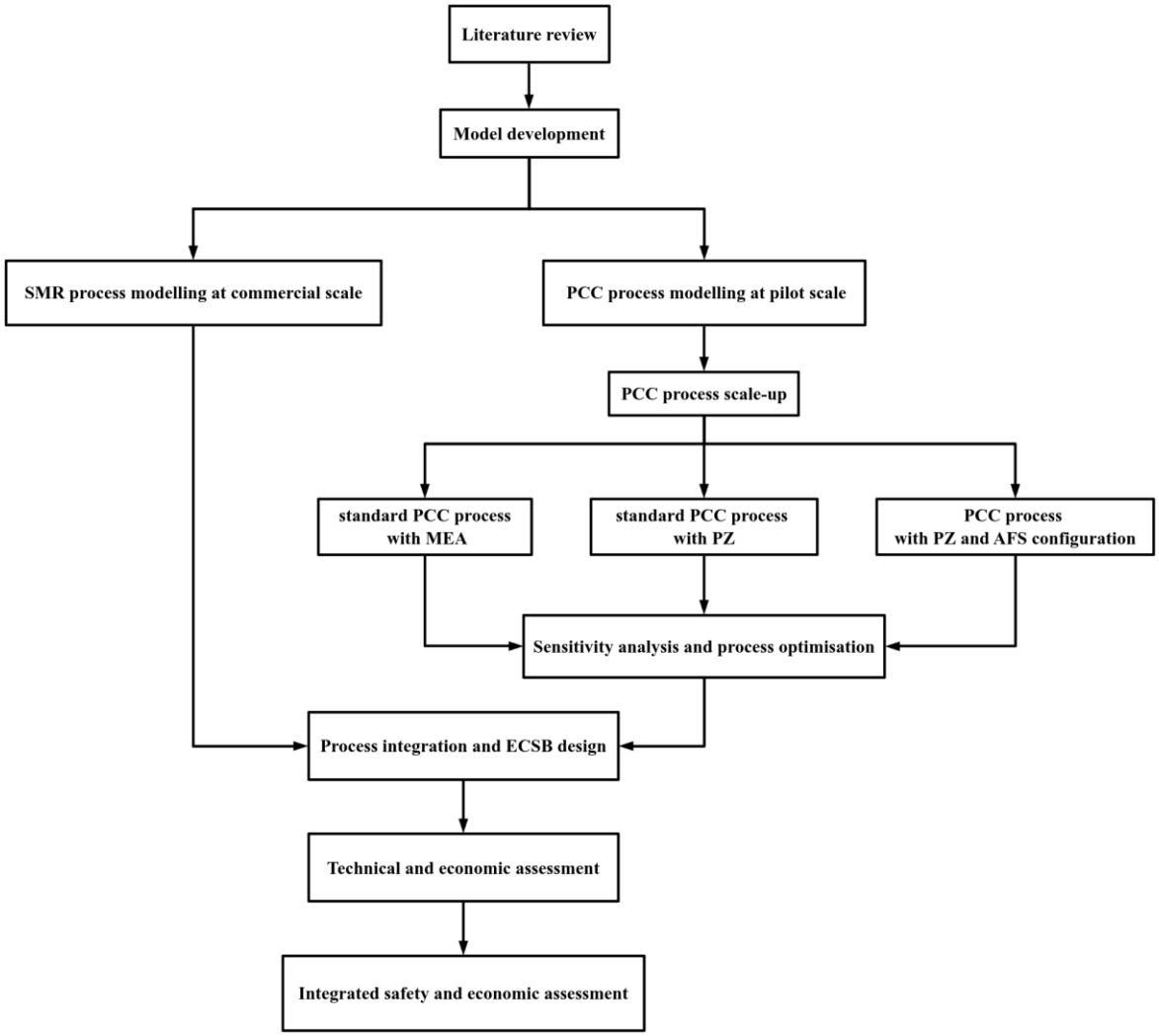

Figure 1.6 Diagram of the research methodology.

1.7.2 The software tool to be used

1.7.2.1 Aspen Plus® V11

Aspen Plus® V11 is a widely used process simulation software. It offers a complete library of physical properties including pure components, electrolyte solutions, Henry's constant, Inorganic, combustion etc. It is also linked to the DECHEMA database, which collects the most complete gas-liquid and liquid-liquid equilibrium data in the world (Aspentech, 2022).

1.7.2.2 Aspen Economic Process Analyzer®

Aspen Economic Process Analyzer™ estimates project capital cost and operating cost by relying on model-based estimations. Key features of this tool include interactive equipment for determining capital and operating costs, as well as the automatic generation of blocks and process flow diagrams (Aspentech, 2022).

1.8 Outline of the report

The outline of this report is as follows:

Chapter 2 reviews previous studies on SMR and PCC processes and provides examples of pilot plants and commercial deployments of BHP. Moreover, the studies on economic, energy and safety performance assessment of BHP process is also presented in this chapter. The findings and research gaps for further research are summarized at the end.

Chapter 3 presents the simulation and scale-up of the PCC process with different solvents and configurations. This includes pilot-scale model development and model validation. The effect of operating parameters on the energy consumption of the PCC process is evaluated. The standard PCC process with MEA is evaluated as a baseline. Then, the PZ-based PCC process is optimized to determine the best operating parameters with the lowest energy consumption.

Chapter 4 presents the technical and economic assessment of the BHP process with different solvents and configurations, including model development, model validation, process integration, and new configuration design. The results are also compared with the SMR process without carbon capture.

An integrated model for studying the relationship between potential process safety improvements and economic benefits is proposed in Chapter 5. The interactions between process, economic and safety variables are investigated through modelling and simulation. In addition, a new risk assessment method is proposed. This method is used to evaluate the

overall process risk of BHP and considers the impact of operating parameters on the overall process risk.

Finally, the conclusions drawn from this dissertation and suggestions for future work are discussed in Chapter 6.

Chapter 2. Literature review

2.1 Overview

This chapter presents an overview of previous research related to the BHP process. Section 2.2 reviews the experimental studies, existing pilot plants and commercial deployment of the BHP process. The modelling and simulation studies focused on the SMR process and PCC process are presented in section 2.3. Section 2.4 reviews existing technical and economic analysis studies and process risk assessment studies on BHP process. A summary of the literature review is given in Section 2.5

2.2 Experimental, pilot and commercial study of BHP

2.2.1 Experimental studies for BHP processes

2.2.1.1 Experimental studies for SMR processes

Currently, SMR is the primary hydrogen production technology, with more than 70 % of hydrogen supply coming from SMR technology (Massarweh et al., 2023). Because this technology is already mature, there have been relatively few experimental studies related to SMR in recent years. These studies have mainly focused on modifications of the reforming reactor and catalyst to increase methane conversion.

Research on the modification of reforming reactors mainly focuses on the application of the membrane reactor. This reactor uses the selective permeation of the metal membrane to separate the hydrogen produced in the reforming reaction, thereby breaking the thermodynamic equilibrium limitations (Gallucci and van Annaland, 2013, Lu and Xie, 2016). In early studies, membrane reactors were mainly used to improve H_2 production efficiency in the SMR process. This reactor usually consisted of a fixed bed reactor with a palladium-based alloy membrane. Compared with the traditional fixed bed reactors, the methane conversion

rate in membrane reactors can be increased to 90 % (Sjardin et al., 2006, Li et al., 2008, Shirasaki et al., 2009). In addition, since the membrane reactor greatly improves the conversion rate of CH_4, the WGS reactor is not necessary, which inspired researchers to think about the contribution of membrane reactors to process intensification.

Professor John R. Grace's group from the University of British Columbia has made important contributions to the study on process intensification of steam reforming. Based on the previous studies on membrane reactors, they proposed to use the fluidized bed membrane reactor (FBMR) to achieve the process intensification. An experimental scale FBMR was built as shown in Figure 2.1. The FBMR used $Pd_{77}Ag_{23}$ membrane panels and RK-212 catalyst with a diameter of 0.17 m and a height of 1.7 m (Rakib et al., 2010). The steam reforming and ATR of methane, ethane, and propane in the FBMR were studied (Mahecha-Botero et al., 2009, Rakib et al., 2010, Rakib et al., 2011, Vigneault and Grace, 2015). The results show that the integration of a fluidized bed reactor reduces coke formation caused by heavier hydrocarbons, and the use of a membrane reactor improves the conversion of methane while separating hydrogen. Therefore, the FBMR can integrate the functions of pre-reforming, main reforming, WGS, and separation section into a single unit and can be run for a long time without significant deactivation of catalyst.

Regrettably, membrane reactors have yet to achieve commercial deployment, primarily due to the absence of pilot-scale validation and comprehensive economic feasibility assessments at a commercial scale.

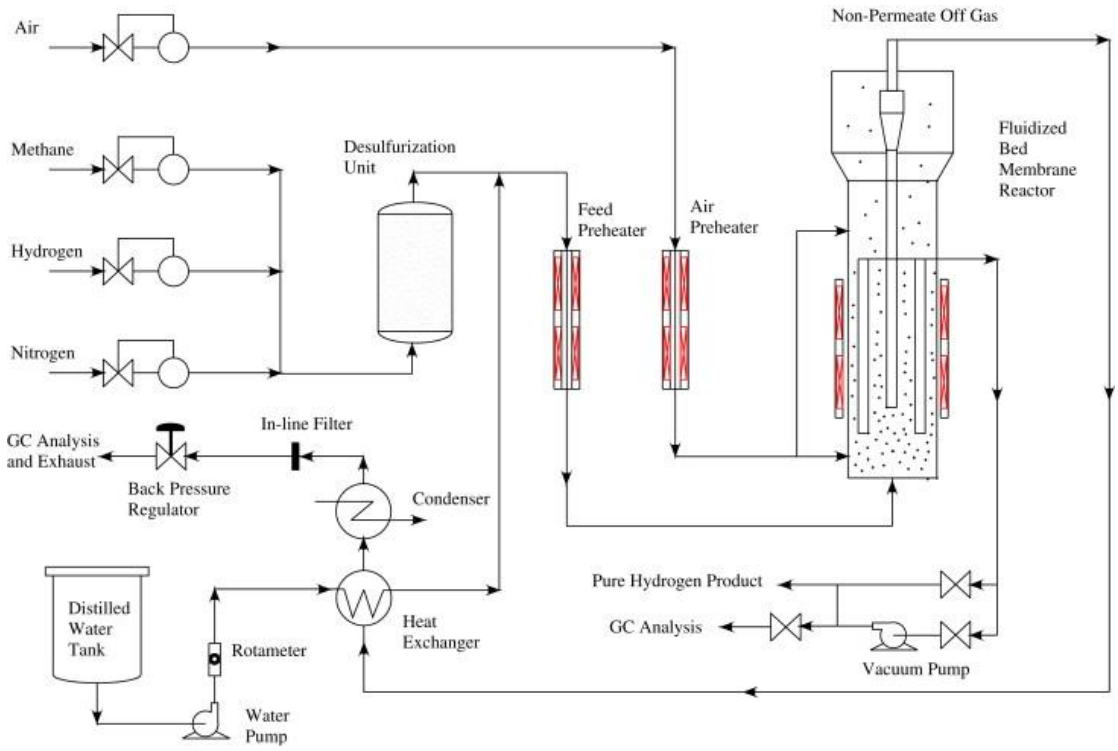

Figure 2.1 The schematic of the FBMR experimental setup (Rakib et al., 2010).

In addition, the research on modification of catalysts mainly focuses on sorption-enhanced steam methane reforming (SESMR) (Ochoa-Fernández et al., 2007, Radfarnia and Iliuta, 2014, Cherbański and Molga, 2018, Ghungrud et al., 2019, Fatigati et al., 2021). The technology combines conventional catalysts with CO_2 sorbents. Compared with traditional SMR processes, SESMR can remove CO_2 in situ, thereby shifting the equilibrium toward the product side and increasing hydrogen production (Wang et al., 2023b). The principle is actually similar to that of membrane reactors, which breaks the thermodynamic equilibrium limitations by removing products in situ.

Among the solid sorbents for SESMR, CaO is widely selected due to its widespread availability in low-cost natural mineralized forms (e.g., limestone or dolomite) and high adsorption capacity (78.6 g CO_2 per 100 g CaO) (Fatigati et al., 2021). Currently, the main challenge facing the development of SESMR is the stability of CaO sorbent. Various strategies have been suggested to enhance the stability of CaO during cyclic CO_2 adsorption,

including the integration of inert metal oxides into the CaO structure and the utilization of efficient Ca-precursors (Liu et al., 2010b, Li et al., 2010, Radfarnia and Iliuta, 2012, Radfarnia and Iliuta, 2014, Chen et al., 2021). A summary of the studies on the SESMR process and their main operating conditions are given in Table 2.1.

Table 2.1 Summary of the SESMR process and their main operating conditions.

Catalysts	CO_2 sorbents	Process temperature/ Pressure (°C)/(bar)	References
Ni-based	hydrotalcite-based	428-467/3.1-7.2	(Ding and Alpay, 2000)
Ni-based	CaO	660-750/2.0-15.0	(Lee et al., 2004)
$Rh/Ce_{\alpha}Zr_{1-\alpha}O_2$	K-promoted hydrotalcite, Li_2ZrO_3	450–600/4.6–15.0	(Halabi et al., 2012b, Halabi et al., 2012a)
$Ni/\gamma\text{-}Al_2O_3$	K_2CO_3-doped-Li_4SiO_4	450-650	(Zhang et al., 2016)
$Ce_{2.5}Ni_{10}Co_{30}$/ $Ce_{2.5}Ni_{20}Co_{20}$	hydrotalcite-based	500-600/10.0	(Ghungrud et al., 2019)
Ni/Al_2O_3	CaO	500-850	(Chen et al., 2021)

2.2.1.2 Experimental studies of the PCC process

Currently, MEA is primary solvent in PCC process (Li et al., 2016). However, it has the issues of volatility, corrosiveness, and high regeneration energy requirements (Otitoju et al., 2021). Some studies pointed out that applying an alternative solvent to MEA is one of the main methods to improve the energy performance in the PCC process (Artanto et al., 2012,

Rabensteiner et al., 2015b, Gao et al., 2019, Mostafavi et al., 2021).

Table 2.2 summarises the reaction kinetics parameters of several solvents, including aminomethyl propanol (AMP), diethanolamine (DEA), diethylenetriamine (DETA), methyl diethanolamine (MDEA), MEA and PZ. The PZ solvent may have a better performance on energy consumption compared with other solvents. It is highly reactive with CO_2 and therefore it can capture the same amount of CO_2 as other solvents but with a significantly lower solvent circulation rate because of its high second-order CO_2 absorption rate constant (k_2) and low activation energy (E_a). Additionally, PZ has lower volatility and higher resistance to degradation (oxidative and thermal) than MEA, which has led to growing interest in PZ for CO_2 capture (Chen et al., 2017, Rochelle et al., 2019, Otitoju et al., 2021).

Table 2.2 The reaction kinetics parameters of different solvents for CO_2 absorption at 25 °C.

Solvent	k_2 (m^3/kmol·s)	E_a (kJ/mol)	Reference
AMP	570	41.7	(Mandal and Bandyopadhyay, 2005)
DEA	576	53.1	(Zhang et al., 2002)
DETA	17510	32.2	(Rayer et al., 2012)
MDEA	6.17	47.9	(Rinker et al., 1996)
MEA	6209	41.2	(Edali et al., 2009)
PZ	70000	33.6	(Derks et al., 2006)
TEA	3	35.8	(Littel et al., 1990)

PZ was initially used as a reaction rate promoter in blends with other solvents such as MEA, MDEA, DEA, etc (Bishnoi and Rochelle, 2002, Ermatchkov et al., 2003, Closmann et al., 2009). Later studies showed that it could be used as a single solvent in a solvent-based PCC process

(Freeman et al., 2010, Plaza and Rochelle, 2011, Rochelle et al., 2011, Nielsen et al., 2013). The studies of PZ from two different pilot plants yielded consistent results. The study from a pilot plant in Dürnrohr achieved a minimum regeneration energy of 2.97 GJ/tonne$_{CO_2}$. Compared to 30 wt.% MEA, the use of 37.5 wt.% PZ reduced the energy consumption of a solvent-based PCC process by 14 % (Rabensteiner et al., 2015a). Another study from a pilot plant in Texas achieved a regeneration energy of 2.87 GJ/tonne$_{CO_2}$ with 40 wt.% PZ. This represented a 14.8 % reduction in energy consumption compared to 30 wt.% MEA (Gao and Rochelle, 2019). These pilot plant results suggest that more energy-efficient carbon capture processes can be developed using PZ as a solvent.

Despite its advantages, PZ is limited by the potential formation of solids, particularly in CO_2-lean streams at temperatures below 20 °C. Under these conditions (low CO_2 loading and low temperatures), PZ can form piperazine hexahydrate (PZ·6H_2O(s)), which may lead to plugging in the lean solvent line. This issue especially occurs during plant start-up and shutdown (Rabensteiner et al., 2015b, Otitoju et al., 2021). In addition, several studies investigated the potential of new configurations in the PCC process to decrease energy requirements, such as exhaust gas recirculation, absorber inter-cooling, stripper inter-heating, 2-stage flash configuration and AFS (Van Wagener et al., 2013, Li et al., 2016, Rezazadeh et al., 2017, Diego et al., 2018, Gao et al., 2019).

The 2-stage flash stripper configuration was first investigated by Van Wagener (2011). The flowsheet of the 2-stage flash configuration is shown in Figure 2.2. This configuration has an 11 % reduction in energy consumption compared to a standard stripper. However, in the pilot-scale investigation, an opposite conclusion was obtained. The energy penalty for the PCC process with the 2-stage flash stripper configuration was 143 kJ/mol$_{CO_2}$. This result is 10 % higher than the energy penalty for the PCC process with a simple stripper. Van et al. attributed this result to the fact that the heat exchanger is undersized for the flash temperature (Van Wagener et al., 2013).

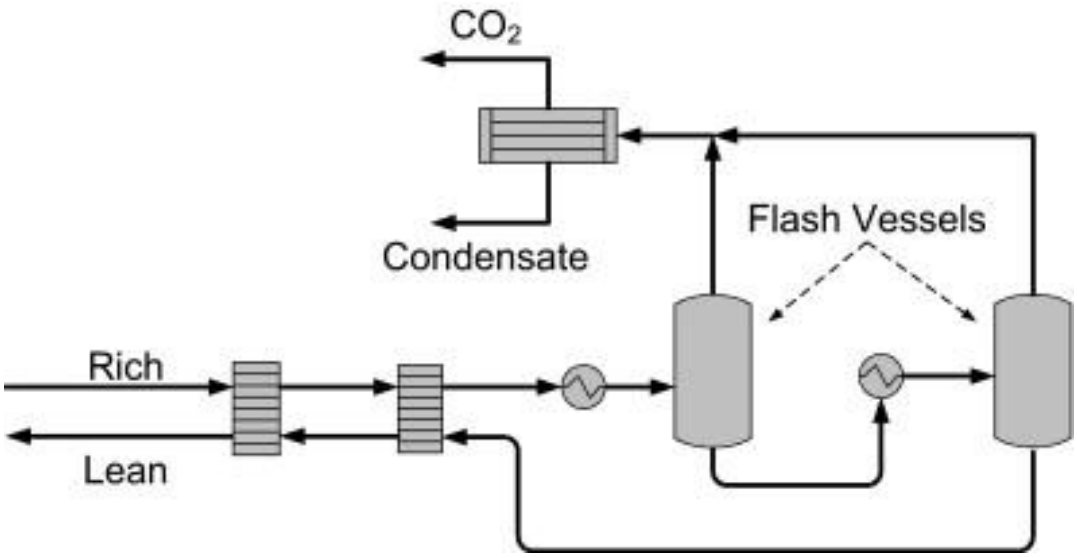

Figure 2.2 The flowsheet of 2-Stage flash stripper (Van Wagener et al., 2013).

Gao et al. (2019) investigated the performance of the absorber intercooler and AFS configurations with 5 mol/L PZ to capture CO_2 from coal-fired flue gas. The flowsheet of the AFS configuration is shown in Figure 2.3. Sixty-eight steady-state operations were conducted at the pilot plant in Texas. As a result, it was proved that AFS configuration can decrease the energy penalty through recovering the latent heat in the hot vapour emission from the stripper.

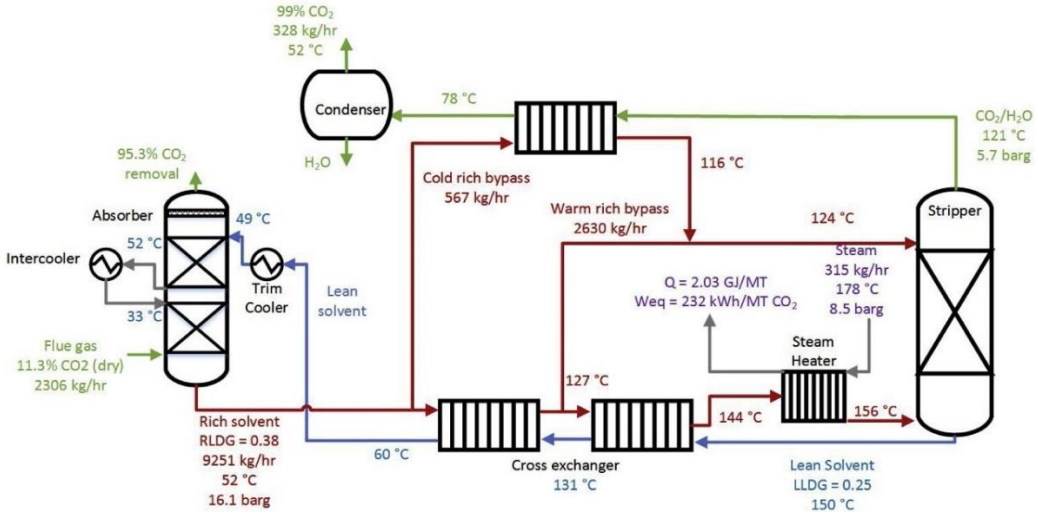

Figure 2.3 Representative conditions for AFS in long term pilot plant (Gao and Rochelle, 2019).

To investigate the performance of the PCC process for different flue gas, Gao and Rochelle (2019) also studied the PZ-based PCC process for the natural gas combined cycle (NGCC). The performance of the absorber with in-and-out and pump-around intercooling was tested. The results indicated that the pump-around intercooling showed a better performance on reducing temperature bulge in the absorber than in-and-out. Furthermore, since the fast reaction rate of PZ solvent, the absorber performance was not highly affected by the lower CO_2 concentration of flue gas from NGCC plants.

Although modifying process configurations improves capture efficiency and energy performance, it inevitably requires additional capital expenditures, such as acquiring heat exchangers and other supplementary process equipment. Conducting an economic evaluation of various process configurations provides a foundation for objectively comparing their energy performance and costs. Therefore, further economic feasibility evaluation of process configurations based on the energy performance evaluation, will help decision makers determine whether the configuration modification is worthwhile.

2.2.2 Pilot project of blue hydrogen plants

Currently, there are two pilot-scale blue hydrogen plants in the world, namely Cryocap^{TM} H_2 project in France and Tomakomai Project in Japan.

2.2.2.1 Port-Jérôme Cryocap^{TM} H_2 pilot plant

Cryocap^{TM} H_2 project cost around € 30 million and was launched in 2015. This pilot plant was connected to Air Liquide's largest SMR unit (Port-Jérôme H_2 plant) located in Port-Jérôme, Normandy, France. A new technology (Cryocap^{TM}) was developed by Air Liquide to capture the CO_2 from the PSA tail gas. Cryocap^{TM} is the first CO_2 capture technology using a cryogenic process. It produced around 300 tonnes per day of liquid CO_2 which is about 55 % of the CO_2 emission in the Port-Jérôme plant (Pichot et al., 2017).

As shown in Figure 2.4, around 2/3 of PSA tail gas is compressed by an 8-stage centrifugal

machine to a high pressure suitable for the carbon capture. The captured CO_2 is purified through partial condensation, distillation, catalytic oxidation, drying, and de-oxygenation to reach a food-grade quality. Lean CO_2 gas from the Cryocap™ H_2 unit contains hydrogen, carbon monoxide, and methane. It is treated by a membrane purification, where H_2 is separated and recycled to the PSA unit to increase hydrogen production (Pichot et al., 2017).

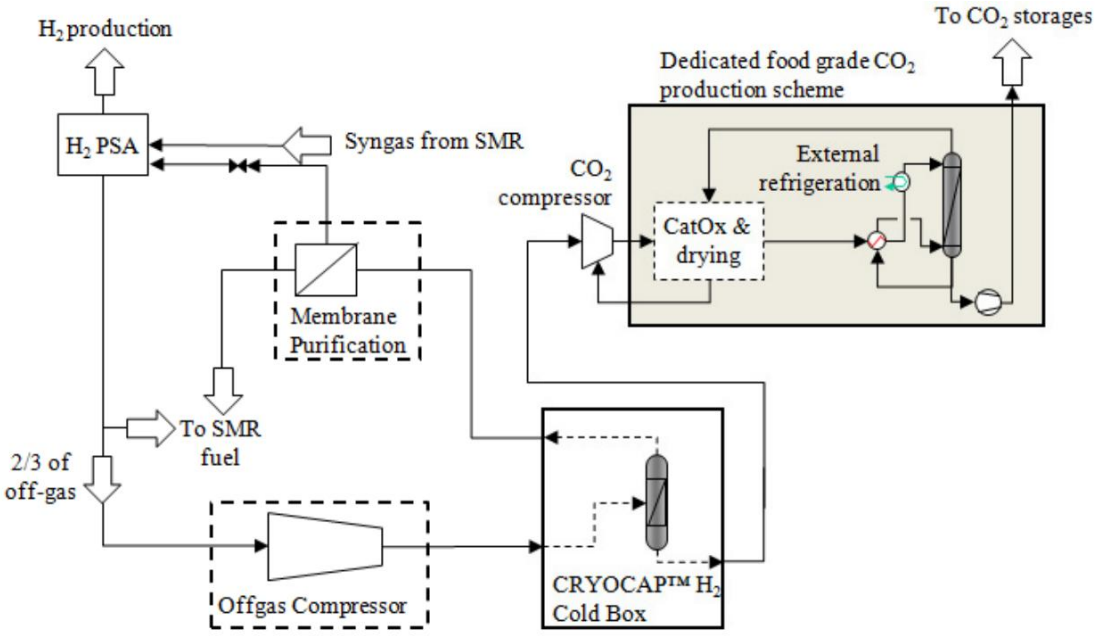

Figure 2.4 Process flow diagram of the Port-Jérôme Cryocap™ H_2 Pilot plant (Pichot et al., 2017).

2.2.2.2 Tomakomai pilot palnt

The Tomakomai project started operating in April 2016 and it located in Tomakomai City, Japan. This project aims to study the feasibility of a PCC plant on a pilot scale. The CO_2 was provided by an SMR unit of Idemitsu Kosan's Hokkaido Refinery. Activated amine (BASF solvent) was used to capture the PSA tail gas with a design capacity of 0.2 million $tonne_{CO2}$/year. The captured CO_2 was compressed and sent into offshore reservoirs (Tanaka et al., 2017).

As shown in Figure 2.5, this two-stage absorption process significantly decreases the reboiler

duty, which is measured at around 0.92 GJ/tonne$_{CO_2}$ for the PSA tail gas. The energy penalty for whole carbon capture plant is lower than 1.3 GJ/tonne$_{CO_2}$, which is around one-third of energy penalty for a conventional CCS process (Sawada et al., 2018).

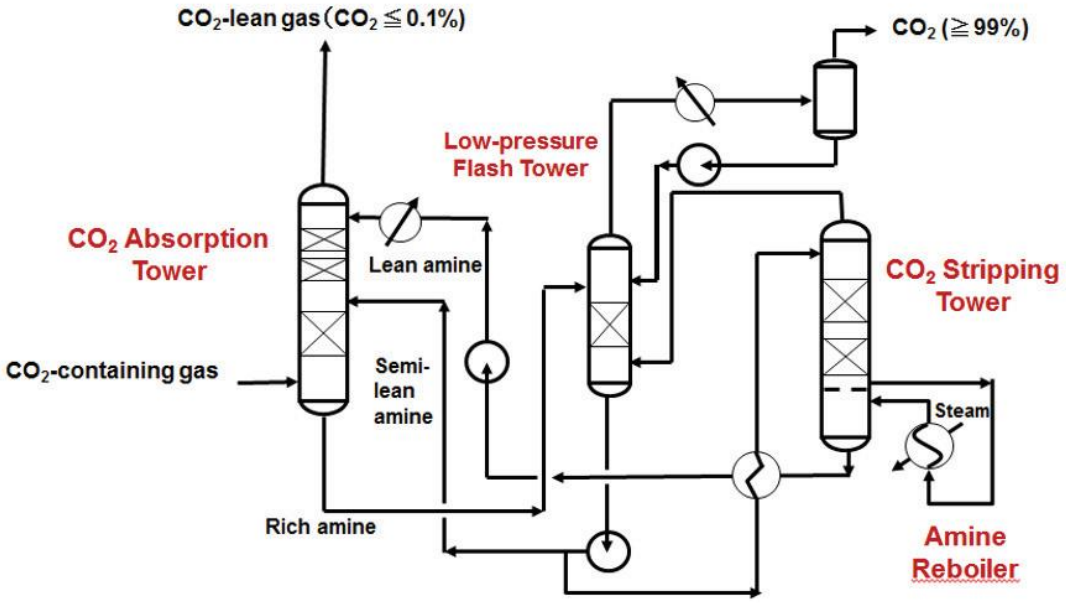

Figure 2.5 Carbon capture process of the Tomakomai project (Tanaka et al., 2017).

2.2.3 Commercial deployment for BHP process

Currently, three commercial-scale blue hydrogen facilities are in operation worldwide, managed by Air Products, Shell and Nutrien. These existing commercial-scale blue hydrogen plants employ physical adsorption or absorption techniques to capture CO_2 from the syngas stream.

2.2.3.1 Air Products Port Arthur project

Port Arthur Project is located in east of Houston, Texas. Air Products retrofitted previous SMR plants with a vacuum swing adsorption (VSA) to capture the CO_2 from the syngas stream. This process captured around 1 million tonne$_{CO_2}$/year in that stream. The compressed CO_2 (approximately 140 bar) was then used in Texas enhanced oil recovery (EOR) projects. This project was funded by the US Department of Energy and was operated in 2013. This blue

hydrogen plant with a total cost of $ 430 million produced 500 tonnes of H_2 per day, which used for petroleum refining (Power et al., 2018).

Air Products developed the most cost-effective CO_2 removal technology for integrated SMRs. The flowsheet of the Air Products Port Arthur project is shown in Figure 2.6. This application was initially based on an MDEA recovery system. However, several major factors led Air Products to select a VSA technology. Firstly, the Port Arthur SMRs were highly integrated with steam/gas turbines and a heat recovery steam generation unit. This level of integration allowed Air Products to produce hydrogen, steam, and power more efficiently than if these products were produced individually. Secondly, compared to VSA technology, the initially proposed MDEA system required more steam for the solvent regeneration process. Thirdly, after detailed analysis, it was concluded that the VSA recovery solution provided the lowest overall cost for carbon captured at the Port Arthur facilities (Baade et al., 2012).

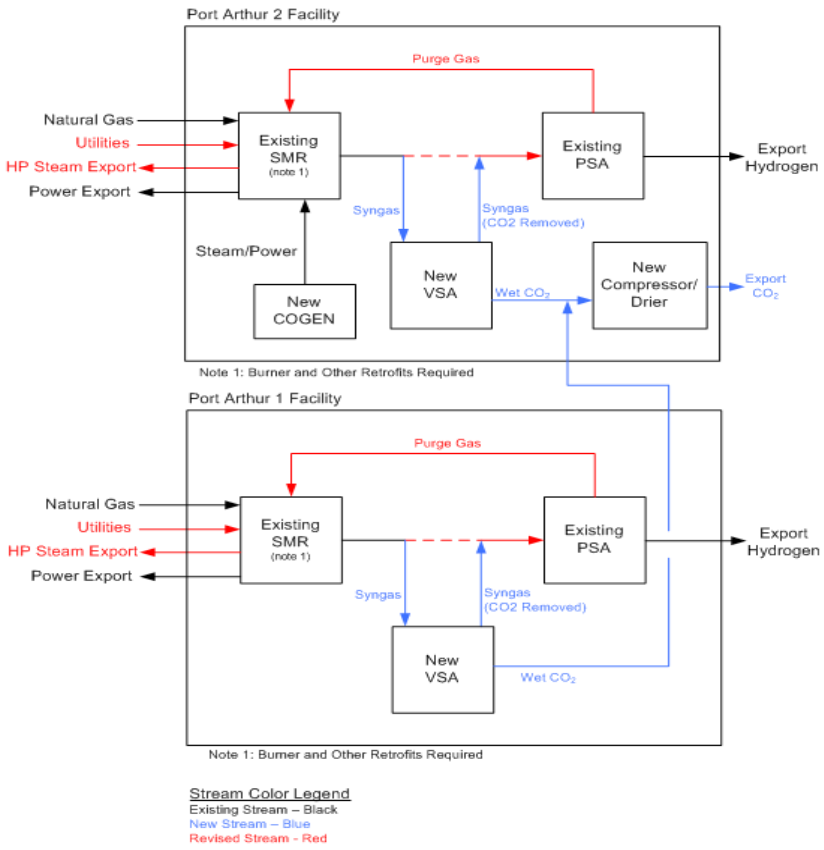

Figure 2.6 The flowsheet of Air Products Port Arthur project (Power et al., 2018).

2.2.3.2 Shell Quest Project

Shell Quest Project is part of the Athabasca Oil Sands Project, which is situated at Scotford Upgrader in Fort Saskatchewan, Canada. The capital cost of this project is estimated about $ 1.35 billion. On November 6, 2015, the Shell Quest project began to capture 35 % of the CO_2 emissions (about 1.2 million tonne/year) from the Scotford SMR units, which produce H_2 for upgrading bitumen. The 3 existing steam methane reformers at Scotford Upgrader produce 900 tonnes of H_2 per day, which is the world's largest SMR plant with CCS currently (Bourne et al., 2014).

Figure 2.7 gives the basic overview of the Shell Quest Project. The CO_2 is captured from syngas by activated amine (Shell ADIPX). Then, CO_2 is released from the solvent in the stripper that produces 95 % pure CO_2 at a pressure slightly above 1 bar. The captured CO_2 is then sent to an injection site near the Scotford Complex and stored in a deep geological formation about 2300 meters underground (Preston, 2018).

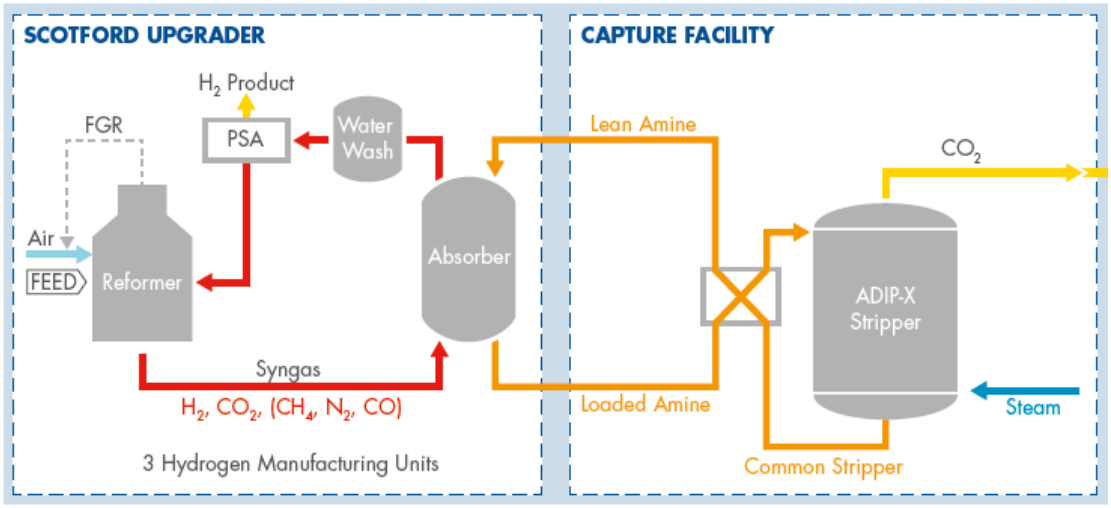

Figure 2.7 Basic overview of Shell Quest Project (Preston, 2018).

2.2.3.3 Alberta Carbon Trunk Line project

Nutrien Fertilizer Facility is a large producer of low-carbon ammonia today, with up to 800 tonnes per day of H_2 production used for fertilizer production. The overall Alberta Carbon

Trunk Line (ACTL) project schematic is shown in Figure 2.8. Liquefied CO_2 from the fertilizer production plant is transported to the ACTL at a pressure of 179.26 bar, which transports the CO_2 to EOR fields at the end of the line for permanent storage. This capture plant is located outside the boundaries of Nutrien's fertilizer plant in Alberta's Industrial Heartland (Terrien et al., 2014)

On June 2, 2020, the ACTL project was announced fully operational, which was estimated to cost $ 0.96 billion. It was a 240 km-long, 16-in-diameter pipelines and gathers industrial CO_2 emissions from Northwest Redwater Partnership Sturgeon Refinery and Nutrien Fertilizer Facility. The ACTL was the largest CCS project, which transports up to 15 million $tonnes_{CO2}$/year used in EOR (Heal and Kemp, 2013).

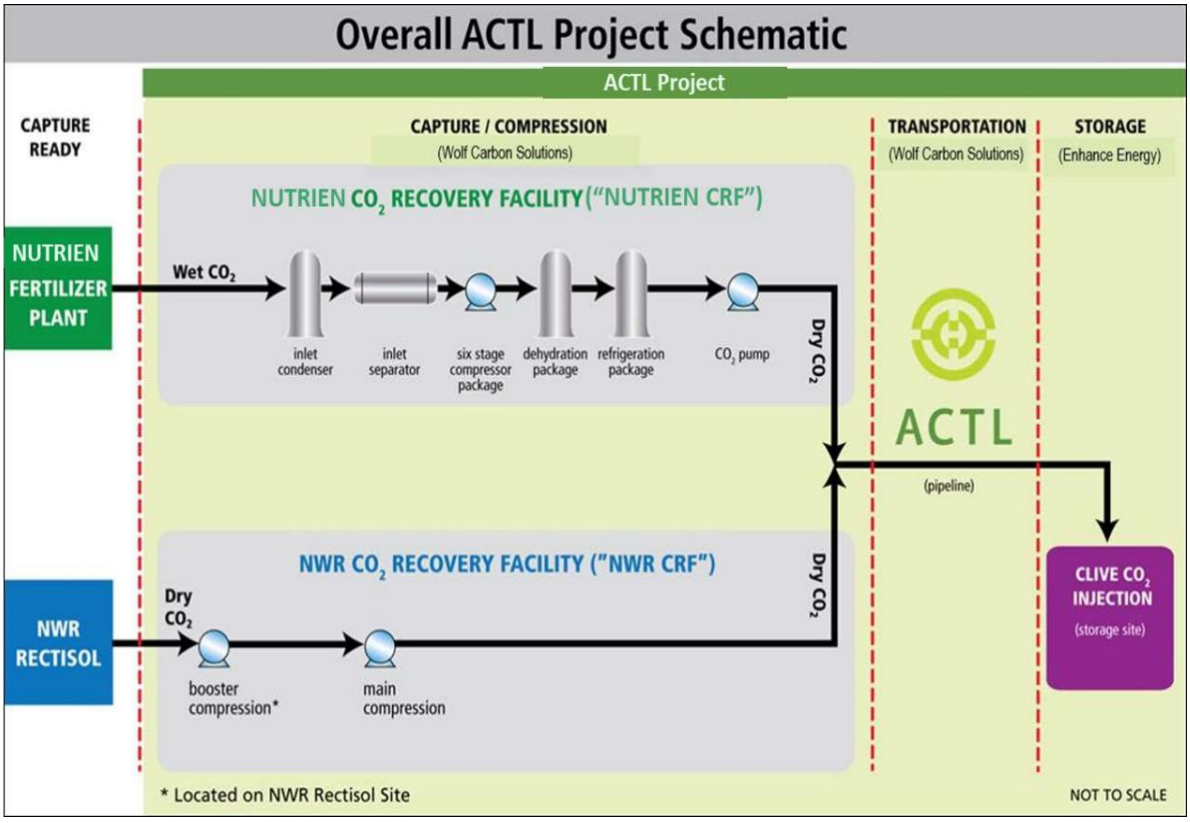

Figure 2.8 Overall ACTL project schematic (Terrien et al., 2014).

2.3 Model-based studies on BHP process

2.3.1 Modelling and simulation studies for SMR process

The SMR is a process that contains multiple units, including desulfurizer, pre-reformer, main reformer, WGS, PSA, etc. Therefore, researchers usually simplify the modelling of some specific units in the SMR process based on their research aims. A common modelling method is to model the reformer based on Gibbs model and model the WGS as an equilibrium reactor (Boyano et al., 2011, Soltani et al., 2014, Sun and Ding, 2014, Salkuyeh et al., 2017). The advantage of this method is that it can accurately simulate the product distribution of the reforming reaction and flexibly adjust the hydrogen yield. However, due to the neglect of catalytic reactions, the prediction of reaction temperature by this method is often on the high side. In addition, the desulfurization and PSA processes are often modelled as separators in order to simplify the simulation procedure (Pellegrini et al., 2020, Antonini et al., 2020, Capocelli et al., 2019). Aspen plus® is the most commonly used software for SMR process modelling. In addition, MATLAB®, COMSOL® and Aspen HYSYS® are often used for reactor modelling.

In a standard SMR process, the CO_2 can be captured from 3 from three primary sources: (I) the syngas stream before the H_2 separation unit; (II) the tail gas following the H_2 separation unit; and (III) the flue gas from the furnace (IEAGHG, 2017). Numerous studies have investigated the performance of CCS at three locations in the SMR process (Soltani et al., 2014, Collodi et al., 2017, Shahid and Kim, 2023, Katebah and Linke, 2022). Figure 2.9 shows the different locations where the carbon capture systems can be installed within the SMR plant. Also, the feed conditions for the three different carbon capture locations in a standard SMR plant is summarized in Table 2.3.

Options 1 and 2 are located before and after the hydrogen separation unit and belong to the pre-combustion process. The primary difference between them is the CO_2 partial pressure

and concentration. The CO_2 partial pressure of option 1 is higher, while Option 2 has a higher CO_2 molar concentration. Both can make CO_2 easier to separate. Option 3 captures CO_2 from flue gases, which is a PCC process. This stream contains all the CO_2 produced during the SMR process (reforming and combustion). Thus, it allows for a higher capture level.

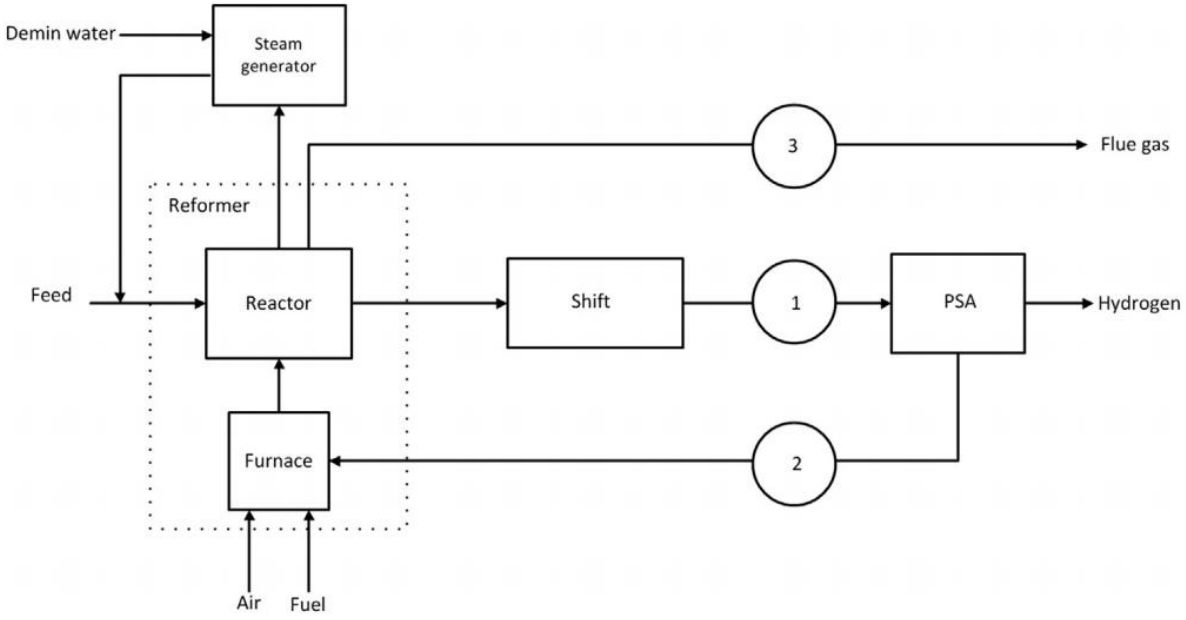

Figure 2.9 Different locations where the CO_2 capture systems can be installed within a standard SMR plant (Soltani et al., 2014).

Table 2.3 Stream feed conditions for different CO_2 removal options in a standard SMR plant (IEAGHG, 2017).

	Option 1	Option 2	Option 3
Pressure (bar)	22.5	2.5	1.2
Mass flowrate (kg/s)	46.36	40.57	150.56
Mole fraction of main components (%):			
CO_2	20.2	64.1	22.6
H_2O	0.2	0.5	17
N_2	0.1	0.2	58.8
O_2	0	0	1.6

Currently, numerous studies have explored the feasibility of carbon capture from option 1 and 2 (Antonini et al., 2021b, Papalas et al., 2020, Pellegrini et al., 2020). Supporters believe that capturing CO_2 from Option 1 and Option 2 is more energy and cost-effective than capturing CO_2 from Option 3. This is because the high CO_2 partial pressure or concentration facilitates CO_2 separation and it is feasible to utilize cost-effective physical adsorption technology (Soltani et al., 2014, Capocelli et al., 2019, Subraveti et al., 2021a).

Opponents argue that CO_2 capture from options 1 and 2 is far from the aim of net-zero emissions, as only 35-60 % of total CO_2 emissions can be captured (Roussanaly et al., 2020, Howarth and Jacobson, 2021). To attain a CO_2 capture rate exceeding 90 %, capturing CO_2 from Option 3 is essential.

In addition, studies also focused on the modification of reactor configurations and the evaluation of operating parameters (Sun and Ding, 2014, Herce et al., 2017, Chompupun et

al., 2018, Papalas et al., 2020, Vo et al., 2021).SESMR has gained significant attention for its potential to increase CH_4 conversion by removing CO_2 in situ. Most of the experimental studies focus on the modification of CO_2 sorbents, while the modelling studies focus more on the modification of reactor configurations. Herce et al. (2017) developed a rate-based model of SESMR with a bubbling fluidized bed reactor, which used dolomite-based solid sorbents to capture CO_2. Papalas et al. (2020) developed a rate-based model of SESMR with two interconnected fluidized bed reactors coupled with chemical looping. Vo et al. (2021) designed an integrated SESMR process, which consisted of a bubbling fluidized-bed reformer and a fast fluidized-bed regenerator. Figure 2.10 gives the schematic diagram of this integrated SESMR process.

These fluidized bed reactors were simulated in Aspen Plus® by modifying correlations and kinetic models. The results of sensitivity analysis indicated that the modification of reactor configurations can increase CH_4 conversion, but the conversion rate is still greatly affected by temperature. In addition, the catalyst to sorbent ratio and the sorbent to carbon ratio also have an impact on methane conversion rate.

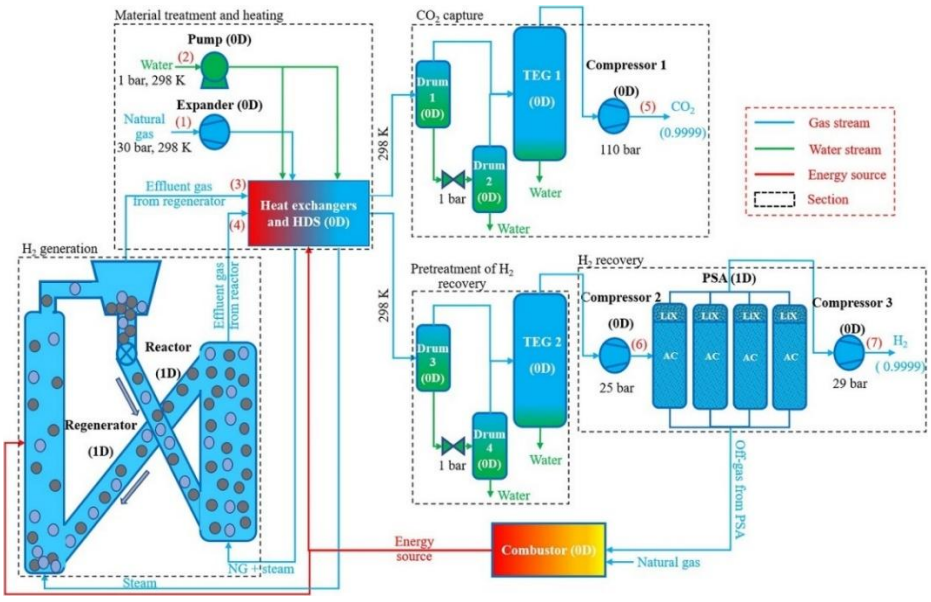

Figure 2.10 Schematic configuration of the developed SESMR process for BHP (Vo et al., 2021).

The effects of operating parameters on the SMR process have been widely studied (Soltani et al., 2014, Sun and Ding, 2014, Papalas et al., 2020, Chen et al., 2021). Because the reforming reaction is a volume expansion process, low pressure is usually beneficial for increasing methane conversion in fixed-bed SMR process. However, the opposite result is observed in the SMR process with membranes. High pressure increases the driving force for H_2 permeation. Therefore, the CH_4 conversion and H_2 yield of the membrane reactor are increased. (Chompupun et al., 2018)

2.3.2 Modelling and simulation studies for carbon capture process

In the early literature, studies on PCC modelling focused on one of the either absorber or stripper due to fewer data from pilot plants being available (Kvamsdal et al., 2009, Lawal et al., 2009, Zhang et al., 2009). As a large amount of pilot plant data is made public, the research on process modelling of PCC is becoming comprehensive and accurate. Currently, the modelling of PCC process usually uses rate-based models and focuses more on the use of new solvents and configurations.

The energy performance of different solvents was evaluated based on data from the pilot plant. The results of the sensitivity analysis showed that parameters such as solvent concentration, CO_2 lean loading, L/G (liquid to gas) ratio, column height, etc. have a significant impact on the energy consumption of PCC process (Abu-Zahra et al., 2007, Lawal et al., 2009, Plaza and Rochelle, 2011, Van Wagener et al., 2013, Rabensteiner et al., 2015a, Gao et al., 2019). Several studies investigated the energy performance of PCC process using PZ at concentrations between 30 wt.% to 50 wt.%. Compared with the energy consumption of the MEA-based PCC process, the PZ-based PCC process achieved a 14.8 % reduction in energy consumption (Rabensteiner et al., 2015a, Gao et al., 2019).

The capture of pre-combustion CO_2 and H_2S by MDEA scrubbing in coal-fired power plants was investigated. Figure 2.11 shows the flow diagram of two capture units for removing H_2S

and CO_2. The H_2S and CO_2 were removed in different absorbers in sequence to ensure that the H_2S content is below 200 ppm(v). The results showed that in the case of low-sulphur coal gasification, the heat duty of the H_2S removal section was always less than 7.8 % of the heat duty required for CO_2 stripping. However, in the case of high-sulphur coal gasification, this proportion became significant, as it may increase to approximately 60 % of the regeneration energy required for CO_2 stripping (Moioli et al., 2016).

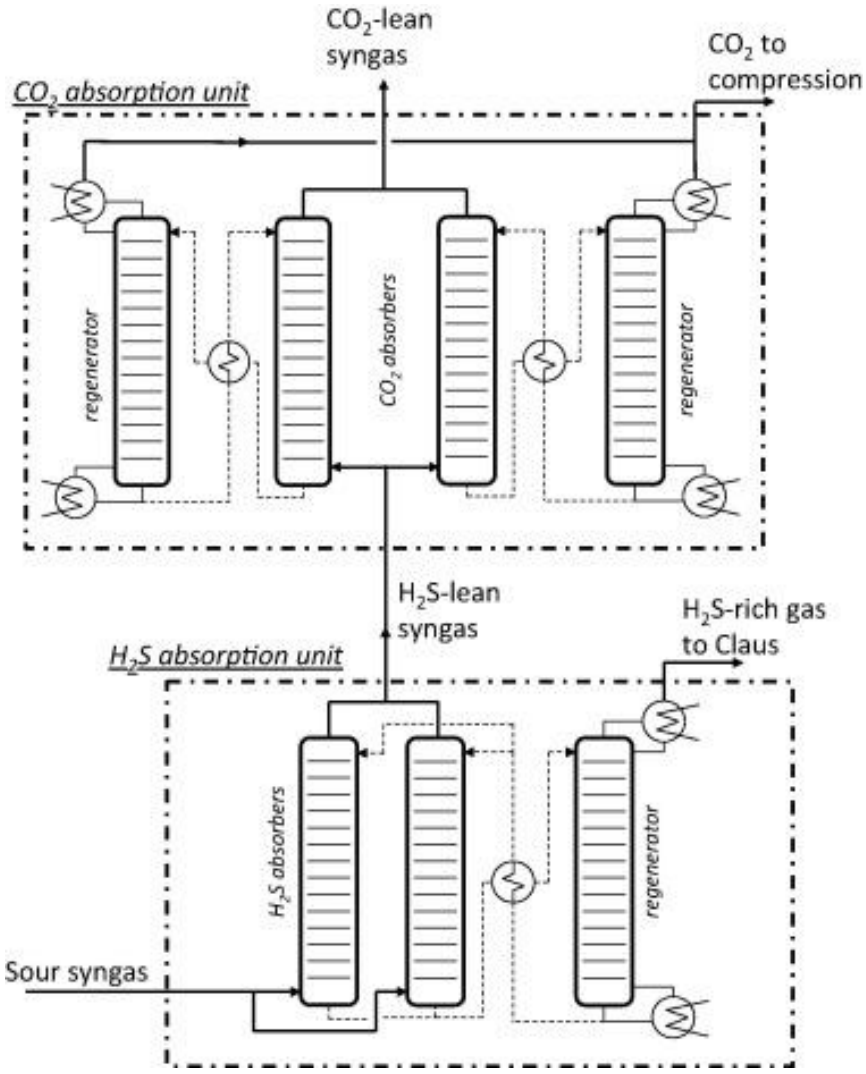

Figure 2.11 Scheme of the capture units for H_2S and CO_2 separation (Moioli et al., 2016).

Several configurations have been proposed to decrease the energy consumption of the PCC process, such as absorber inter-cooling for the absorption process; rich-split process and

parallel exchanger arrangement for the heat exchange process; AFS, stripper inter-heating and lean vapour recompression for the regeneration process (Li et al., 2016, Gao and Rochelle, 2019, Antonini et al., 2021a, Otitoju et al., 2021, Mostafavi et al., 2021). These configurations were simulated in Aspen Plus® at steady state and proved to decrease energy consumption in PCC process. The combinations of configurations can further reduce the energy consumption (Li et al., 2016, Gao and Rochelle, 2019). Some studies have shown that the modification of configuration can reduce operating and total expenditure. However, these complex process configurations resulted in higher capital costs (Mostafavi et al., 2021).

Capocelli et al. (2019) evaluated the feasibility of capturing CO_2 from flue gases using physical adsorption technology. A commercial-scale rapid vacuum pressure swing adsorption (RVPSA) unit was proposed to capture CO_2 from flue gases of SMR plant. The simulation results illustrated that the energy consumption of the RVPSA unit was 0.63 GJ/tonne$_{CO_2}$ at a capture level of 90 %.

2.4 Economic, energy and safety performance assessment of BHP process

2.4.1 Technical and economic assessment of BHP process

Currently, large amount of research supports BHP as a low-carbon, short-term solution during the transition period from grey hydrogen to green hydrogen (Cammeraat et al., 2022, Okonkwo et al., 2021, Massarweh et al., 2023). While most researchers highlight the benefits of blue hydrogen technology in reducing overall carbon emissions, a few claim that blue hydrogen has higher greenhouse gas emissions than grey hydrogen. For instance, Howarth and Jacobson (2021) point out that the footprint of BHP is more than 20 % higher than burning natural gas directly, due to an additional energy consumption increase of at least 39 % when capturing CO_2 from the flue gases. However, this paper is considered to have overestimated the CO_2 emissions and natural gas leakage in BHP process during simulation

(Romano et al., 2022, Diab et al., 2022).

The main challenge of BHP is high cost and increased energy consumption due to the integration of the PCC process. Several studies carried out the technical and economic analysis of SMR process with and without MEA-based PCC process (Roussanaly et al., 2020, Khan et al., 2021, Subraveti et al., 2021a, Li et al., 2024). The conclusions of these studies are largely consistent, slight variations arise mainly from the differences in the assumed capacities of the SMR plants and the costs of natural gas feedstock. A summary of these results is provided in Table 2.4. These results indicate that integration of an SMR plant with a carbon capture process significantly increases both capital and operating costs, leading to a substantial rise in the levelized cost of hydrogen. Obviously, the transition from grey hydrogen to blue hydrogen in commercial-scale SMR plant still faces significant cost challenges. It is of great significance to find ways to decrease the capital and operating costs of blue hydrogen plants.

Table 2.4 The economic performance of a standard SMR plant with and without carbon capture (Roussanaly et al., 2020, Khan et al., 2021, Subraveti et al., 2021a, Li et al., 2024).

	SMR plant	SMR plant with carbon capture
Capital cost (million $)	111.5-117.2	178.2-222.3
Operating cost (million $/year)	62.9-70.7	91.2-114.9
Levelized cost of hydrogen ($/tonne$_{H_2}$)	900-1490	1411-1917
CO_2 avoid cost ($/tonne$_{CO_2}$)	N/A	67-77

Some studies proposed to use physical adsorption technology instead of solvent-based PCC to achieve a reduction in the cost of BHP. VSA process with different adsorbents (Zeolite 13X, UTSA-16 and IISERP MOF2) were investigated and compared with MEA-based absorption

approach. Among them, UTSA-16 and IISERP MOF2 are widely studied metal–organic framework used for CO_2 capture. The results showed that the VSA technology with IISERP MOF2 had the lowest CO_2 avoided cost (83 $/tonne$CO_2$). However, it was still higher than that of the MEA-based PCC process (67-77 $/tonne$_{CO2}$) (Subraveti et al., 2021b).

In addition, Salkuyeh et al. (2017) studied whether alternative hydrogen production methods have cost and energy advantages over the SMR process when combined with carbon capture. The energy and economic performance SMR, ATR, syngas chemical looping (SCL), and chemical looping reforming (CLR) with or without CCS were investigated. The results showed that when CCS is integrated, the CLR option has the highest thermal efficiency, and the hydrogen production cost is only about 70 % of the other technologies.

2.4.2 Process risk assessment of BHP process

Currently, research on process safety and risk assessment is extensive. Relevant risk metrics cover mathematical, analytical, empirical, probabilistic, and computational approaches. There have been many studies discussing how to classify these methods, as shown in Table 2.5. In this thesis, the risk assessment methods are classified into index-based approach and risk-based approach.

Table 2.5 Classification of risk assessment methods.

Categories	References
(a) overall approach; (b) individual approach	Kidam et al. (2016)
(a) index-based approach; (b) consequence-based approach; (3) risk-based approach	Abidin et al. (2018)
(a) relative ranking approach; (b) advanced mathematical approach; (c) risk-based approach; (d) graphical approach; (e) hybrid approach; (f) equation-based approach	Jafari et al. (2018)
(a) hazard-based approach; (b) risk-based approach; (c) cost optimal approach	Park et al. (2020)
(a) index-based approach; (b) risk-based approach; (c) graphical approach; (d) Safety, health and environmental-based approach	Gao et al. (2021)

2.4.2.1 Index-based risk assessment methods

Index-based risk assessment methods aim to establish a set of numerical scales that can be used to compare process risks (Park et al., 2020). Khan and Abbasi (1998) highlight the most significant advantages of using an index-based risk assessment approach, including: rapid identification of hazards, provision of comparable net scores, and flexibility in decision making.

The most pioneering index-based risk assessment method can be traced back to the Dow's fire and explosion index (F&EI), which is widely used in fire and explosion risk assessment (AICHE, 1994). However, this method may not be suitable for BHP as it overemphasizes the hazards from the raw materials. This limitation is common in early studies of index-based risk assessment methods and can be attributed to reduced sensitivity resulting from an excessive

focus on a single hazard. The similar limitations can be seen in prototype index of inherent safety (PIIS) (Lawrence, 1996), inherent safety index (ISI) (Heikkilä, 1999) and i-Safe Index (Palaniappan et al., 2004).

Some new studies have attempted to overcome this problem, such as integrated inherent safety index (I2SI) (Khan and Amyotte, 2004), process stream index (PSI) (Shariff et al., 2012) and inherent system safety index (ISSI) (Sultana and Haugen, 2022). These methods comprehensively consider the impact of the chemical materials, equipment, and the properties of mixtures on the system risk.

Among them, I2SI is based on a framework similar to the hazard and operability analysis (HAZOP) (Khan and Abbasi, 1997) procedure and can simultaneously evaluate the hazard potential and economic evaluation of the process design. PSI was integrated with a process simulator to obtain mixture data as input for the index calculation.

2.4.2.2 Risk-based risk assessment methods

Risk-based risk assessment methods consist of the severity and likelihood of consequences. is usually implemented by generating credible risk scenarios, selecting risk models, and calculating the likelihood and severity of risks based on various process options (Gao et al., 2021). Common hazard identification methods include HAZOP (Khan and Abbasi, 1997) and hazard identification and ranking (HIRA) (Khan and Abbasi, 1998).

HAZOP is one of the best approaches for hazard identification and evaluation during the design and operation process. This method identifies possible deviations in the system and determines the specific initial events that cause the deviations to infer the possible consequences and severity of accidents caused by such deviations (Khan and Abbasi, 1997). The HIRA method estimates the severity and toxic effects of fire and explosion accidents based on the total energy and inventory of the equipment. This method considers the effect of process parameters on the severity of the consequences (Khan and Abbasi, 1998).

The likelihood of consequences can be estimated by event tree analysis (ETA) and fault tree analysis (FTA). For example, the ETA is employed to assess the likelihood of success or failure for each relevant mitigative safeguard, as well as to determine the overall risk associated with each resulting scenario. FTA aims to determine the likelihood of the top event occurring based on the known probabilities of bottom events. The top event represents the most critical failure, while bottom events are fundamental failures that cannot be broken down further. Events that connect the bottom and top events are referred to as intermediate events. (Ruijters and Stoelinga, 2015).

Risk-based analysis is widely used in SMR process. Past studies have shown that high-pressure reactors such as desulfurizers and reforming reactors are usually the most dangerous units in SMR process. Full-bore ruptures of these units can result in the most dangerous flash fires and affect large areas (Jafari et al., 2012, JAFARI et al., 2013, Mohammadfam and Zarei, 2015)

In addition, some studies combined risk analysis with economic evaluation to analyse the interaction between economic and safety variables in SMR process. The results showed that some risk reduction measures, such as reducing the purge gas pressure discharged from the gas compressor and increasing the syngas temperature entering the condenser, have a negative impact on economic benefits. These studies provide suggestions for risk-economic trade-offs in commercial-scale hydrogen production (Ade et al., 2022).

Some new risk-based assessment methods, such as system hazard identification, prediction and prevention (SHIPP) and multi-criteria decision-making (MCDM) methods, were proposed to investigate the efficiency and safety performance of different hydrogen production technologies (Rathnayaka et al., 2011b, Chau et al., 2022a). The results showed that while electrolysis-based technologies (AWE, PEM and SOEC) have environmental advantages, they demonstrate greater uncertainties compared to non-renewable technologies such as SMR, ATR and Pox (Chau et al., 2022a).

The appraisal procedure of SHIPP is shown in Figure 2.12. It defines system risk based on whether a series of protection layers fail to account for operational behaviour and adjusts the accident likelihood using the Bayesian updating mechanism. This method enables the identification of critical safety areas and functions, as well as the assessment of the failure probabilities of these safeguards (Rathnayaka et al., 2011b).

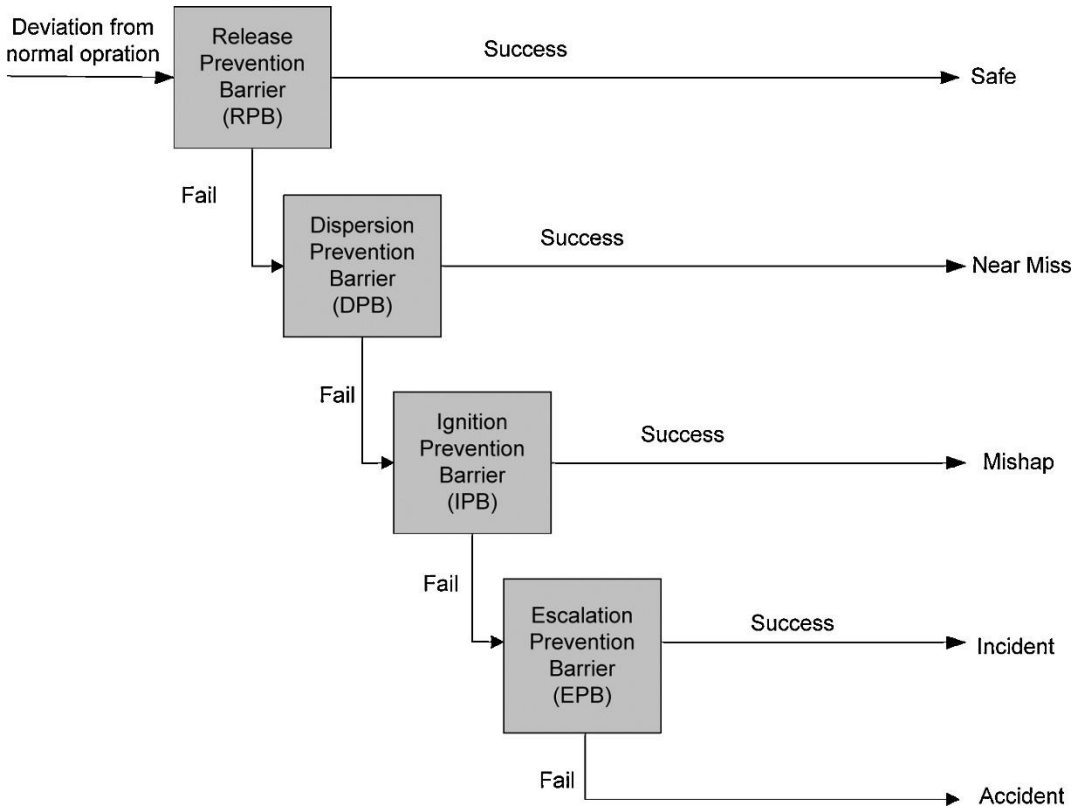

Figure 2.12 Appraisal procedure of SHIPP (Rathnayaka et al., 2011a).

2.5 Summary

The literature review of the BHP carried out in this chapter has shown that:

1) BHP is considered a low-carbon, short-term solution in the transition from grey hydrogen to green hydrogen. The cost and energy consumption increase due to the integration of carbon capture processes as well as potential safety issues are two major challenges to the commercial deployment of BHP.

2) Many recent studies on BHP have focused on capturing carbon from syngas streams and tail gas. However, a significant limitation of these studies is that only 35-60 % of the total carbon emissions in the process are captured, as CO_2 from flue gas is released into the atmosphere. To fully decarbonize the process, addressing CO_2 capture from flue gas is essential. This study investigated the performance of SMR integrated with PCC process. The CO_2 from flue gas of SMR process was captured by solvent-based PCC technology, achieving nearly 90 % CO_2 removal.

3) The primary approaches to minimizing the energy penalty involve the use of new solvents and new process configurations. Many studies showed that PZ solvent has better energy performance and has been suggested as a potential substitute for MEA solvent in PCC process. Some new configurations such as AFS are considered to not only decrease the energy consumption of the PCC process but also reduce costs. This study used PZ solvent and AFS configuration to reduce the energy consumption of the PCC process. In addition, an energy and cost-saving configuration was developed to reduce cost and energy consumption of BHP process.

4) Unlike risk assessments that focus on the hydrogen production process, risk assessments for BHP require investigating any economic impacts that may occur while proposing process improvements to reduce associated risks. Since risk assessment and economic assessment are equally important in commercial-scale BHP, a method is needed to assess overall process risk from a holistic perspective. An index-based risk assessment approach may be more appropriate for commercial-scale BHP processes because it can quickly identify hazards and provide comparable net scores. This study proposed a new risk assessment method to evaluate the overall process risk of commercial-scale BHP. In addition, an integrated model was developed to investigate the relationship between potential process safety improvements and economic benefits.

Chapter 3. Modelling, simulation and performance assessment of large-scale PCC process using PZ and AFS configuration

3.1 Overview

This chapter investigated the energy performance of the large-scale PCC process using PZ and advance flash stripper configuration. It encompasses model development, model validation, model scale-up, energy performance assessment and process optimisation. The modelling and simulation of PCC process were conducted using Aspen Plus® V11. Section 3.2 provides the descriptions of the process configurations. Section 3.3 details the development of solvent-based PCC models using MEA and PZ in Aspen Plus® V11. Section 3.4 focuses on pilot-scale model validation, and Section 3.5 provides an overview of the scale-up process. Section 3.6 discusses the effect of three parameters on energy performance of the large-scale PCC process with PZ and AFS configuration. Section 3.7 presents the process optimisation. The conclusions of this chapter are presented in Section 3.8.

3.2 Process description

3.2.1 Standard solvent-based PCC process

The standard PCC process includes the absorber, the stripper, a cooler, a cross-flow heat exchanger and pumps. The flue gas from hydrogen plant is first sent to a quench scrubber/direct contact cooler where it is scrubbed with caustic soda or sodium bicarbonate solution for further cooling and desulfurization. This decreases the SO_x in the flue gas to less than 1 ppm (for reducing solvent degradation).

The cooled flue gas is blown into the absorber, where the CO_2 is captured through counter-

current contact with a CO_2-lean solvent, resulting in a CO_2-rich solvent. The treated gas exits from top of the absorber and washed by water to minimise the carryover of amine.

The CO_2-rich solvent is preheated using the regenerated CO_2-lean solvent from the stripper before being pumped into the stripper. Inside the stripper, the CO_2 is separated from the CO_2-rich solvent at 105-140 °C and is released from the top of the stripper. The CO_2-rich gas is subsequently directed to a compressor and a dehydration system.

A process flowsheet illustrating the standard PCC process configuration is provided in Figure 3.1.

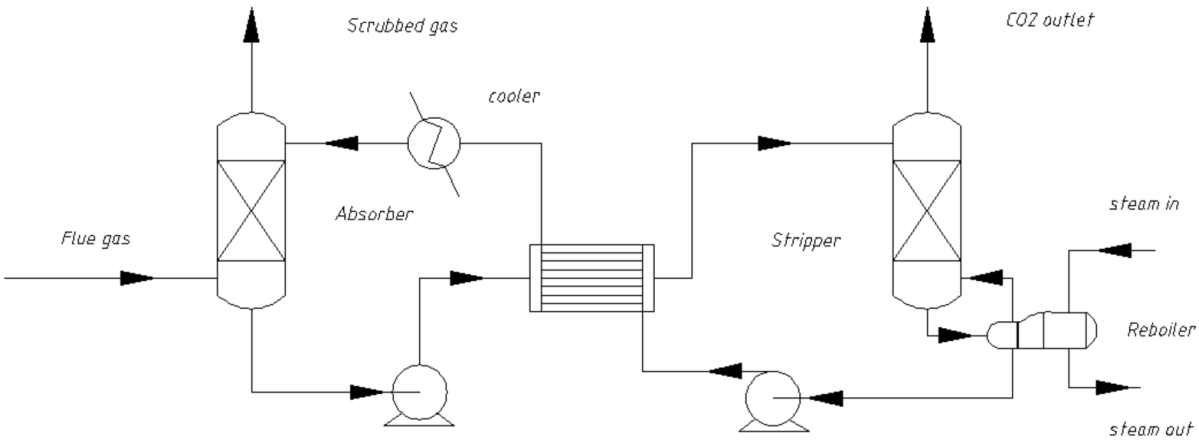

Figure 3.1 Standard configuration of the solvent-based PCC process.

3.2.2 PCC process with AFS

The AFS configuration was developed and tested at a pilot plant by researchers at the University of Texas at Austin (Gao et al., 2019, Gao and Rochelle, 2019). In contrast to the standard configuration of the PCC process, the solvent exiting the absorber is divided into two streams: a cold-rich bypass and a warm-rich bypass. The cold-rich bypass is heated by hot vapor from the top of the stripper and then combined with a portion of the warm-rich bypass before being fed to the top of the stripper. The remaining rich solvent is preheated using the regenerated lean solvent and a steam heater before being directed to a flash tank

located at the bottom of the stripper. In this setup, the flash tank and steam heater perform the functions of the reboiler in the standard stripper configuration. Compared to the standard striper configuration, the AFS enhances energy performance by recovering latent heat from hot vapour. The flowsheet of the AFS is presented in Figure 3.2.

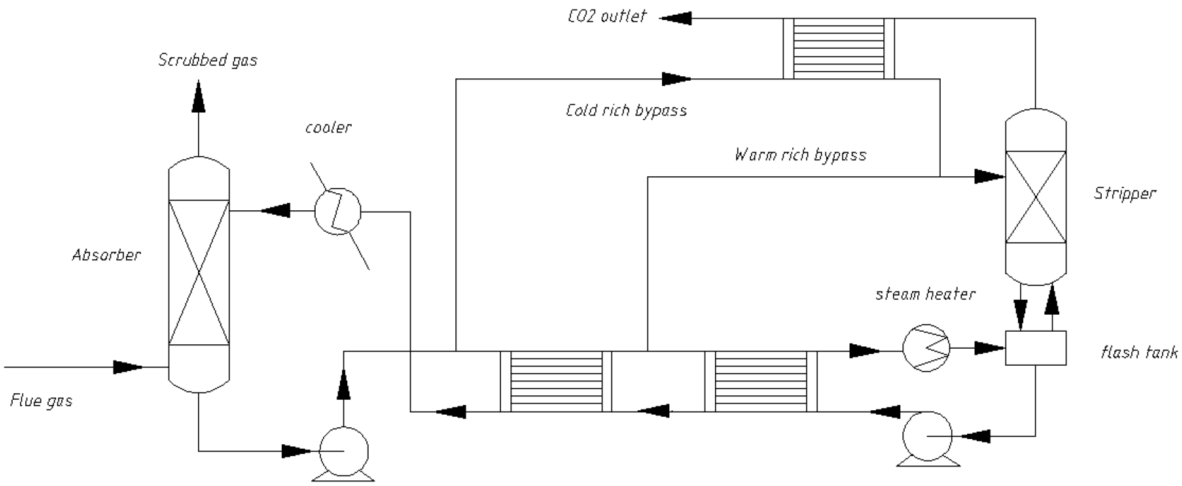

Figure 3.2 The AFS configuration of the solvent-based PCC process.

3.3 Model development

The rate-based models of the solvent-based PCC process were developed in Aspen Plus® V11. These models incorporate the electrolyte chemistry (component speciation) and correlations for determining mass transfer, heat transfers, hydrodynamic properties, physical properties, thermodynamic properties, and kinetic properties. The assumptions used in the model includes:

- Liquid and vapour phases both are comprised of thin film and bulk regions.
- No accumulation in the bulk regions as well as the liquid and gas films.
- Mass transfer within these films occurs by steady-state molecular diffusion only.
- The bulk regions of both liquid and vapour phases are assumed to have uniform compositions.

- The vapour phase is composed of only CO_2, H_2O, N_2, O_2 and MEA or PZ.
- Gas and liquid flow counter-currently.

3.3.1 Thermodynamic and kinetic models

Aspen Plus® incorporates various physical properties methods to model a chemical process. The electrolyte Non-Random-Two-Liquid (Elec-NRTL) model is selected for liquid properties due to the presence of ions. It was proposed by Chen and Evans (1986) and describes the excess Gibbs energy in aqueous electrolyte solutions. This model provides key information such as interface of vapour-liquid equilibrium and driving forces of bulk interface which makes it suitable for kinetic simulations focusing on rates of mass transfer.

The Redlich-Kwong (RK) equation of state (Redlich and Kwong, 1949) is used for vapour properties, which is the most widely used equation to represent the non-ideal equilibrium behaviour of gas-phase in CO_2-H_2O-MEA systems. The components and ions in the gas and liquid phase are listed in Table 3.1.

Table 3.1 The components and ions in the gas and liquid phase.

Gas phase	Liquid phase		
CO_2	H_2O	MEA	PZ
H_2O	H_3O^+	$MEAH^+$	PZH^+
N_2	CO_2	$MEACOO^-$	$PZCOO^-$
O_2	CO_3^{-2}	HCO_3^{-1}	$PZ(COO^-)_2$

The chemistry of CO_2 absorption with aqueous MEA and PZ is presented by both equilibrium and rate-based reactions. The liquid film is characterised by the equilibrium reactions which

are defined as (Ermatchkov et al., 2006, Canepa et al., 2013)

$$2H_2O \leftrightarrow H_3O^+ + OH^- \quad (3.1)$$

$$H_2O + HCO_3^- \leftrightarrow H_3O^+ + CO_3^{2-} \quad (3.2)$$

$$H_2O + MEAH^+ \leftrightarrow H_3O^+ + MEA \quad (3.3)$$

$$H_2O + PZH^+ \leftrightarrow H_3O^+ + PZ \quad (3.4)$$

$$H_2O + H^+PZCOO^- \leftrightarrow H_3O^+ + PZCOO^- \quad (3.5)$$

The temperature-dependent equilibrium constants (K_{eq}) for reactions (3.1) – (3.5) are determined as follows. It was proposed by Austgen et al. (1989) and govern the dissociation of weak electrolytes in an aqueous solution.

$$In(K_{eq}) = A + \frac{B}{T} + C \cdot In(T) + DT \quad (3.6)$$

The rate-based reactions are presented in reactions (3.7) – (3.14), where reactions (3.7) and (3.8) are the forward and reverse reactions involved in bicarbonate formation (Canepa et al., 2013); reactions (3.9) - (3.12) are the forward and reverse reactions for carbamate formation (Li et al., 2024); reactions (3.13) and (3.14) are the forward and reverse reactions associated with iminodiacetate formation (Otitoju et al., 2021).

$$CO_2 + OH^- \rightarrow HCO_3^- \quad (3.7)$$

$$HCO_3^- \rightarrow CO_2 + OH^- \quad (3.8)$$

$$MEA + H_2O + CO_2 \rightarrow H_3O^+ + MEACOO^- \quad (3.9)$$

$$H_3O^+ + MEACOO^- \rightarrow MEA + H_2O + CO_2 \quad (3.10)$$

$$PZ + H_2O + CO_2 \rightarrow H_3O^+ + PZCOO^- \quad (3.11)$$

$$H_3O^+ + PZCOO^- \rightarrow PZ + H_2O + CO_2 \quad (3.12)$$

$$PZCOO^- + H_2O + CO_2 \rightarrow H_3O^+ + PZ(COO^-)_2 \quad (3.13)$$

$$H_3O^+ + PZ(COO^-)_2 \rightarrow PZCOO^- + H_2O + CO_2 \quad (3.14)$$

The reaction rate (r) for reactions (3.7) – (3.14) are estimated by the power law expressions (Zhang et al., 2009). The kinetic expression is defined as

$$r = kT^n \exp\left(-\frac{E_a}{RT}\right) \prod_{i=1}^{N} C_i^{a_i} \quad (3.15)$$

Where:

k: pre-exponential factor

T: absolute temperature

n: temperature exponent

E_a: activation energy

R: universal gas constant

N: number of components in the reaction

C_i: concentration of component *i*

a_i : the stoichiometric coefficient of component *i* in the reaction equation

The values of the parameters for the equilibrium and the rate-based reactions are shown in Table 3.2 and 3.3. They were determined based on a combination of experimental data and literature correlations.

The equilibrium constants in Table 3.2 were derived using the empirical correlation proposed by Austgen et al. (1989), as shown in Equation (3.6). The constants A, B, C, and D were fitted from experimental vapor-liquid equilibrium and calorimetric data reported in the literature, including the works of Posey and Rochelle (1997) and Canepa et al. (2013). These studies

conducted systematic measurements across a range of temperatures and concentrations to ensure accurate representation of electrolyte behaviour in aqueous amine systems.

The kinetic parameters listed in Table 3.3 were obtained from previous experimental studies that used stopped-flow techniques, conductivity measurements, and reaction modelling to quantify the forward and reverse rate constants. The values were adopted from well-established sources such as Pinsent et al. (1956), Bishnoi and Rochelle (2000), and Ermatchkov et al. (2003).

Table 3.2 The parameters for the equilibrium reactions (Posey and Rochelle, 1997, Canepa et al., 2013).

Equation no.	A	B	C	D
3.1	131.889	-13455.8	-22.4768	0
3.2	216.051	-12432.1	-35.4821	0
3.3	-3.03832	-7008.357	0	-0.0031348
3.4	18.135	3814.4	0	-0.0151
3.5	14.042	3443.1	0	0

Table 3.3 Kinetic parameter for the rate-controlled reactions (Pinsent et al., 1956, Hetzer et al., 1968, Bishnoi and Rochelle, 2000, Ermatchkov et al., 2003).

Equation no.	k	E_a (J/mol)
3.7	4.32×10^{13}	55380.82
3.8	2.38×10^{17}	123105.18
3.9	4.77×10^{11}	41239.04
3.10	2.18×10^{18}	59098.51
3.11	7.41×10^{10}	33567.91
3.12	7.94×10^{21}	65837.09
3.13	3.62×10^{10}	33567.91
3.14	5.56×10^{25}	768226.73

3.3.2 Transport properties models

This model incorporates various transport properties, including the mixture viscosity, binary diffusivity, thermal conductivity, and liquid surface tension. These transport properties are critical for performing mass transfer, heat transfer calculations using the Elec-NRTL model. The corresponding correlations used to estimate the thermophysical properties of the vapour and liquid phases are summarized in Table 3.4.

Table 3.4 The corresponding correlations for estimate the thermophysical properties.

Thermo-physical properties	Relevant correlations	Source
Vapour mixture viscosity	Chapman-Enskog-Brokaw model	(Bird et al., 2007)
Liquid mixture viscosity	Jones-Dole electrolyte model	(Horvath, 1985)
Vapour phase binary diffusion coefficients	Chapman-Enskog and Wilke-Lee models	(Wilke and Chang, 1955)
Liquid phase binary diffusion coefficients	Wilke-Change model	(Wilke and Chang, 1955)
Thermal conductivity of the vapour mixture	Wassiljewa-Mason-Saxena model	(Aspen, 2008)
Thermal conductivity of the liquid mixture	Riedel correlation	(Aspen, 2008)
Mixture surface tension	Hakim-Steinberg-Stiel model	(Horvath, 1985)
Mass transfer and interfacial area	Bravo et al. (1985) correlation	(Bravo et al., 1985)
Heat transfer coefficient	Chilton-Colburn analogy	(Chilton and Colburn, 1934)
Liquid holdup	Bravo et al. 1992 correlation	(Bravo et al., 1992)

The absorber and the stripper are modelled as RadFrac columns, and each column was divided into 20 stages. This method allows the packed tower to be divided into a user-defined number of theoretical stages which helps to observe the thermodynamic state of the vapour and liquid streams leaving a stage. RadFrac model is designed to simulate a wide range of

multi-stage fractionation processes, including absorption, stripping, azeotropic distillation, and extractive distillation. This model supports the application of the rate-based modelling approach for absorber and stripper columns, providing a more dependable method for assessing the performance of solvent-based PCC process (Aspentech, 2022).

The bulk properties of the gas and liquid phases were estimated by counter-current flow model. It accurately predicts the column flows and determines the gas and liquid bulk properties by averaging the conditions at inlet and outlet (Razi et al., 2013). The "Discrxn" option was used to model the film resistance of liquid phase, where the rapid reaction between CO_2 and solvent occurs. This option also accounts for both chemical reactions and diffusion resistance within the liquid film. In this study, the liquid phase was divided into ten discretization points. The "Film" option was applied to model the vapour phase film resistance. This option considers diffusion resistance but does not account for chemical reactions, eliminating the requirement of vapour phase to be discretized into small segments.

The heat exchanger is modelled as a heater and a cooler connected by a heat flow. In addition, the mass balance of the whole process was achieved by adding solvents and water supplementation to address system losses. Table 3.5 details mass flowrate of the make-up solvents and water. The flow rates of the make-up streams for MEA, PZ, and water were determined through a component-wise mass balance using Aspen Plus®.

Table 3.5 The results of solvents and water make-up in MEA-based and PZ- based PCC process.

	MEA-based PCC process	PZ-based PCC process
Flowrate of solvent make-up (kg/h)	0.13	2.06
Flowrate of H_2O make-up (kg/h)	46.61	2.46

3.4 Model validation

The validation of the MEA-based and PZ-based PCC models is conducted through comparison with pilot-scale experimental data. The MEA-based PCC model is verified using data from 22 test cases performed at the Tarong PCC pilot plant in Australia (Li et al., 2016). These tests used an MEA solvent with a concentration of 24.1-34.1 wt.% and flue gas containing 11-14 vol% CO_2. The absorber was 0.35 m in diameter and included four sections (1.782 m each), packed with Mellapak M250X. The stripper was 0.25 m in diameter and included two sections (3.582 m each), packed with Mellapak M350X.

For the PZ-based PCC model, validation is performed using experimental data from University of Texas (Plaza and Rochelle, 2011, Van Wagener, 2011). These experiments involved a PZ solvent with concentrations between 28-44 wt.% and flue gas containing 12.2 vol% CO_2. The absorber and stripper both had a diameter of 0.428 m and were composed of two sections (3.04 m each), packed with Mellapak 2X. The detailed operating conditions for the MEA-based and PZ-based PCC pilot plants are provided in Table 3.6, 3.7, 3.8, 3.9 and 3.10.

Table 3.6 Details of the pilot plant data for absorber (Cases 1-11) used as input into the rate-based PCC model using MEA (Li et al., 2016).

Cases of absorber	1	2	3	4	5	6	7	8	9	10	11
Lean solvent temperature (°C)	31.7	31.4	31.3	35.5	33.9	34.8	35.3	33.5	32.4	37.5	35.6
Solvent circulation rate (kg/min)	32.0	32.3	27.3	31.6	27.1	33.3	36.1	32.3	24.2	24.6	32.3
MEA concentration (wt.%)	25.1	24.1	27.9	25.5	31.6	29.6	29.2	30.3	33.5	34.1	29.3
Lean loading (mol_{CO_2}/mol_{MEA})	0.279	0.294	0.284	0.280	0.314	0.333	0.347	0.316	0.254	0.278	0.414
Rich loading (mol_{CO_2}/mol_{MEA})	0.466	0.480	0.469	0.471	0.481	0.486	0.488	0.494	0.494	0.489	0.525
Intel flue gas temperature (°C)	51.7	50.5	48.1	51.3	53.6	54.2	55.8	65.5	66.1	63.9	49.8
Inlet flue gas flow rate (kg/s)	8.16	8.19	8.14	8.16	8.05	8.07	8.08	8.05	10.77	10.74	8.13
Inlet flue gas pressure (bar)	1.050	1.046	1.052	1.055	1.064	1.062	1.062	1.062	1.076	1.072	1.061

Table 3.7 Details of the pilot plant data for absorber (Cases 12-22) used as input into the rate-based PCC model using MEA (Li et al., 2016).

Cases of absorber	12	13	14	15	16	17	18	19	20	21	22
Lean solvent temperature (°C)	38.7	38.7	39.4	39.3	39.2	39.7	40.5	39.6	39.4	39.6	39.5
Solvent circulation rate (kg/min)	21.3	21.3	27.4	27.3	27.3	32.4	27.3	27.3	27.2	27.5	27.3
MEA concentration (wt.%)	32.3	32.8	29.2	29.2	28.9	26.2	27.4	28.1	28.3	28.5	28.5
Lean loading (mol_{CO_2}/mol_{MEA})	0.285	0.291	0.285	0.285	0.280	0.314	0.288	0.295	0.297	0.283	0.283
Rich loading (mol_{CO_2}/mol_{MEA})	0.486	0.500	0.488	0.488	0.491	0.499	0.503	0.511	0.512	0.492	0.492
Intel flue gas temperature (°C)	48.3	48.8	58.3	59.4	56.7	61.8	60.7	60.0	56.1	58.2	57.9
Inlet flue gas flow rate (kg/s)	8.09	8.13	9.98	9.97	9.95	9.97	9.95	9.95	9.93	9.98	9.96
Inlet flue gas pressure (bar)	1.056	1.055	1.078	1.076	1.077	1.072	1.074	1.079	1.077	1.078	1.079

Table 3.8 Details of the pilot plant data for stripper (Cases 1-11) used as input into the rate-based PCC model using MEA (Li et al., 2016).

Cases of stripper	1	2	3	4	5	6	7	8	9	10	11
Condenser temperature (°C)	30.2	29.0	26.2	29.6	32.0	29.9	29.4	25.4	26.9	24.8	28.8
Stripper pressure (bar)	1.801	1.786	1.757	1.880	1.873	1.931	1.936	1.896	2.211	2.199	1.503
CO_2 desorption rate (kg/h)	71.6	71.0	70.6	73.6	72.6	76.8	76.7	76.0	93.9	94.2	49.3
Reboiler temperature (°C)	116.9	116.4	117.0	117.6	117.2	117.1	115.9	117.5	125.3	125.8	104.7
Heating duty (GJ/tonne$_{CO_2}$)	4.48	4.45	4.35	4.5	4.33	4.51	4.6	4.49	4.01	4.04	4.55
CO_2 product purity (vol.%)	97.7	97.7	97.8	97.7	97.6	97.8	97.8	98.0	98.9	99.0	98.1

Table 3.9 Details of the pilot plant data for stripper (Cases 12-22) used as input into the rate-based PCC model using MEA (Li et al., 2016).

Cases of stripper	12	13	14	15	16	17	18	19	20	21	22
Condenser temperature (°C)	24.6	23.8	19.3	20.5	18.1	20.8	19.7	19.3	17.5	18.7	17.1
Stripper pressure (bar)	1.850	1.802	2.007	1.980	2.002	1.985	2.002	2.011	2.000	2.013	2.002
CO_2 desorption rate (kg/h)	73.2	71.2	84.2	83.5	84.1	82.3	84.3	84.5	84.3	84.2	84.3
Reboiler temperature (°C)	119.9	118.7	121.5	121.1	121.2	119.9	121.7	121.3	121.1	121.4	121.6
Reboiler duty (GJ/tonne$_{CO_2}$)	3.86	3.88	4.10	4.12	4.15	4.28	4.18	4.10	4.11	4.12	4.11
CO_2 product purity (vol.%)	98.4	98.7	99.5	98.6	99.5	99.1	99.3	99.1	99.2	99.4	99.6

Table 3.10 Details of the pilot plant data used as input into the rate-based PCC model using PZ (Plaza and Rochelle, 2011, Van Wagener, 2011).

Cases	1	2	3	4	5	6	7	8	9	10	11	12	13	14
Absorber														
PZ concentration (wt.%)	38.9	40.2	43.9	41.1	39.9	41.2	40.7	40.2	40.1	39.5	29.1	29.7	29.4	28.3
Solvent circulation rate (kg/h)	62.4	64.2	63.0	65.4	50.4	76.8	64.2	51.0	75.6	64.8	74.4	73.2	60.6	48.6
Lean temperature (°C)	49.9	46.5	49.5	39.7	44.1	45.4	48.2	44.9	51.7	45.3	44.8	48.6	46.5	42.6
Lean loading (mol_{CO_2}/mol_{Alk})	0.261	0.308	0.254	0.386	0.284	0.303	0.305	0.298	0.267	0.331	0.316	0.274	0.257	0.262
Stripper														
Stripper pressure (bar)	1.378	1.377	1.378	1.378	1.378	1.377	4.135	4.137	3.157	3.155	3.155	3.447	3.445	3.445
CO_2 desorption rate (kg/h)	118.8	93.6	129.6	39.6	100.8	111.6	93.6	82.8	115.2	64.8	79.2	115.2	111.6	93.6
Condenser temperature (°C)	14.9	15.5	9.0	22.0	11.3	4.7	19.6	16.2	20.1	25.2	8.0	11.5	4.8	4.8
Condenser rate (kg/h)	72.0	28.8	68.4	7.2	39.6	43.2	18.0	14.4	39.6	46.8	14.4	39.6	36.0	32.4
Reboiler temperature (°C)	108.2	104.0	107.9	86.5	104.7	103.1	126.5	128.5	128.0	117.1	118.7	126.6	127.2	126.0
Reboiler duty (kW)	130.6	101.0	155.5	45.9	111.1	125.3	112.7	105.6	141.3	79.0	99.8	134.6	129.0	114.5

The validation results of model predictions against experimental data for PCC models are as follows. The validation results for all cases in MEA-based PCC model are shown in Figure 3.3, 3.4, 3.5 and 3.6. Figure 3.7 shows the validation results of MEA-based PCC model for the temperature profile of absorber in Case 22. The MEA-based PCC model validation results of rich loading, capture level, CO_2 product purity, and reboiler duty in Case 22 are given in Table 3.11.

Capture level is calculated with the equation (3.16):

$$Capture\ level = \frac{CO_2\ in flue\ gas - CO_2\ in\ outlet\ gas}{CO_2\ in\ flue\ gas} \times 100\% \quad (3.16)$$

The relative deviation for all model predictions against experimental data was calculated by equation (3.17).

$$Relative\ deviation\ (\%) = \frac{|experimental\ data - model\ predictions|}{experimental\ data} \times 100\% \quad (3.17)$$

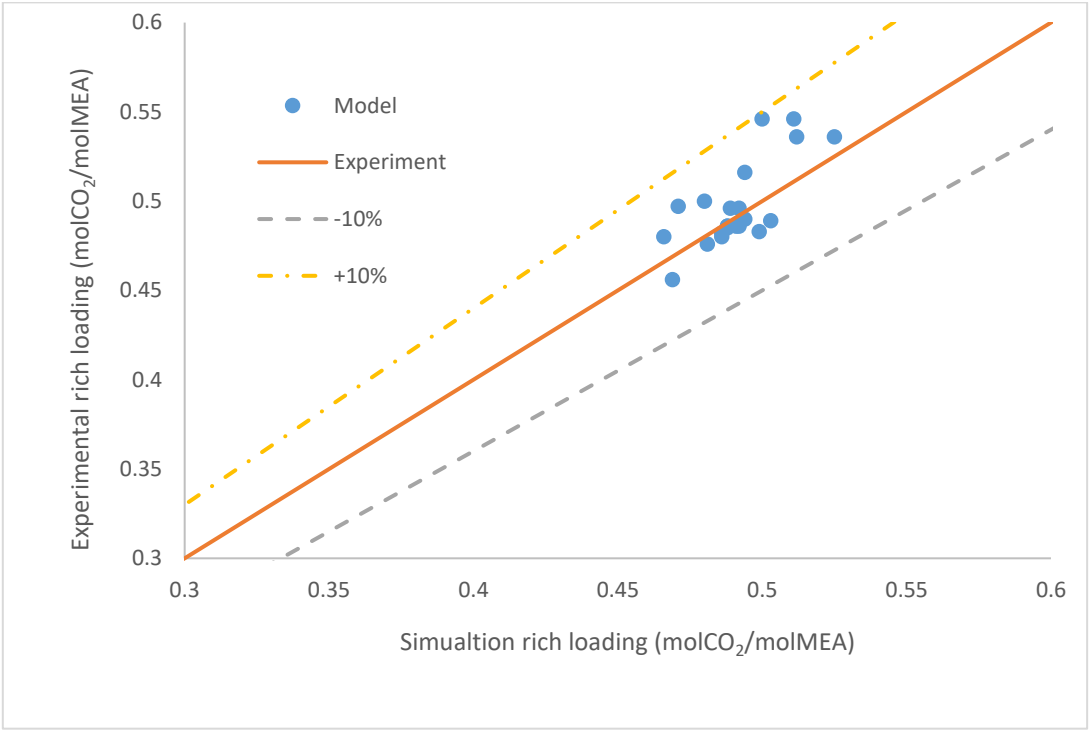

Figure 3.3 Validation results of CO_2 rich loading in MEA-based PCC process.

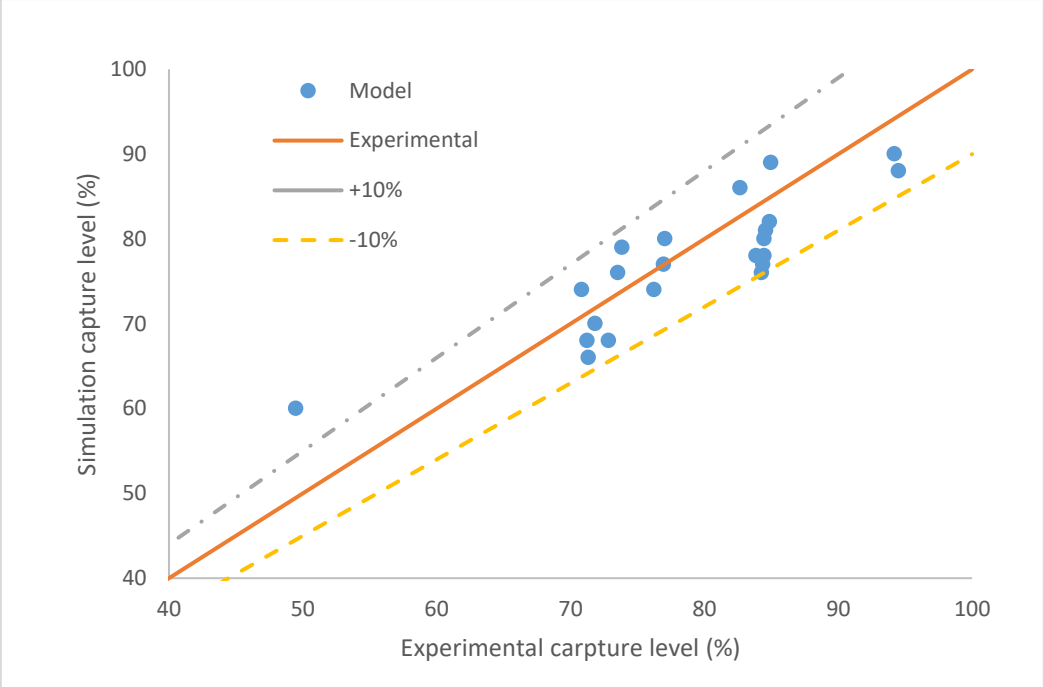

Figure 3.4 Validation results of CO_2 capture level in MEA-based PCC process.

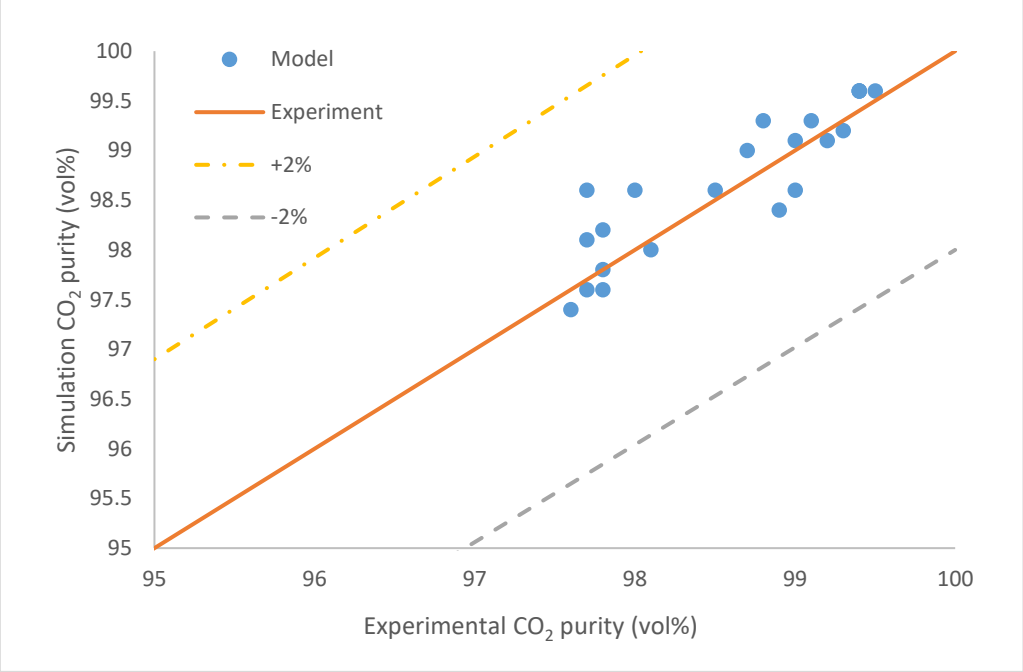

Figure 3.5 Validation results of CO_2 product purity in MEA-based PCC process.

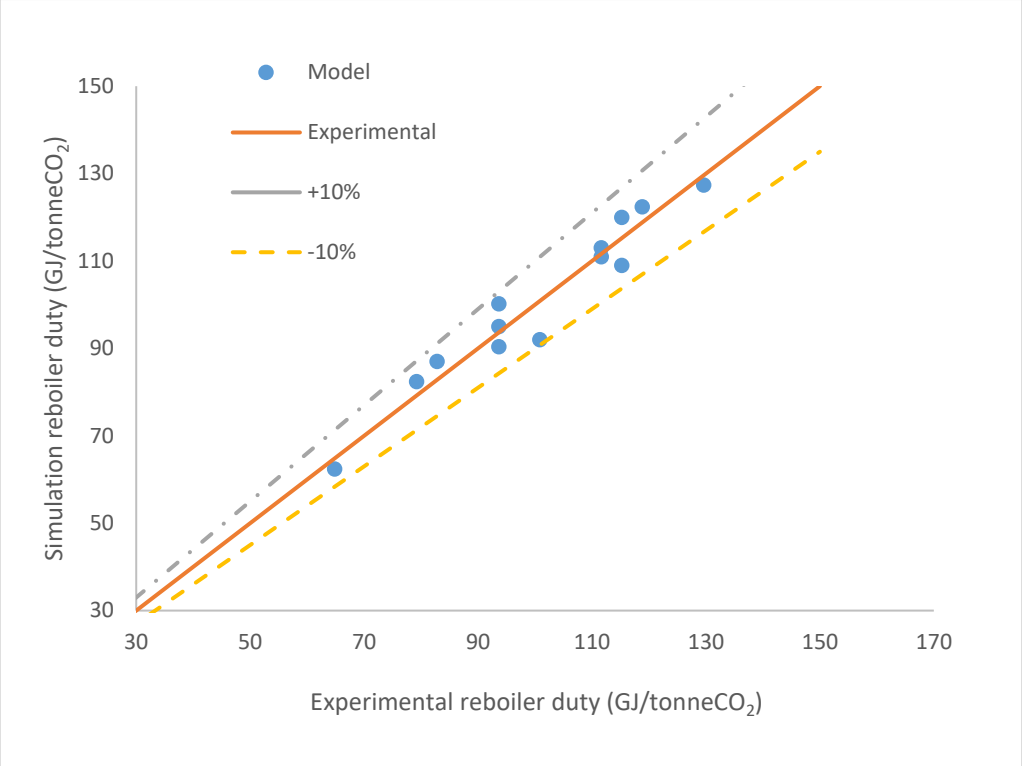

Figure 3.6 Validation results of reboiler duty in MEA-based PCC process.

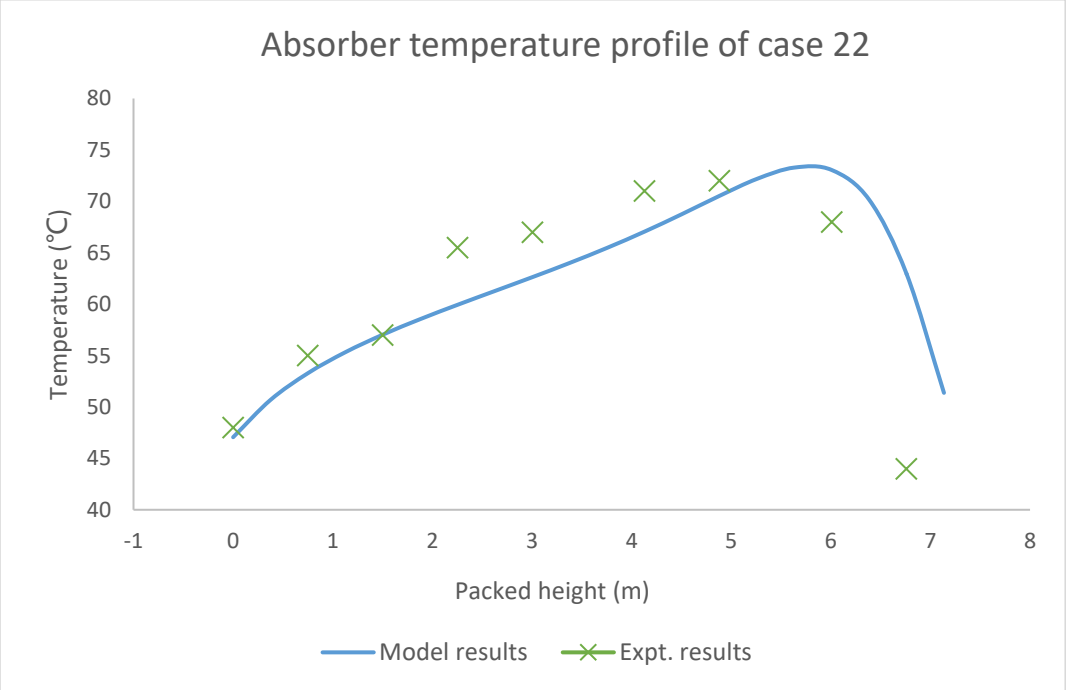

Figure 3.7 Validation results of absorber temperature profile in MEA-based PCC process.

Table 3.11 Model validation for case 22 in MEA-based PCC process.

Parameter	Experiment	Simulation	Relative deviation (%)
Rich loading (mol_{CO_2}/mol_{Alk})	0.492	0.487	1.42
Capture level (%)	84.44	80.05	5.22
CO_2 product purity (vol%)	99.6	99.7	0.1
Reboiler duty ($GJ/tonne_{CO_2}$)	4.12	4.24	3.41

Figure 3.3 compares the simulation results and experimental data for CO_2 rich loading. This is an important indicator reflecting the absorption capacity of the solvent. The validation results indicate that the model can accurately describe the experimental results of the pilot plant. The relative deviation between the simulation results and the experimental data is less than ±10 %. Figure 3.4 shows the validation results of CO_2 capture level. The results show that the simulation results can predict the experimental data with an average relative deviation of 4.47 %. Figure 3.5 compares the simulation results and experimental data for CO_2 product purity. The simulation results are highly consistent with the experimental results, with a relative deviation of less than ±2 % in all 22 cases. Reboiler duty is an important indicator of energy consumption in PCC process. Figure 3.6 shows the validation results of reboiler duty in MEA-based PCC process. The model accurately predicted the experimental results, with a relative deviation of less than ±10 %.

The validation results for all cases in PZ-based PCC model are shown in Figure 3.8, 3.9 and 3.10. Figure 3.11 shows validation results of PZ-based PCC model for absorber temperature profile in Case 1. The PZ-based PCC model validation results of rich loading, capture level, CO_2 desorption rate, rich solvent flow rate and reboiler duty in Case 1 are shown in Table 3.12.

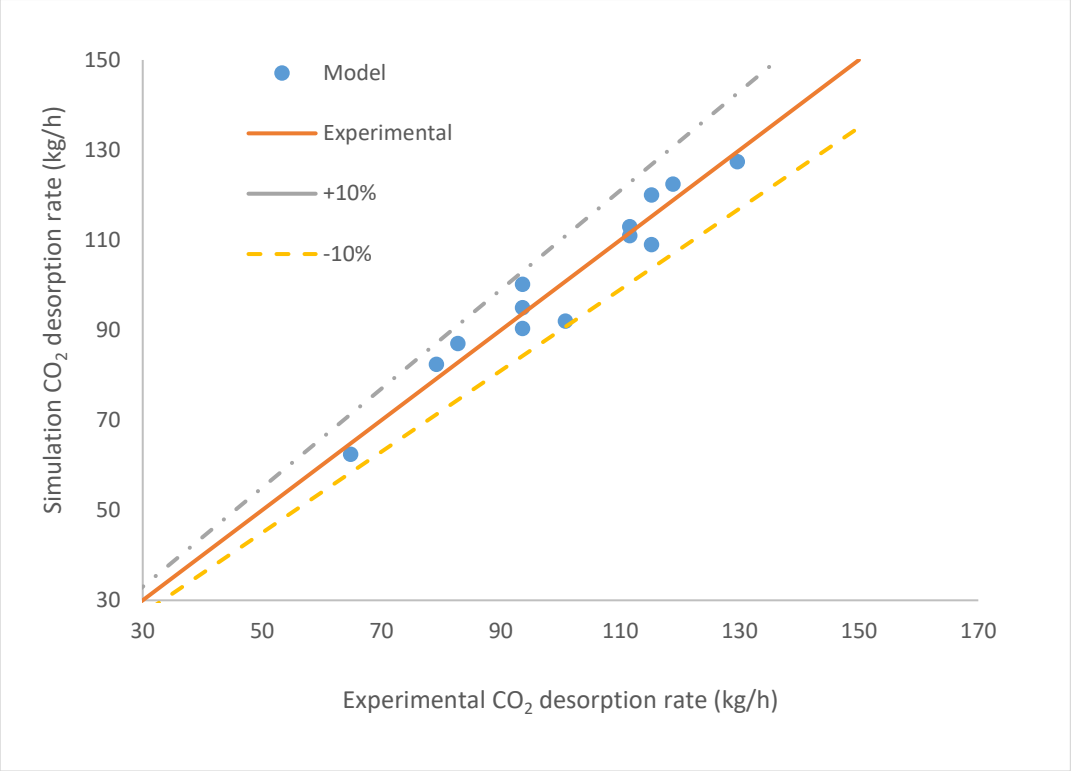

Figure 3.8 Validation results of CO_2 desorption rate in PZ-based PCC process.

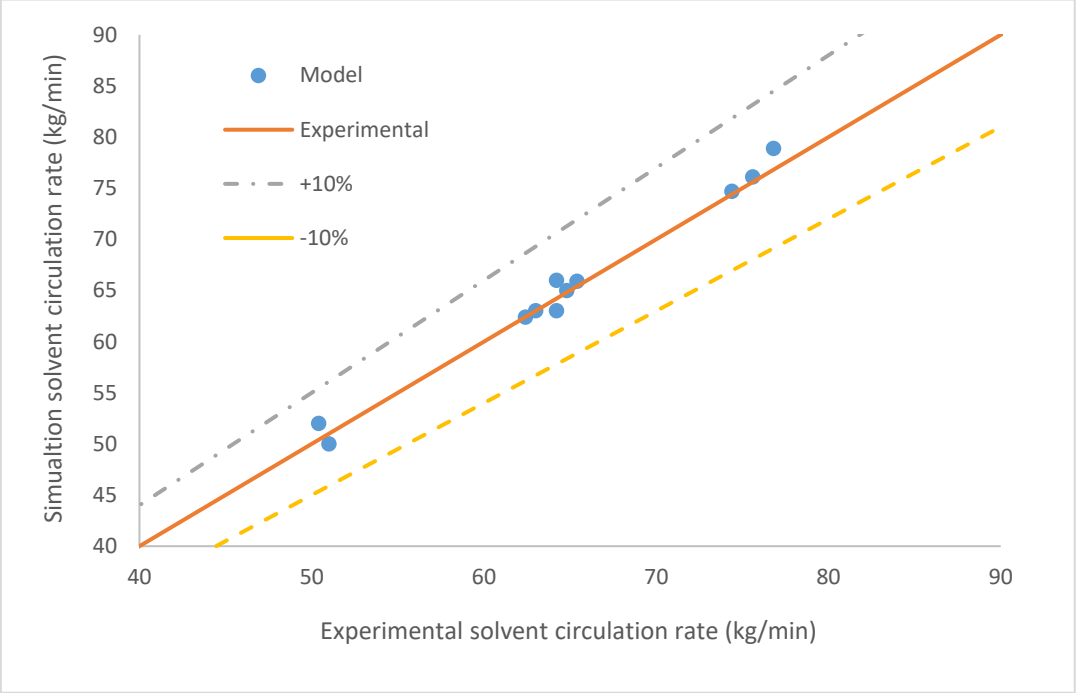

Figure 3.9 Validation results of solvent circulation rate in PZ-based PCC process.

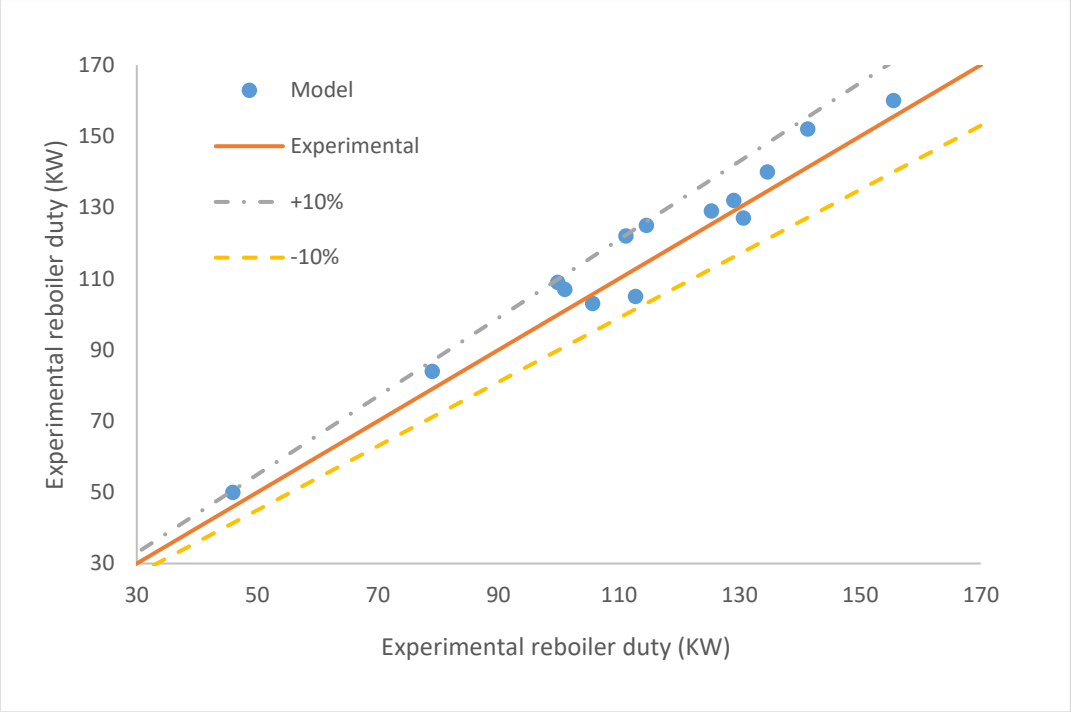

Figure 3.10 Validation results of reboiler duty in PZ-based PCC process.

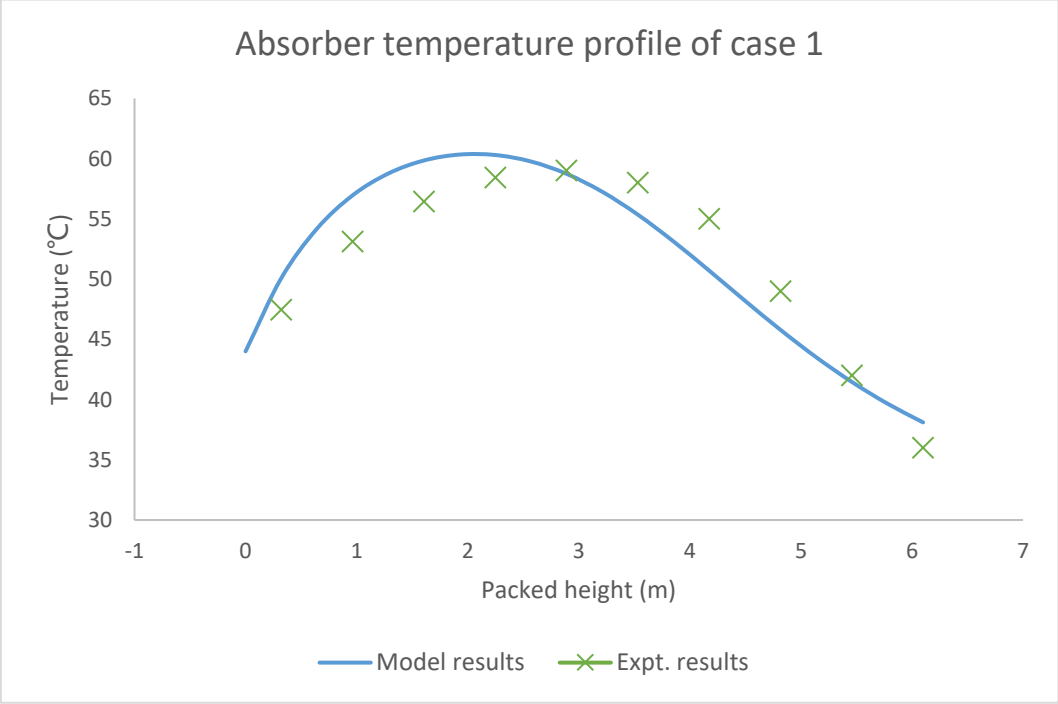

Figure 3.11 Validation results of absorber temperature profile in PZ-based PCC process.

Table 3.12 Model validation for case 1 PZ-based PCC process.

Parameter	Experiment	Simulation	Relative deviation (%)
Rich loading (mol_{CO_2}/mol_{Alk})	0.385	0.384	0.26
Capture level (%)	85.8	81.3	5.47
CO_2 desorption rate (kg/h)	118.8	122.4	3.03
Rich solvent flow rate (kg/s)	1.09	1.09	0
Reboiler duty (KW)	130.5	127.1	2.76

Figure 3.8 compares the simulation results and experimental data for CO_2 desorption rate. The validation results illustrate that the model can accurately predict the experimental results of the pilot plant. The relative deviation between the simulation results and the experimental data is less than ±10 %. The solvent circulation rate is an important indicator for estimating operating expenditure. Figure 3.9 compares the simulation results and experimental data for solvent circulation rate. The simulation results are highly consistent with the experimental results, with an average relative deviation less than 1 %. Figure 3.10 shows the validation results of reboiler duty in PZ-based PCC process. The model accurately predicted the experimental results, with a relative deviation of less than ±10 %.

The MEA-based and PZ-based PCC models demonstrated satisfactory accuracy, with deviations from the experimental results remaining within ±10 %.

3.5 Model Scale-up for PCC process

The solvent-based PCC models are scaled up to achieve 90 % of CO_2 capture from the commercial-scale SMR plant. This capture level is widely used assumption based on the trade-off between operating cost and CO_2 removal rate (Brandl et al., 2021). The character of flue gas from the SMR plant is obtained from the IEA report (IEAGHG, 2017). The mass flowrate of the flue gas is 72.1 kg/s, which consists of N_2 (61 mol%), CO_2 (20.7 mol%), H_2O (17.5 mol%), and O_2 (0.8 mol%). The assumptions for model scale-up are as follows:

- The CO_2 lean loading and CO_2 absorption capacity were assumed to be consistent with the rate-based models at pilot scale.
- The solvents concentration in lean solvents were assumed to be consistent with the rate-based models at pilot scale.
- The same operating pressures of the pilot plant will be applied for the commercial-scale model.

3.5.1 The calculation of MEA-based PCC model scale-up

The solvent circulation rate is calculated following the method proposed by Agbonghae et al. (2014), which relies on the solvent absorption capacity that obtained from simulation. The column diameters is estimated by the generalised pressure drop correlation (GPDC) method described by Sinnott (2005). It first calculates the flow parameters that represent the L/G ratio entering the packed column. Subsequently, the modified gas load is obtained from the GPDC. Finally, the column diameter is estimated based on the gas mass flow rate per unit cross-sectional area.

The solvent mass flow rate, L (kg/s) is calculated by equation (3.16):

$$\text{Solvent mass flow rate (L)} = \frac{G \cdot F_{CO_2} \cdot M_{MEA}}{M_{CO_2} \cdot \Delta\alpha \cdot W_{MEA}} \quad (3.16)$$

Where:

G: flue gas mass flow rate (kg/s)

F_{CO_2}: CO_2 mass fraction

M_{MEA}: MEA molar mass (kg/kmol)

M_{CO_2}: CO_2 molar mass (kg/kmol)

$\Delta\alpha$: MEA absorption capacity (mol_{CO_2}/mol_{MEA})

W_{MEA}: MEA concentration (wt.%)

The flow parameter (F_{LV}) is calculated with equation (3.17) and the values of liquid and vapour density are obtained from the pilot-scale simulation.

The flow parameter (F_{LV}) = $\frac{L}{G}\sqrt{\frac{\rho_V}{\rho_L}}$ (3.17)

Where:

L: solvent mass flowrate (kg/s)

G: flue gas mass flowrate (kg/s)

ρ_V: vapour density (kg/m^3)

ρ_L: liquid density (kg/m^3)

The column pressure drop is 42 mm of water/metre of packing height, which is selected based on the recommendation of operation at the highest economical pressure drop.

F_{LV} is calculated by the equation (3.17) while k_4 is obtained from Figure 3.12 (Sinnott, 2005).

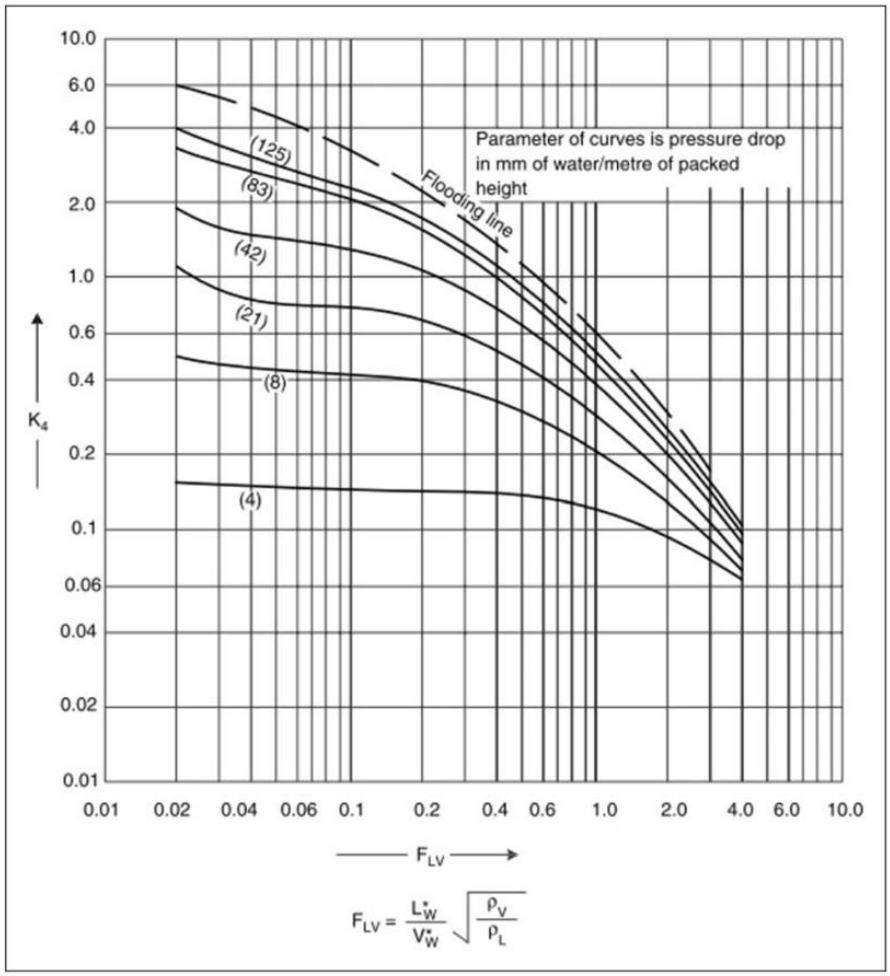

Figure 3.12 Diagram of generalised pressure drop (Sinnott, 2005)

Gas mass flow rate per unit cross-sectional area, V_W (kg/m²s) is calculated by equation (3.18)

$$V_W = \sqrt{\frac{k_4 \cdot \rho_V (\rho_L - \rho_V)}{13.1 F_P (\frac{\mu_L}{\rho_L})^{0.1}}} \quad (3.18)$$

Where:

k_4: modified gas load

F_P: packing factor (m^{-1})

μ_L: liquid viscosity (Ns/m^2)

3.5.2 Summary of calculation result for the absorber and the stripper

Table 3.13 and 3.14 provide the input parameters and the results of the scale-up calculations for MEA-based and PZ-based PCC models. The input specifications (ρ_L, ρ_V, F_P, μ_L, and L/G ratio) are obtained from the pilot-scale PCC models that developed in Aspen Plus®. The calculated flow parameter (F_{LV}) is used to extract the gas load parameter (K_4) from the GPDC diagram (see Figure 3.12). The gas mass flowrate per cross-sectional area (V_W) is calculated by equation (3.18).

Table 3.13 The calculation results of absorber and stripper in MEA-based PCC model.

Parameters	absorber	stripper
L/G ratio	7.16	12.61
ρ_V (kg/m^3)	1.15	1.99
ρ_L (kg/m^3)	1003.29	916.56
F_{LV}	0.2425	0.5879
k_4	1.01	0.58
F_P (m^{-1})	259	359
μ_L(Ns/m^2)	0.0012	0.0003
V_W (kg/m^{2}s)	1.15	0.99
A (m^2)	62.56	40.93
Result		
L (kg/s)	516.4	516.4
D (m)	8.92	7.22

Table 3.14 The calculation results of absorber and stripper in PZ-based PCC model.

Parameters	absorber	stripper
L/G ratio	4.95	10.09
ρ_V (kg/m^3)	1.167	1.575
ρ_L (kg/m^3)	1085.8	1040.1
F_{LV}	0.1622	0.3931
K_4	1.3	0.81
F_P (m^{-1})	207.1	207.1
μ_l (Ns/m^2)	0.0011	0.0003
V_W (kg/m^{2}s)	1.55	1.47
A (m^2)	46.43	23.95
Result		
L (kg/s)	356.7	356.7
D (m)	7.69	5.52

3.5.3 Commercial-scale PCC plant simulation

The PCC simulation was scaled up based on the pilot plant models to achieve 90 % of CO_2 capture from the commercial-scale SMR plant. The commercial-scale PCC simulation was operated under similar conditions as the pilot scale. The simulation was implemented using Aspen Plus®.

Table 3.15 presents the specifications for MEA-based and PZ-based PCC simulations at commercial scale. The simulations were performed in Aspen Plus® V11. The performance of standard PCC processes at commercial scale is summarized in Table 3.16 and the flowsheet of the standard PCC plant at commercial scale is given in Figure 3.13.

Table 3.15 Column dimensions for PCC plants at commercial scale.

	Parameters	Value
MEA-based PCC plant	Absorber column diameter (m)	8.9
	Absorber packing height (m)	10
	Absorber packing type	Mellapak M250X
	Stripper column diameter (m)	7.2
	Stripper packing height (m)	10
	Stripper packing type	Mellapak M350X
PZ-based PCC plant	Absorber column diameter (m)	7.8
	Absorber packing height (m)	10
	Absorber packing type	Mellapak 2X
	Stripper column diameter (m)	6.5
	Stripper packing height (m)	10
	Stripper packing type	Mellapak 2X

Table 3.16 The performance of commercial-scale PCC plants with standard configuration.

	Parameters	Value
MEA-based PCC plant	Solvent circulation rate (kg/s)	516
	Lean loading (mol_{CO_2}/mol_{MEA})	0.283
	Capture level (%)	90
	MEA concentration (wt.%)	30
	MEA make-up (kg/h)	64.71
	H_2O make-up (kg/s)	0.719
	Absorber pressure (bar)	1.1
	Stripper pressure (bar)	2.4
PZ-based PCC plant	Solvent circulation rate (kg/s)	250-475
	Lean loading (mol_{CO_2}/mol_{Alk})	0.287
	Capture level (%)	90
	PZ concentration (wt.%)	30-44
	PZ make-up (kg/h)	327.32-11757.6
	H_2O make-up (kg/s)	3.39-14.76
	Absorber pressure (bar)	1.1
	Stripper pressure (bar)	1.8

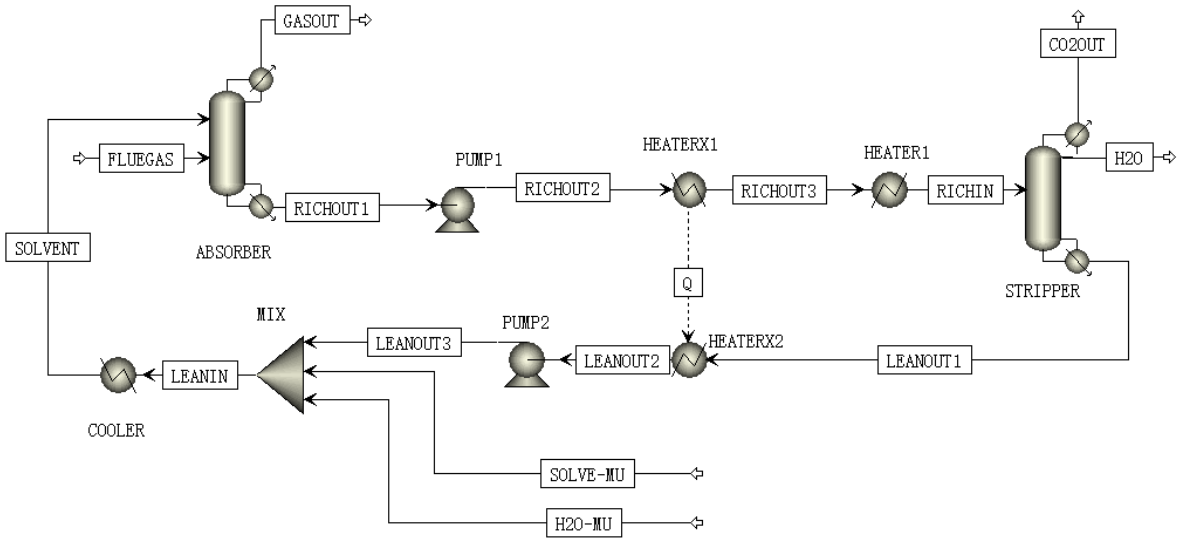

Figure 3.13 The process flowsheet for commercial-scale PCC plant in Aspen Plus® V11.

In the AFS configuration, additional heat exchangers and splitters are included in the system. The stripper is modelled with the Radfrac block, while the heat exchangers are represented by two heater blocks connected with a heat stream. The stripper is set up with 20 stages. Stage 1 to stage 19 represent the packed sections. The stage 20 (last stage) is the flash tank. To minimize solvent degradation, stage 20 is modelled with a lower solvent hold-up and shorter residence time compared to the other stages. The performance of PZ-based PCC process with AFS configuration at commercial-scale is detailed in Table 3.17. Figure 3.14 gives the model topology for the PCC process with AFS configuration in Aspen Plus® V11.

Table 3.17 The performance of PZ-based PCC plant with AFS configuration at commercial scale.

Parameters	Value
Solvent circulation rate (kg/s)	456-475
Lean loading (mol_{CO_2}/mol_{MEA})	0.287
Capture level (%)	90
PZ concentration (wt.%)	30-38
PZ make-up (kg/h)	273.65-1884.95
H_2O make-up (kg/s)	0.01-5.89
Absorber pressure (bar)	1.1
Stripper pressure (bar)	1.4

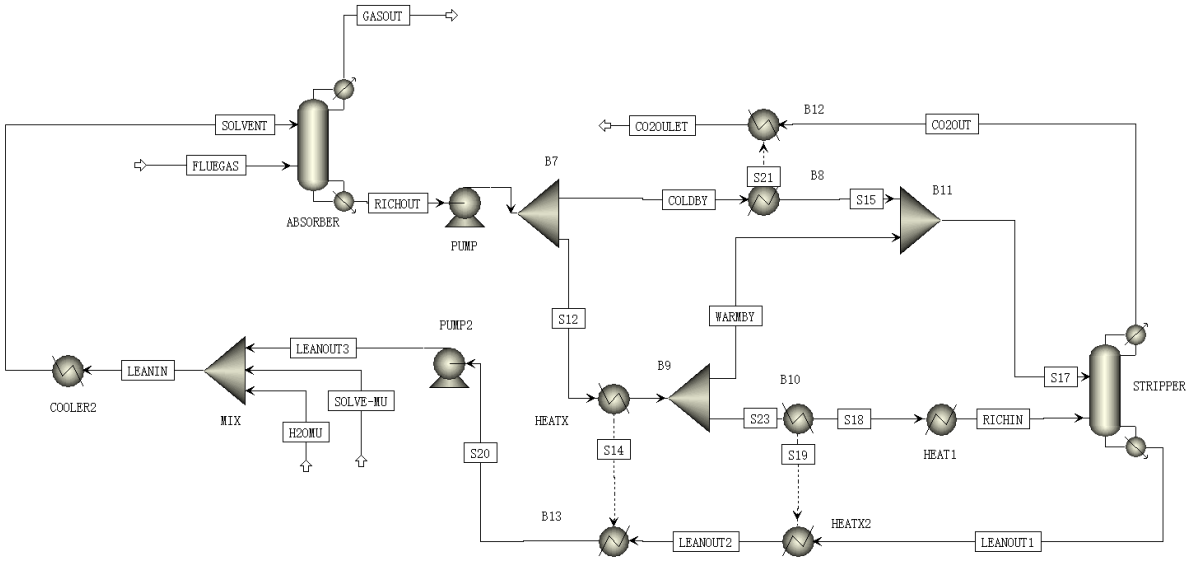

Figure 3.14 The flowsheet of the PCC process with AFS configuration in Aspen Plus® V11.

3.6 Energy performance assessment

The energy performance of PCC plant using PZ solvent with different concentration was evaluated at first. The 30 wt.% MEA was evaluated as a benchmark. The heat duty for reboiler,

cooling duty for condenser and electric duty for pumps was unified into the ratio representing the energy required in gigajoules per tonne of CO_2 (GJ/tonne$_{CO_2}$). This approach provides a consistent basis for comparing energy consumption and helps in identifying the best concentration choice.

Then, the effects of three parameters on energy performance of PCC process were studied, including CO_2 lean loading, stripper pressure and column height. The energy performance of PCC process with different solvents and configurations was compared.

3.6.1 Energy performance of different solvents

Table 3.18 outlines the contributions of heat duty, cooling duty and electric duty to the energy performance of different solvents, with values normalized per tonne of CO_2 captured. The heat duty arises from the reboiler, while the electric duty stems from the pumps. The 30 wt.% MEA exhibits the highest heat duty at 4.286 GJ/tonne$_{CO_2}$ and electric duty at 7.255 MJ/tonne$_{CO_2}$. Compared to the PCC processes using 30, 38 and 44 wt.% PZ, the PCC process using 30 wt.% MEA shows a higher energy demand for solvent regeneration. Furthermore, the energy required for CO_2 capture rises as PZ concentration increases. This is because when the lean loading of PZ is low, the amount of stripping steam required to achieve this low lean loading dominates the energy consumption. Therefore, the higher the PZ concentration, the stronger the absorption capacity of the solvent, the more difficult the desorption of CO_2, and the higher the heat duty of reboiler. Similar findings were reported by Gaspar et al. (2016).

Table 3.18 The energy performance of PCC process with different solvents.

Solvents	Heat duty (GJ/tonne$_{CO_2}$)	Cooling duty (GJ/tonne$_{CO_2}$)	Electric duty (GJ/tonne$_{CO_2}$)	Total duty (GJ/tonne$_{CO_2}$)
30 wt.% MEA	4.286	4.720	0.007	9.013
30 wt.% PZ	3.780	4.341	0.003	8.125
38 wt.% PZ	3.885	3.778	0.003	7.668
44 wt.% PZ	4.276	3.348	0.002	7.625

The cooling energy consumption includes the flue gas cooling duty (from GASCOOLE), the regenerated solvent cooling duty (from COOLER) and the condenser duty of the stripper (from STRIPPER). The highest cooling duty of 4.72 GJ/tonne$_{CO_2}$ was observed in the PCC process using 30 wt.% MEA. For the PCC process with PZ, increasing the PZ concentration from 30 to 44 wt.% led to reductions in cooling duty by 8 %, 19 %, and 29 %, respectively. The primary contributor to these changes is the regenerated solvent cooling duty (from COOLER). A decrease in solvent circulation rate reduces the cooling demand for the regenerated solvent, thereby lowering the overall cooling duty.

3.6.2 Parametric study

An energy performance study of different solvents showed that PZ has a lower energy consumption than MEA in the solvent regeneration process. In addition, as the PZ concentration decreases, the heat required for solvent regeneration further decreases. Considering that when capturing the same amount of CO_2, reducing the solvent concentration leads to an increase in the solvent circulation rate, which increases the operating cost. Therefore, a 30 wt.% PZ solvent was selected in the parametric study based on energy-economy trade-off.

In this section, the effects of three parameters on energy consumption and solvent circulation rate were studied, including CO_2 lean loading, stripper pressure and column height. The energy performance of standard PCC process with 30 wt.% MEA, the standard PCC process with 30 wt.% PZ, and the PCC process with 30 wt.% PZ and AFS configuration was investigated.

3.6.2.1 Effect of different CO_2 lean loading

The effect of varying CO_2 lean loadings on energy consumption and solvent circulation rate is presented in the Figures 3.15 and 3.16. The Figure 3.15 presents that the energy consumption of the standard PCC process using 30 wt.% MEA decreases as the CO_2 lean loading increases. This is because the increase in CO_2 loading reduces the loading gap between the lean and rich solvent. Therefore, as the lean loading increases, CO_2 is more easily separated from the rich solvent.

The energy consumption of standard PCC process with 30 wt.% PZ attained a minimum at the lean loading of around 0.2 $mol_{CO_2}/mol_{solvent}$. This is because when the lean loading is low, the amount of stripping steam required to achieve this low lean loading is dominant in the energy consumption. When the lean loading is high, the heating up of the solvent at these high solvent circulation rates is dominant in the energy consumption (Abu-Zahra et al., 2007).

The same trend can be found in the PCC process with 30 wt.% PZ and AFS configuration. In addition, the AFS configuration enhances energy efficiency, which attained a lowest energy consumption of 3.25 $GJ/tonne_{CO_2}$ at lean loading of 0.2 $mol_{CO_2}/mol_{solvent}$.

The effect of different lean loads on solvent circulation rate is presented in Figure 3.16. The increase in CO_2 lean loading leads to an increase in the solvent circulation rate. This is because the increase in lean loading reduces the absorption capacity of the solvent. Thus, the required solvent circulation rate increases to capture the same amount of CO_2. The selection of CO_2 lean loading requires a trade-off between energy and economy, as an increase in solvent circulation rate may incur additional operating costs.

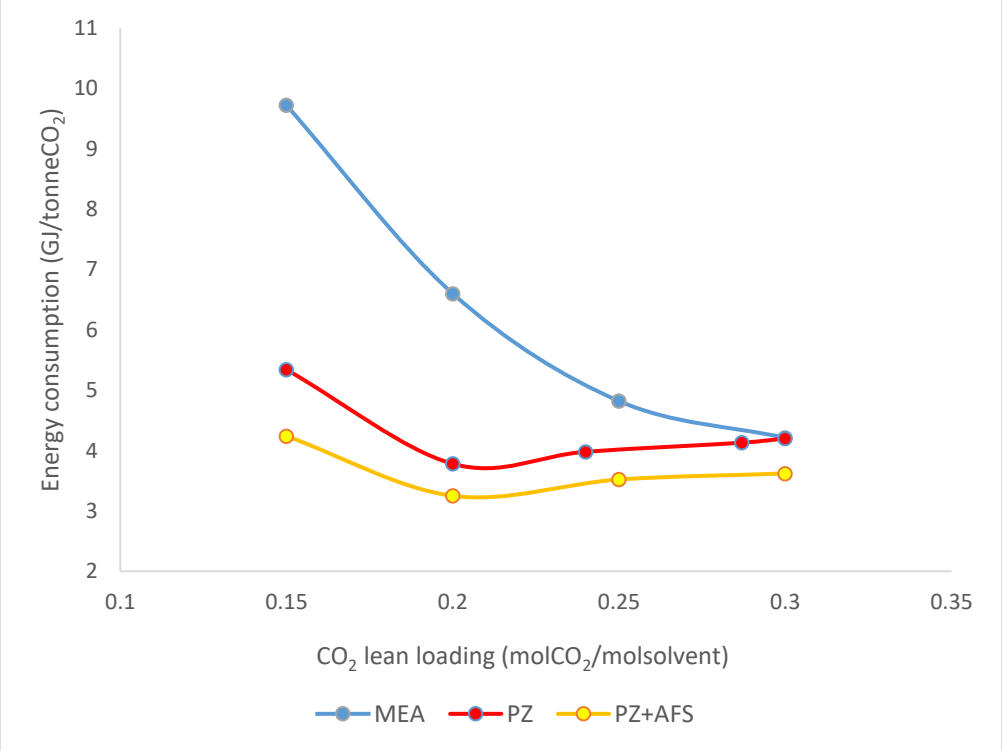

Figure 3.15 Effect of varying CO_2 lean loads on energy consumption of PCC process.

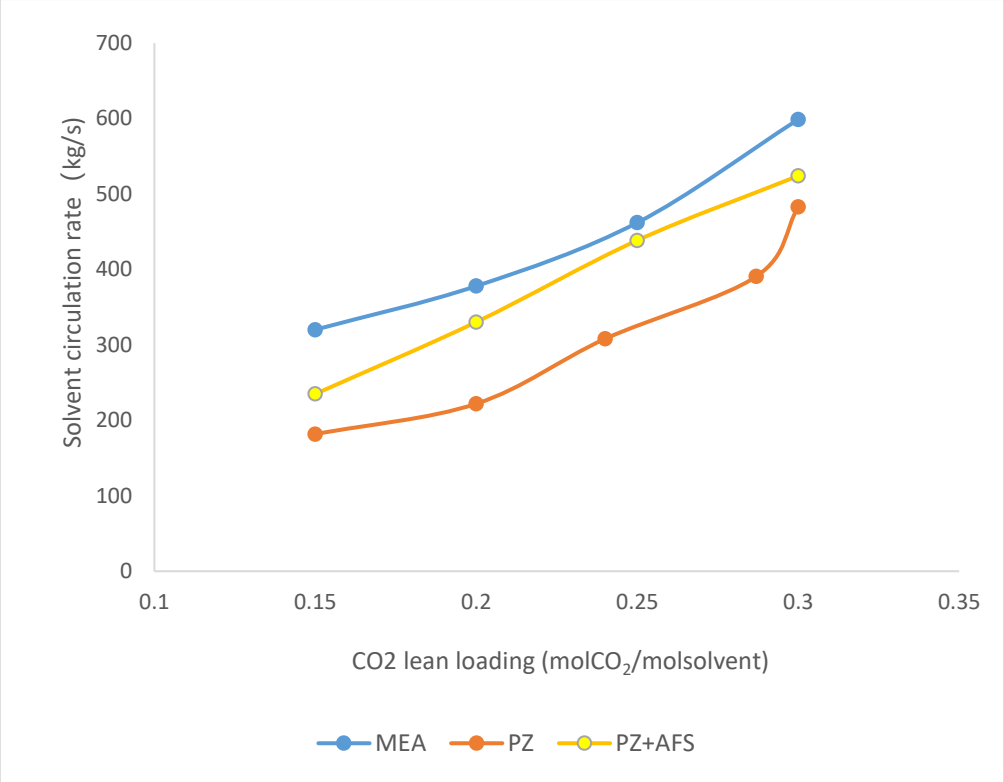

Figure 3.16 Effect of varying lean loads on solvent circulation rate of PCC process.

3.6.2.2 Effect of different stripper pressure

Figures 3.17 and 3.18 show the impact of different stripper pressure on energy consumption and solvent circulation rate. In Figure 3.17, it is shown that as the operating pressure of the stripper increases, the energy consumption reduces. This is because the increase in stripper pressure leads to an increase in the temperature inside the stripper. Therefore, the rich solvent temperature at the stripper outlet also increases. Higher rich solvent temperature increases the amount of heat that can be used for exchange, which leads to a reduction in the energy consumption for solvent regeneration. Since the reason for the reduction in energy consumption due to an increase in stripper pressure is independent of the solvent absorption capacity, the solvent circulation rate remains unchanged, which can be seen in Figure 3.18.

Nonetheless, it is reasonable to anticipate that increased amine degradation rates and heightened corrosion issues may arise under these higher pressure conditions.

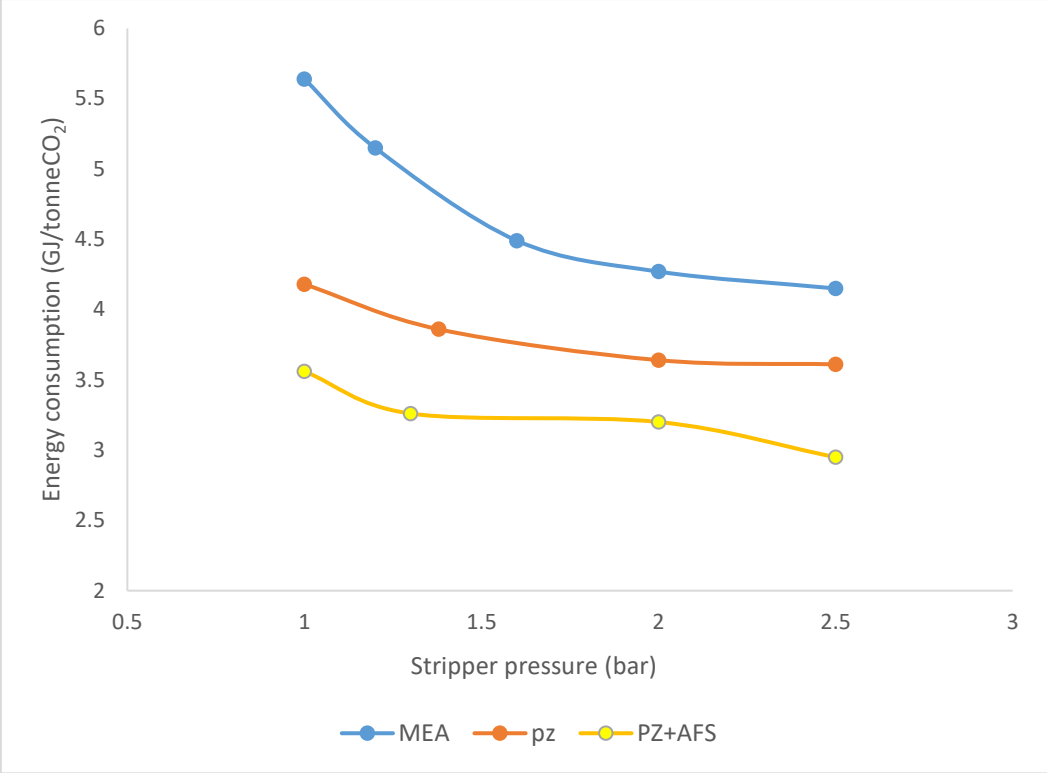

Figure 3.17 Effect of different stripper pressure on energy consumption of PCC process.

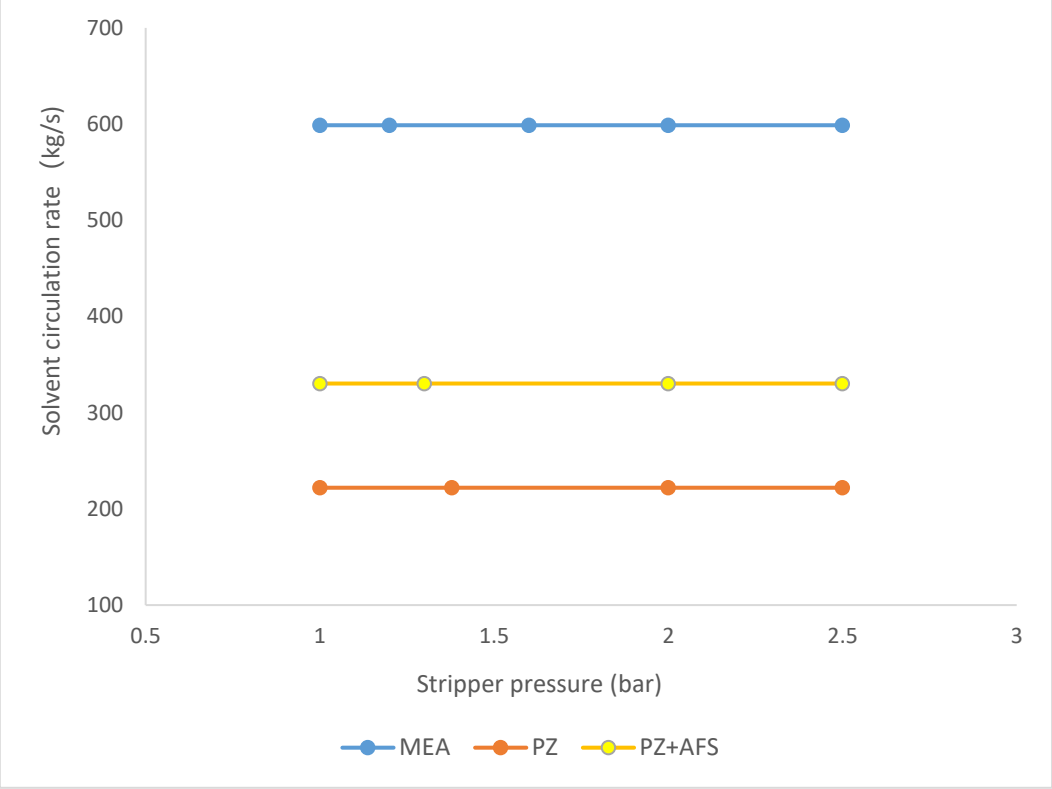

Figure 3.18 Effect of different stripper pressure on solvent circulation rate of PCC process.

3.6.2.3 Effect of varying column height

The effect of varying column height on energy consumption and solvent circulation rate are shown in the Figures 3.19 and 3.20. The results showed that the increase in column height is beneficial to reducing energy consumption and solvent circulation rate. This is because the increase in column height increases the contact time between the solvent and the flue gas, which enhances the absorption of CO_2, thereby reducing the solvent circulation rate. When the solvent absorption capacity remains unchanged, the reduction in solvent circulation rate leads to a reduction in energy consumption. Although the increase in column height contributes to the reduction of both energy consumption and operating costs, the potential increase in capital costs may be more concerning.

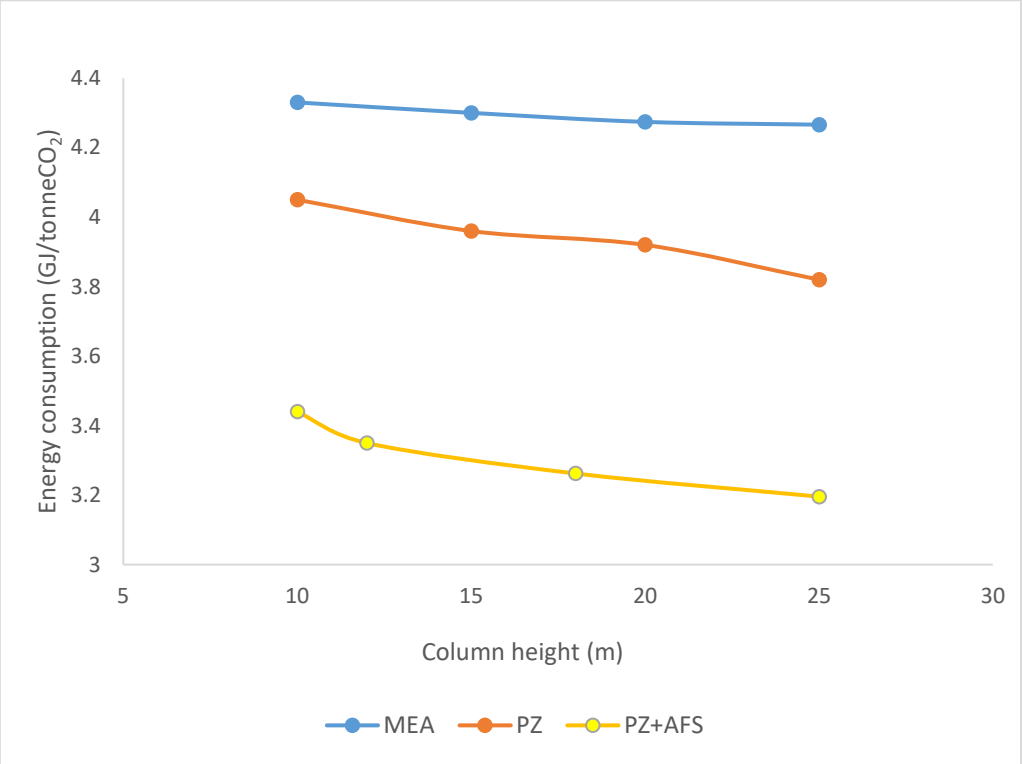

Figure 3.19 Effect of varying column height on energy consumption of PCC process.

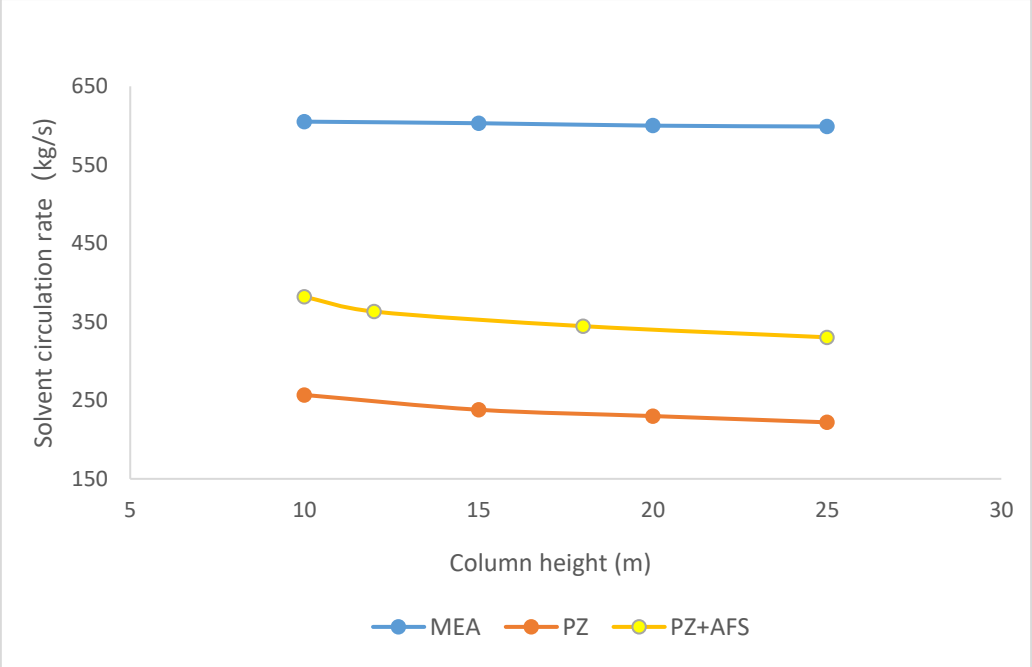

Figure 3.20 Effect of varying column height on solvent circulation rate of PCC process.

3.7 Process optimisation with respect to energy consumption

3.7.1 Definition of the optimum process

The energy consumption in the PCC process plays a critical role, as it significantly impacts the overall thermal efficiency of the BHP plant. The optimum process is identified as the one with the lowest energy requirements across the three evaluated parameters: CO_2 lean loading, stripper pressure and column height.

The capture level of 90 % CO_2 removal was chosen for the optimization, which is widely used assumption based on the trade-off between operating cost and capture level. The 30 wt.% PZ was selected according to the results in section 3.6.1. The standard PCC process using 30 wt.% MEA was selected as a baseline case. Two optimum processes were defined as case (a): the standard PCC process using 30 wt.% PZ and case (b): the PCC process using 30 wt.% PZ and AFS configuration.

The optimum lean loading was determined to be 0.21 and 0.20 $mol_{CO_2}/mol_{solvent}$ for case (a) and case (b), respectively. Higher stripper pressures consistently reduced energy consumption. However, considering the ammonia degradation and corrosion issues, the

optimum stripper pressure was 2.5 bar, which was the maximum considered in this study. Increasing the column height resulted in lower energy consumption but will greatly increase capital costs. Therefore, a column height of 25 m will be used in the process optimization based on energy and economic trade-off. As discussed earlier, the key specifications of the two optimum processes are shown in Table 3.19.

Table 3.19 Key specifications of the optimum processes.

	30 wt.% PZ	30 wt.% PZ + AFS configuration
Capture level (%)	90	90
Solvent concentration (wt.%)	30	30
CO_2 lean loading ($mol_{CO_2}/mol_{solvent}$)	0.21	0.20
Stripper pressure (bar)	2.5	2.5
Column height (m)	25	25

3.7.2 The optimum processes

The defined processes in Table 3.19 were simulated with Aspen Plus® V11. The results of optimum process are shown in Table 3.20. The simulation results of the baseline case are also presented in Table 3.20 for a clear comparison with the optimum process results.

Table 3.20 Optimum process results.

	Baseline case	Case (a)	Case (b)
CO_2 lean loading ($mol_{CO_2}/mol_{solvent}$)	0.30	0.21	0.20
CO_2 rich loading ($mol_{CO_2}/mol_{solvent}$)	0.47	0.52	0.52
Column height (m)	20	25	25
Stripper outlet temperature (°C)	123.5	122.9	121.9
Solvent circulation rate (kg/s)	599.9	382.0	330.3
Energy consumption ($GJ/tonne_{CO_2}$)	4.27	3.44	3.19

The optimal processes identified demonstrated lower energy consumption compared to the baseline, with reductions of 19 % for the standard PCC process using 30 wt.% PZ and 25 % for the PCC process with 30 wt.% PZ and AFS configuration. These reductions could lead to significant decreases in operating costs. However, it is worth noting that capital costs may increase as process operating conditions change and column height increase. While operating costs may also increase due to heightened corrosion occurring at high operating pressures (Abu-Zahra et al., 2007).

3.8 Conclusion

This chapter presented the development of steady-state models for the solvent-based PCC process in Aspen Plus® V11. These models were validated with experimental data from a pilot plant. The validation results present good agreement, with model predictions falling within ±10 % of the measured values. The validated pilot-scale PCC models were then scaled up to achieve 90 % CO_2 capture from the commercial-scale SMR plant. The energy performance of the commercial-scale PCC process with PZ and AFS configuration was evaluated and compared with the commercial-scale PCC process using 30 wt.% MEA and standard configuration (baseline). The key findings of this chapter are as follows:

- The energy performance evaluation of different solvents showed that PZ has a clear advantage in energy performance compared with MEA. The regeneration energy of the standard PCC process decreases from 4.29 GJ/tonne$_{CO_2}$ with 30 wt.% MEA to 3.78 GJ/tonne$_{CO_2}$ with 30 wt.% PZ.
- The parametric study showed that energy consumption of PZ regeneration is lower than that of MEA. In addition, the energy consumption of standard PCC process can be further decreased by using AFS configuration.
- The CO_2 lean loading have a major effect on the energy performance. Therefore, it is a primary subject in the optimisation of solvent-based PCC process. The energy consumption of the standard PCC process decreases as the CO_2 lean loading increases. The minimum energy consumption is attained by the standard PCC process using 30 wt.% PZ at the lean loading around 0.2 mol$_{CO_2}$/mol$_{solvent}$.

- Increasing stripper pressure and column height are both beneficial to reducing energy consumption. However, higher stripper pressure and column height may result in additional capital and operating costs.
- The increase of CO_2 lean loading leads to the increase of solvent circulation rate. The increase of stripper pressure has little effect on the solvent circulation rate. The increase in column height is beneficial to reducing the solvent circulation rate. The effects of these three parameters on the solvent circulation rate show three different trends. This is because the factors that affect energy consumption are different.
- The results of process optimisation indicate that the lowest energy consumption of 3.19 GJ/tonne$_{CO_2}$ is achieved by the optimal process with 30 wt.% PZ and AFS configuration, which is a significant reduction compared to 4.17 GJ/tonne$_{CO_2}$ in the baseline case.

Chapter 4. Technical and economic performance assessment of BHP using new configuration through modelling and simulation

4.1 Overview

This chapter investigates the technical and economic performance of the commercial-scale BHP with a new configuration. It includes model development, model validation, model integration, energy performance assessment and economic performance assessment, conducted using Aspen Plus® V11. The standard configuration of the BHP process with 30 wt.% MEA was investigated as a benchmark. The energy consumptions and costs of the standard BHP process using PZ is compared with energy and cost-saving blue hydrogen production (ECSB) process using PZ. Section 4.2 outlines the process configurations. Section 4.3 focusses on model development of the standard SMR process in Aspen Plus® V11. Model validation at the commercial scale is addressed in Section 4.4. Section 4.5 introduces the process integration and ECSB process design. Section 4.6 discusses the methodology of technical and economic performance evaluation. The results and discussion are given in Section 4.7. The chapter conclusions are summarized in Section 4.8.

4.2 Process description

4.2.1 Standard SMR process

To evaluate the energy and cost performance of a hydrogen plant with and without carbon capture process. A standard SMR process without any carbon capture system is selected as reference process for comparing the different carbon capture configurations.

The Figure 4.1 illustrates the standard SMR process. Natural gas is initially pre-heated to 135 °C by flue gas and then pressurized to over 30 bar. Then, natural gas is split into fuel and

feedstock. The fuel is burned in the steam reformer furnace, supplying heat for the entire system. The feedstock is further heated to 380 °C in the pre-heater coil located in the convective section of the main reformer (IEAGHG, 2017). After that, it is mixed with recycled hydrogen from a PSA unit in a desulfurization system, where sulphur components are removed to protect downstream catalysts from poisoning.

The desulfurized feedstock is blended with high pressure steam to maintain a fixed steam to carbon (S/C) ratio of approximately 2.6-3.0. Then, this mixture is directed to the pre-reformer, where heavier hydrocarbons (ethane, propane, etc.) are converted to CH_4 and other co-products (i.e. CO_2, H_2 and CO). The residual heavier hydrocarbons in the product gas are required to be less than 500 ppmv. Pre-reformer is a fixed-bed reactor with a Ni-based catalyst, designed to minimize the coking and sintering in the following steps. Also, it takes over part of the reforming duty from the main reformer, which increases the process efficiency.

The product gas exiting the pre-reformer is further heated to the required temperature (around 900-950 °C) and then sent to the main reformer. In the radiant section of the main reformer, the product gas from the pre-reformer enters the catalyst-filled tubes from the top, where un-shifted syngas (containing H_2, CO, CO_2, CH_4 and H_2O) is produced under high-temperature and high-pressure conditions. The residual methane typically between 3.3 % and 4.0 % on dry molar basis. Additionally, the total amount of process steam must be more than the stoichiometric requirement to avoid coke formation on the catalyst.

Hot flue gas (800-1000 °C) exiting the furnace is discharged into the convective section located on top of the furnace. The main reformer is designed to recover as much heat as possible from the flue gas in this section. As steam reforming reactions are highly endothermic, additional heat must be provided to ensure the required conversion, primarily through the combustion of natural gas fuel and the PSA tail gas. Flue gas is also used to pre-heat the combustion air.

The syngas (un-shifted) exiting the main reformer tubes is directed to the waste heat boiler where it is cooled to approximately 320 °C. The heat recovered during this process is used to produce high pressure steam. The cooled syngas (un-shifted) is sent to the WGS reactor,

where the excess steam converts most of the CO to CO_2 and H_2 on a catalyst bed. In this chapter, the high temperature WGS reactor was chosen for its reliable performances and ease of operation during start-up and shutdown. Residual CO from the WGS reactor is typically between 2.5 % and 3.5 % on a dry molar basis.

The shifted syngas is further cooled in the air cooler to separate condensed water from the shifted syngas before being fed into a hydrogen separation unit. The PSA unit is usually used to purify the shifted syngas. This involves a cyclic adsorption process comprising of multiple adsorption beds to produce the H_2 product with a purity exceeding 99.99 %. The PSA unit typically recovers 85 % to 90 % of the hydrogen from the syngas (IEAGHG, 2017). The regeneration of the PSA adsorbent bed involves desorbing impurities and residual hydrogen through depressurisation, forming PSA tail gas. This tail gas is used as fuel in the burner.

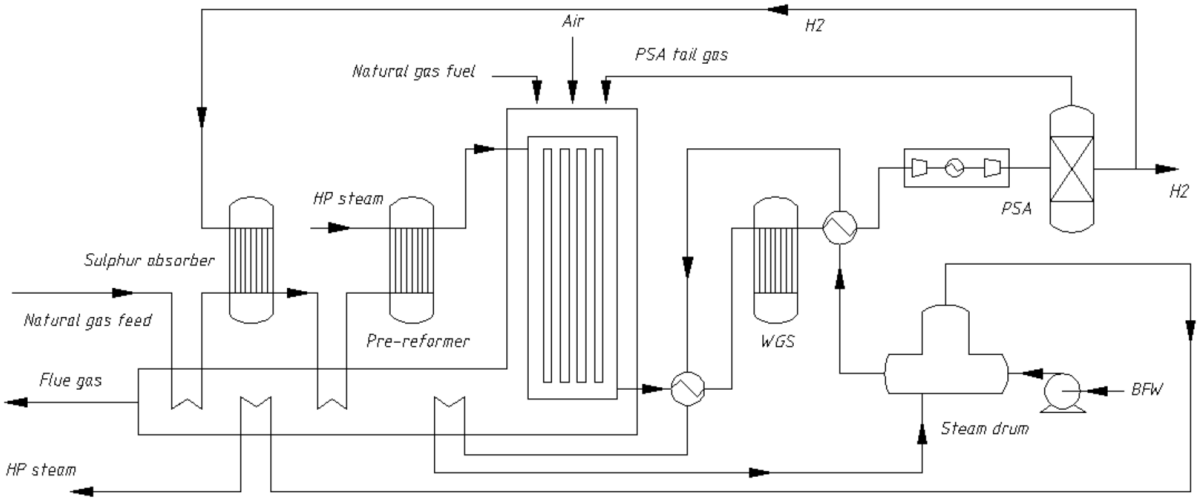

Figure 4.1 Diagram of standard SMR process.

4.2.2 Standard BHP process

Figure 4.2 illustrates the standard BHP process, which integrates an SMR process and a PCC process. The standard SMR process is adopted, which is described in the previous section. The flue gas from the SMR plant is cooled to an appropriate temperature and introduced into an absorber. In the absorber, the CO_2-lean solvent captures CO_2 from flue gas through counter-current contact, yielding the CO_2-rich solvent. The scrubbed gas is then released from top of the absorber. The CO_2-rich solvent is preheated by the regenerated CO_2-lean solvent from the stripper before being pumped into the stripper. In the stripper, the CO_2 is

separated from rich solvent at temperatures ranging from 110-140 °C and is then released from the top of the stripper.

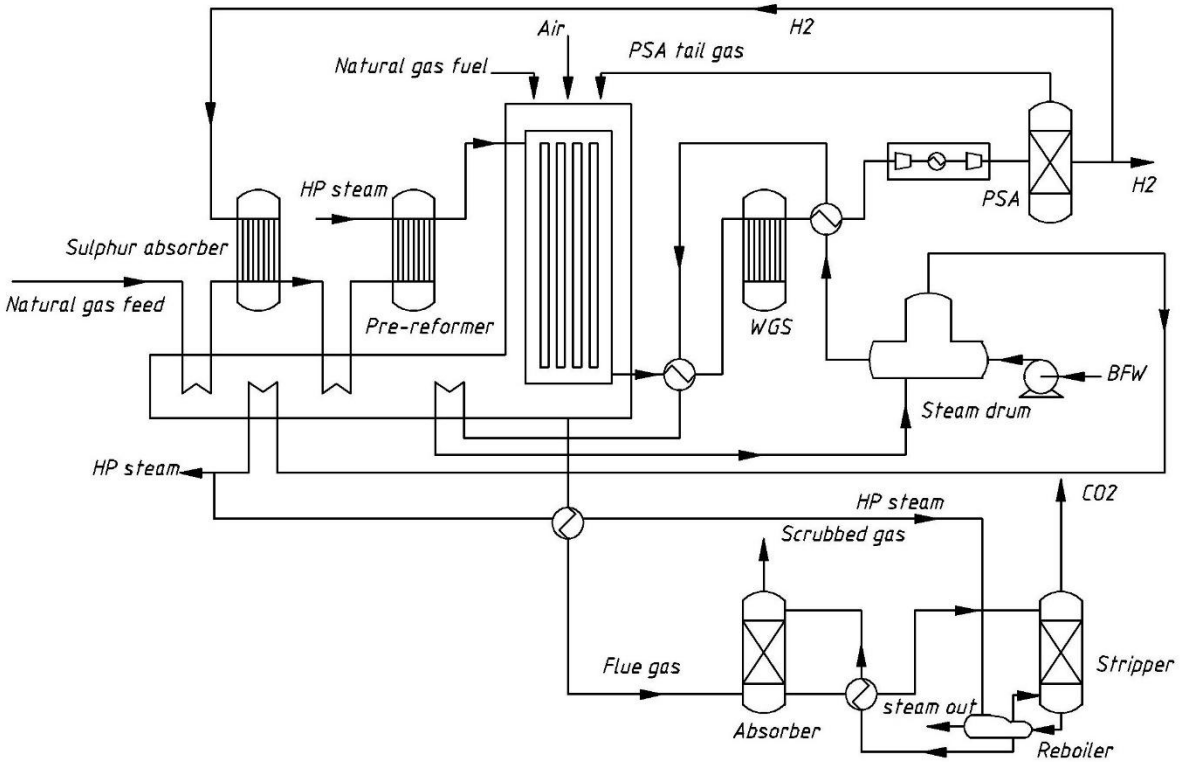

Figure 4.2 Diagram of standard BHP process.

4.2.3 BHP process with energy and cost-saving configuration

An energy and cost-saving configuration is proposed to decrease the cost and energy consumption of the BHP process. This ECSB process is characterized by: (I) the application of PZ as a solvent in PCC process, known for its high CO_2 absorption efficiency; (II) an optimized heat exchange system that recovers the waste exergy from flue gas; and (III) the implementation of AFS which simplifies the stripper design and reduces capital cost.

Figure 4.3 shows the design of energy and cost-saving configuration. The standard SMR process is adopted while the wasted exergy in the flue gas is recovered to support the solvent regeneration process. Furthermore, the AFS was used in the PCC process. The rich solvent exiting the absorber is divided into two streams: a cold-rich bypass and a warm-rich bypass. The cold-rich bypass is heated by hot vapor from the top of the stripper and then combined with a portion of the warm-rich bypass before being fed to the top of the stripper. The

remaining rich solvent is preheated using the regenerated lean solvent, flue gas and a steam heater before being directed to a flash tank located at the bottom of the stripper. In this setup, the flash tank and steam heater perform the functions of the reboiler in the standard stripper configuration.

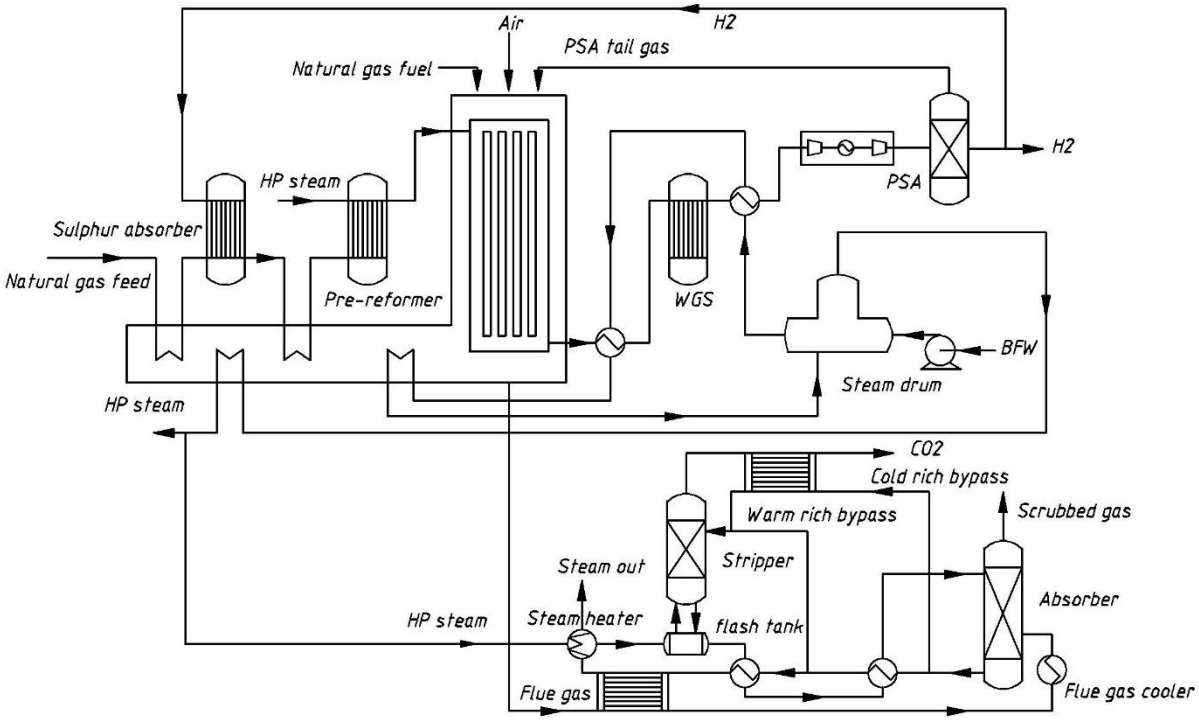

Figure 4.3 Diagram of the ECSB process.

4.3 Model development

4.3.1 SMR model development and simulation procedure

A steady-state SMR process was modelled and simulated in Aspen Plus® V11. Since the steam reforming reaction and WGS reaction are fast enough in the presence of catalysts and the production of hydrogen is very close to the equilibrium value, the thermodynamic approach is used for modelling (Lu and Xie, 2016).

The Peng-Robinson (PR) equation of state was selected for simulation as its suitability for non-polar compounds such as CO_2, CH_4, H_2 and N_2. This equation of state was first proposed by Peng and Robinson (1976) and widely used in hydrocarbon processes such as petrochemical processes, refinery, and gas processing.

$$P = \frac{RT}{V-b} - \frac{a(T)}{V(V+b)+b(V-b)} \quad (4.1)$$

Where:

P: pressure

R: universal gas constant

T: temperature

V: molar volume

a: attraction parameter related to intermolecular forces

b: repulsion parameter related to molecular size

The flowsheet of the SMR plant in Aspen Plus® V11 is shown in Figure 4.4. The assumptions for the model development include:

- Steady-state equilibrium model.
- The H_2 separation rate of PSA is assumed to be 87 %, as PSA units generally recover between 85 % and 90 % of hydrogen from syngas (IEAGHG, 2017).
- All sulphur components are removed during the desulfurization process.
- Complete combustion in the furnace, thus no NO_x and SO_2.

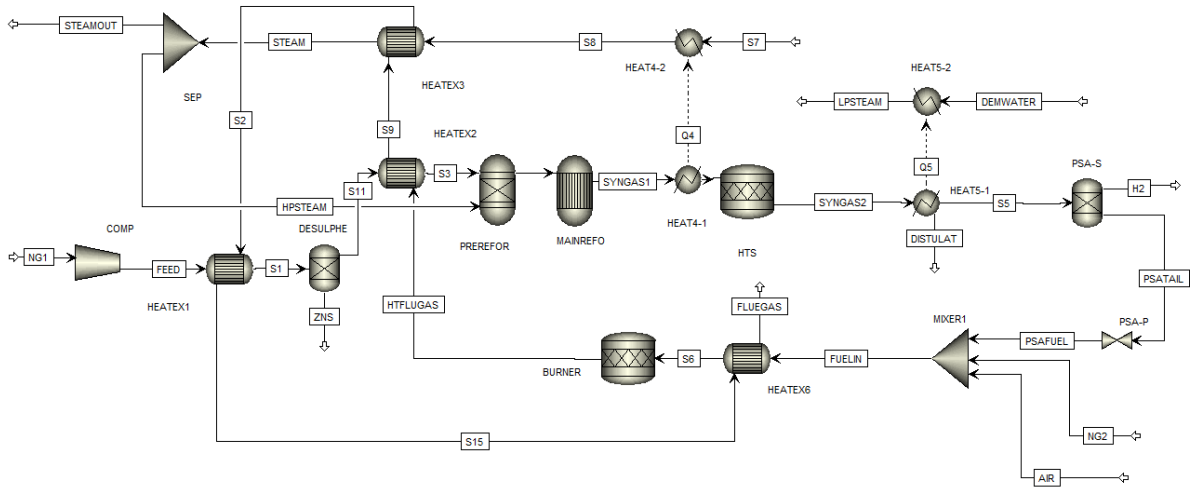

Figure 4.4 The flowsheet of the commercial scale SMR plant in Aspen Plus® V11.

After being pressurized and preheated, natural gas and high-pressure steam are fed into the main reformer, with a S/C ratio maintained at approximately 2.7. Temperature variations in the flue gas and the main reformer inlet flow are modelled using two heat exchanger blocks. The main reformer is modelled as a Gibbs reactor, where the main reactions (4.2) and (4.3) are equilibrium-limited and highly endothermic.

$$CH_4 + H_2O \leftrightarrow CO + 3H_2, \Delta H_{298}^0 = 206\ kJ/mol \quad (4.2)$$

$$CH_4 + 2H_2O \leftrightarrow CO_2 + 4H_2, \Delta H_{298}^0 = 164.9\ kJ/mol \quad (4.3)$$

After being cooled to 330 °C, the syngas is directed to the WGS reactor. The stoichiometric reactor is selected to model the WGS reactor for adjusting the CH_4 conversion rate. The reaction involved is:

$$CO + H_2O \leftrightarrow CO_2 + H_2, \Delta H_{298}^0 = -41.1\ kJ/mol \quad (4.4)$$

In the PSA unit, pure hydrogen is separated from the shifted syngas. The PSA tail gas is combusted with natural gas in the furnace to supply heat for the system. The furnace is modelled as a Gibbs reactor.

4.3.2 Main specifications of the simulation

The commercial-scale SMR plant is simulated to generate 200 tonne$_{H_2}$/day. The main reformer is designed to operate at 900 °C and 30 bar. The operating conditions of main blocks in the simulation are given in Table 4.1. The selection of these values refers to the design of Boyano et al. (2011), Soltani et al. (2014), (IEAGHG, 2017).

Table 4.1 The operating conditions of main blocks.

Block	Main specifications	Value
Desulfurization	Temperature (°C)	377
	Pressure (bar)	30
Pre-reformer	Temperature (°C)	660
	Pressure (bar)	29
Main reformer	Temperature (°C)	906
	Pressure (bar)	28.5
WGS	Temperature (°C)	413
	Pressure (bar)	27.8
PSA	Temperature (°C)	40
	Pressure (bar)	25
Furnace	Temperature (°C)	950
	Pressure (bar)	1.034

4.4 Model validation of commercial-scale SMR process

The commercial-scale SMR process was verified using data obtained from the IEA report IEAGHG (2017), which presents six cases of a commercial-scale SMR plants producing 100000 $m^3_{H_2}$/day with and without CCS. Among them, the Base Case (SMR process without carbon capture) was chosen for the validation as it provides a detailed description of the key parameters in a standard SMR plant. In this case, the natural gas consumption is approximately 27.1 tonnes/hour, with 86 % of the natural gas used as feedstock and the remainder as fuel. The process requires around 86 tonnes of high-pressure steam per hour. The whole process includes desulfurization, pre-reformer, main reformer, WGS and PSA. It produces about 200 tonnes/day of H_2 and emits about 2000 tonnes/day of CO_2. Detailed information about the Base Case is given in Table 4.2, 4.3 and 4.4.

Table 4.2 Key operating parameters and material balance of Base Case (part I) (IEAGHG, 2017).

Description	Natural gas	Natural gas feedstock to hydrogen plant	Natural gas fuel to burners	Purified feedstock to pre-reformer	WGS reactor inlet
Temperature (°C)	9	128	121	500	320
Pressure (MPa)	7.00	3.71	0.50	3.39	2.80
Molar flow rate (kmol/h)	1696.6	1455.8	240.4	5514.0	8370.3
Mass flow rate (kg/h)	30563	26231	4332	98874	101667
Moler fraction of each composition					
CO_2	0.0200	0.0200	0.0200	0.0053	0.0492
CO	0.0000	0.0000	0.0000	0.0000	0.1156
Hydrogen	0.0000	0.0000	0.0000	0.0053	0.5171
Nitrogen	0.0089	0.0089	0.0089	0.0023	0.0015
Oxygen	0.0000	0.0000	0.0000	0.0000	0.0000
Methane	0.8900	0.8900	0.8900	0.2350	0.0238
Ethane	0.0700	0.0700	0.0700	0.0185	0.0000
Heavier hydrocarbons	0.0111	0.0111	0.0111	0.0029	0.0000
H_2O	0.0000	0.0000	0.0000	0.7307	0.2927

Table 4.3 Key operating parameters and material balance of Base Case (part II) (IEAGHG, 2017).

Description	WGS reactor outlet	PSA inlet	PSA tail gas	Flue gas	High pressure steam export
Temperature (°C)	320	35	28	136	395
Pressure (MPa)	2.80	2.58	0.13	0.02	4.23
Molar flow rate (kmol/h)	8370.3	6596.9	2106.3	8659.4	2556.0
Mass flow rate (kg/h)	101667	69711	60658	257698	46053
Moler fraction of each composition					
CO_2	0.0492	0.1627	0.5095	0.2123	0.0000
CO	0.1156	0.0464	0.1454	0.0000	0.0000
Hydrogen	0.5171	0.7563	0.2369	0.0000	0.0000
Nitrogen	0.0015	0.0020	0.0062	0.6083	0.0000
Oxygen	0.0000	0.0000	0.0000	0.0102	0.0000
Methane	0.0238	0.0302	0.0945	0.0000	0.0000
Ethane	0.0700	0.0700	0.0700	0.0185	0.0000
Heavier hydrocarbons	0.0111	0.0111	0.0111	0.0029	0.0000
H_2O	0.0000	0.0000	0.0000	0.7307	0.2927

Table 4.4 Key operating parameters and material balance of Base Case (part III) (IEAGHG, 2017).

Description	Demi water	Hydrogen products	H_2 recycle	High pressure Steam to process	Low pressure steam to deaerator
Temperature (°C)	15	40	40	400	177
Pressure (MPa)	0.60	2.50	2.51	4.29	0.44
Molar flow rate (kmol/h)	5095.7	4461.5	29.1	5290.1	30.0
Mass flow rate (kg/h)	91800	8994	59	95301	540
Moler fraction of each composition					
CO_2	0.0000	0.0000	0.0000	0.0000	0.0000
CO	0.0000	0.0000	0.0000	0.0000	0.0000
Hydrogen	0.0000	0.9999+	0.9999+	0.0000	0.0000
Nitrogen	0.0000	0.0000	0.0000	0.0000	0.0000
Methane	0.0000	0.0000	0.0000	0.0000	0.0000
Ethane	0.0700	0.0700	0.0000	0.0000	0.0000
Heavier hydrocarbons	0.0111	0.0111	0.0000	0.0000	0.0000
H_2O	0.0000	0.0000	0.0000	1.0000	1.0000

Table 4.5 presents the steady-state model validation results, including methane conversion rate, hydrogen production, flue gas mass flow rate, syngas molar flow rate and CO_2 molar concentration in flue gas. The relative deviations between model predictions and IEA data are mostly within 5 %, demonstrating that the steady-state model accurately predicts the performance of SMR plant.

Table 4.5 Comparison of IEA data (IEAGHG, 2017) and model predictions for SMR plant performance.

Parameter	IEA data	Model prediction	Relative deviation (%)
CH_4 conversion rate (%)	84.6	86.5	2.25
H_2 production (kg/h)	8994	8914	0.89
Flue gas mass flow rate (kg/h)	257698	259584	0.73
CO_2 molar concentration in flue gas (%)	21.23	20.67	2.64
Syngas molar flow rate (kmol/h)	8370.3	8396.2	0.31
Molar flow rate of PSA inlet stream (kmol/h)	6596.9	6615.4	0.28
Molar flow rate of PSA tail gas (kmol/h)	2106.3	2193.7	4.15
Molar fraction of CO_2 in main reformer	0.0492	0.0495	0.61
Molar fraction of CO in main reformer	0.1156	0.1113	3.72
Molar fraction of H_2 in main reformer	0.5171	0.5172	0.02
Molar fraction of CH_4 in main reformer	0.0238	0.0245	2.94
Molar fraction of N_2 in main reformer	0.0015	0.0016	6.67

4.5 Process integration and ECSB design

The model development of the standard PCC process and the PPC process with AFS configuration is described in this section. The integration of standard SMR process with PCC process was carried out using Aspen Plus® V11. The flowsheet for the standard BHP process

is presented in Figure 4.5. In the standard configuration, the flue gas was typically cooled to 40 °C before entering the PCC process to minimize solvent losses due to evaporation at higher temperatures. The flue gas cooling system was modelled as a heater block (**GASCOOLE**).

To minimize the energy penalty associated with solvent regeneration in the PCC process, an optimized heat exchange system was developed. The system recovers wasted exergy from the flue gas stream in the SMR process and utilizes it to heat the rich solvent in the PCC process through a heat exchanger. This configuration was simulated by two heater blocks (**HEAT9-1 and HEAT9-2**) connected by a heat stream (**QEX**). The AFS configuration was chosen to lower the capital cost of the stripper as it eliminates the need for a condenser and a reboiler. The flowsheet of ECSB process developed in Aspen Plus® V11 is shown in Figure 4.6.

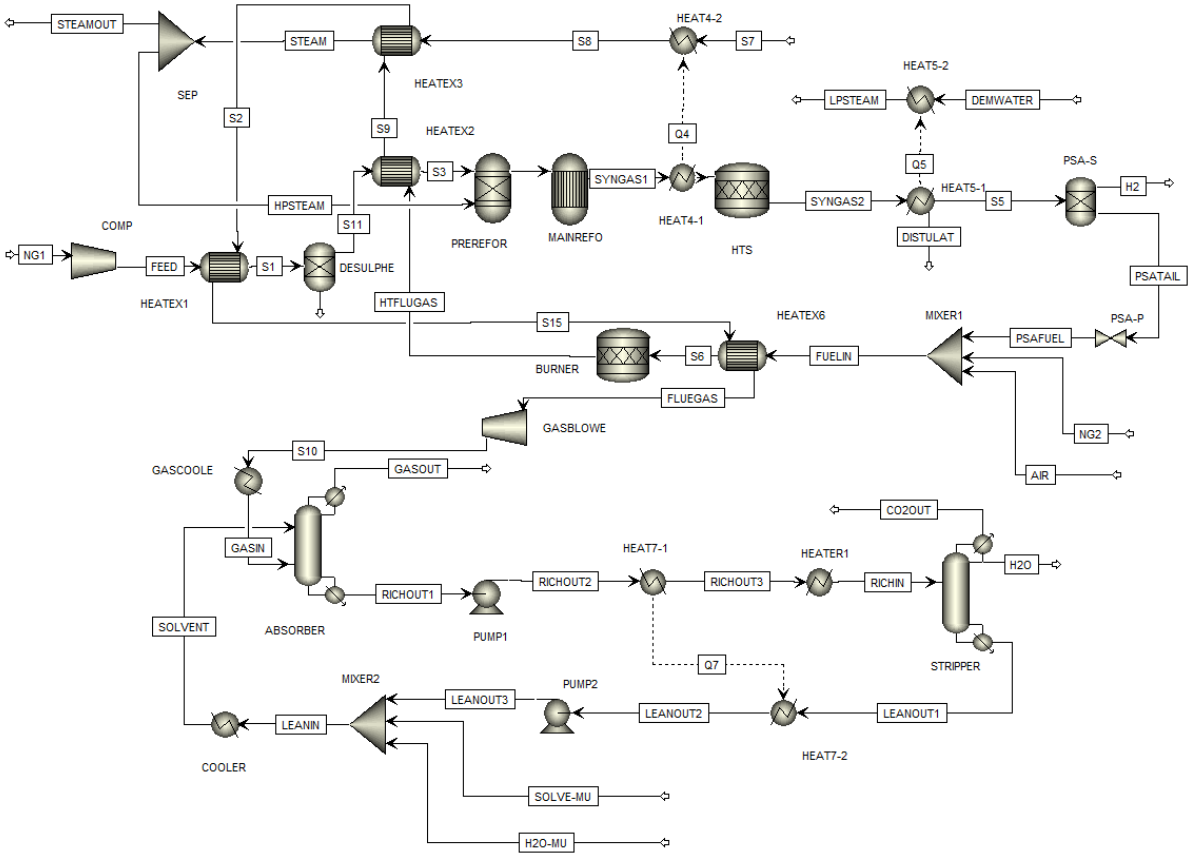

Figure 4.5 The flowsheet of standard BHP in Aspen Plus® V11.

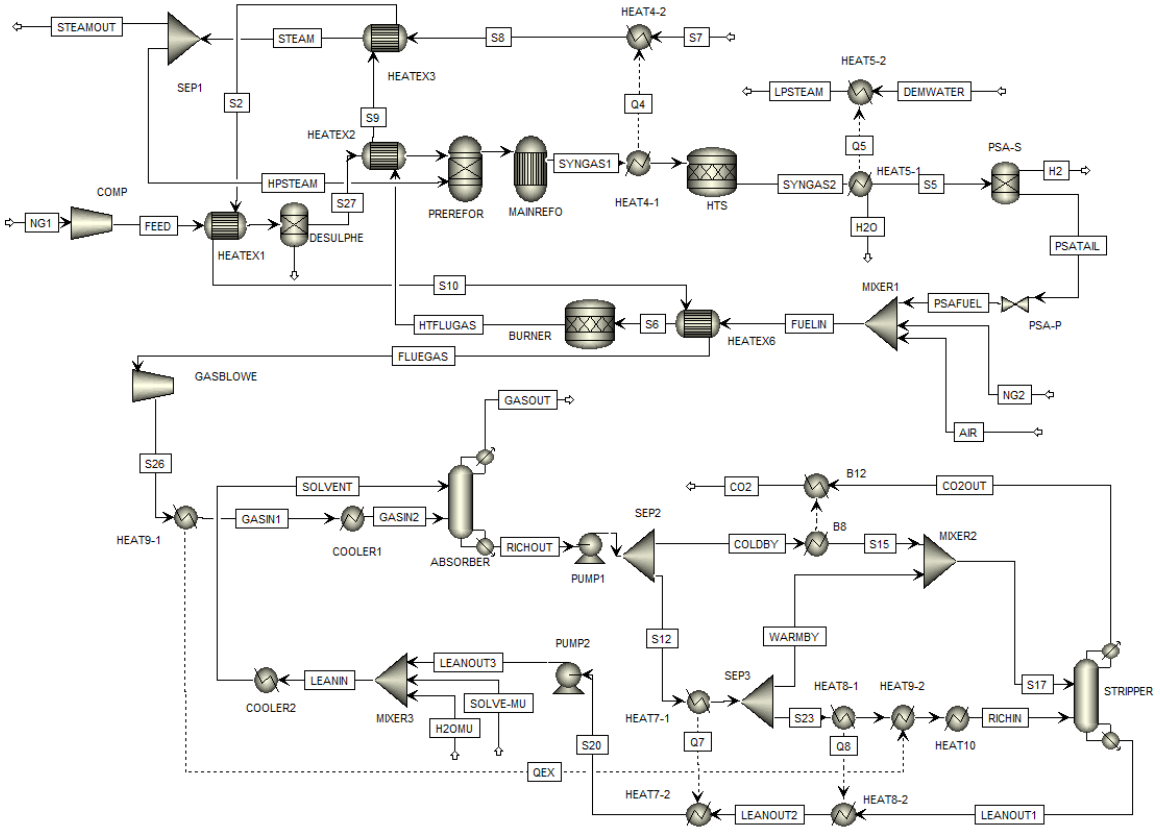

Figure 4.6 The flowsheet of ECSB in Aspen Plus® V11.

4.6 Technical and economic evaluation

4.6.1 Energy performance evaluation

The energy performance of commercial-scale BHP process with different solvents and configurations was evaluated. The SMR process without carbon capture served as the baseline for comparison. The duty of heat for reboiler, cooling for condenser and electricity for pumps was unified as the ratio in GJ/tonne$_{CO_2}$. The energy consumption of different units in BHP process was converted to equivalent work (MW). The rise in overall energy consumption was defined as the energy penalty, calculated by Eq. (4.5):

$$Energy\ penalty = \left(\frac{Energy\ demand\ with\ PCC - Energy\ demand\ without\ PCC}{Energy\ demand\ without\ PCC}\right) \times 100 \qquad (4.5)$$

4.6.2 Economic performance evaluation

The economic performance evaluation for the BHP process was conducted with the Aspen Economic Process Analyzer® (APEA) based on the detailed process flowsheet presented in Figure 4.5 and 4.6. The developed models were transferred to APEA, where each equipment was sized and costed according to relevant design standards. APEA calculates the direct equipment cost (DEC) in BHP process such as the fixed-bed reactors, PSA, heat exchangers, compressors, pumps, and columns. The process stream pipes and splitters were not included as project components in cost estimation (Otitoju et al., 2021).

The capital expenditure (CAPEX) is estimated using the DEC. The operational expenditure (OPEX) comprised both fixed and variable annual operating and maintenance (O&M) costs. The fixed O&M costs are assumed as 3 % of the CAPEX (Otitoju et al., 2021), covered items such as labour costs, maintenance cost, and overhead charges. The variable O&M costs accounted for consumables and utilities, including natural gas, steam, solvent, and other utility requirements. The solvent loss were estimated at 1.5 kg/tonne$_{CO_2}$ for MEA (Lepaumier et al., 2011) and 0.05 kg/tonne$_{CO_2}$ for PZ (Manzolini et al., 2015). Detailed pricing information for consumables and utilities is provided in Table 4.6.

Table 4.6 The reference prices of consumables and utilities in February 2023 (IEA, 2021, Otitoju et al., 2021, TE, 2023, GPP, 2023).

Item	value
Natural gas price ($/mmbtu)	3.64
Electricity price ($/kWh)	0.406
Make-up water cost ($/tonne)	3
Make-up MEA cost ($/tonne)	1500
Make-up PZ cost ($/tonne)	8000

The total annual costs (TAC) consist of annual capital costs (ACC) and annual O&M costs. The ACC is determined using Eq. (4.6) (Karimi et al., 2011), where *n* represents the project lifespan

and *i* denotes the interest rate. For hydrogen production projects, typical assumptions of *n*=25 and *i*=10 % are used to ensure the cost analysis aligns with the realistic economic conditions and benefits of such projects (Collodi et al., 2017).

$$ACC = \frac{CAPEX}{[(1+i)^n - 1]/i(1+i)^n} \quad (4.6)$$

4.7 Results and discussion

4.7.1 Energy performance results

Figure 4.7 illustrates the energy performance of commercial-scale BHP process with different solvents and configurations. The results clearly show that changes in both solvent and configuration significantly impact the overall energy consumption of the BHP process, with both factors contributing almost equally to these variations. The adoption of the PZ solvent and the ECSB configuration notably reduces the energy penalty of the PCC process, although it has minimal effect on the SMR process. Furthermore, using 30 wt.% PZ yields the most significant reduction in energy penalty. This observation aligns with the energy performance of different solvents in a standalone PCC plant which are shown in Chapter 3.

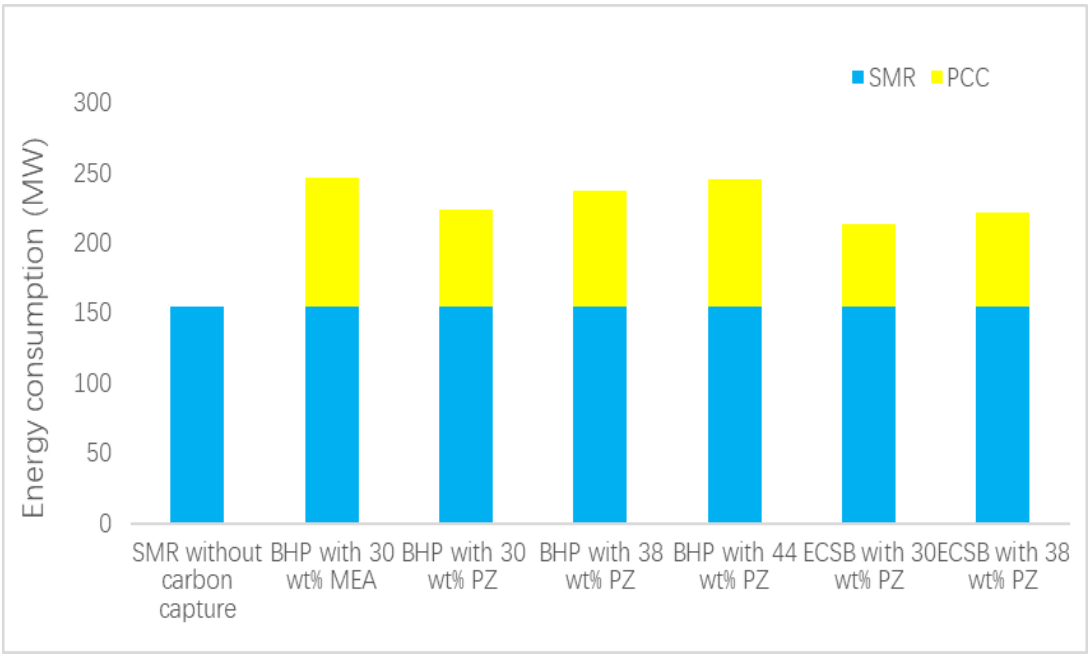

Figure 4.7 Energy performance of commercial-scale BHP process with different solvents and configurations.

Table 4.7 provides a breakdown of the energy required to operate each unit. The SMR process without carbon capture consumes a total of 154.61 MW, with 95.9 % of this energy allocated to heating the reactors. Adding the PCC process slightly increases the energy demand of the SMR process, mainly due to the higher energy requirements of the air blower. This is because the furnace in the SMR process supplies all the energy for the PCC process, which necessitates additional natural gas combustion to generate extra steam for solvent regeneration. Consequently, the flue gas flowrate increases, requiring more energy from the air blower to direct the additional flue gas into the absorber.

Among the tested solvents and configurations, the highest energy penalty of 59.3 % is observed in the BHP process using 30 wt.% MEA, driven primarily due to the significant energy requirement for solvent regeneration. In contrast, using 30 wt.% PZ considerably lowers the energy penalty associated with solvent regeneration. The implementation of the new configuration further decreases the energy penalty from the carbon capture process. The lowest total energy consumption for BHP process is achieved with ECSB process using 30 wt.% PZ. Compared to BHP process using 30 wt.% MEA, the energy penalty of ECSB process using 30 wt.% PZ is reduced by 36.35 %.

Table 4.7 The detailed energy requirements for operating each unit in the BHP process.

	SMR without carbon capture	BHP with 30 wt.% MEA	BHP with 30 wt.% PZ	BHP with 38 wt.% PZ	BHP with 44 wt.% PZ	ECSB with 30 wt.% PZ	ECSB with 38 wt.% PZ
Hydrogen production							
Natural gas compressor (MW)	4.93	4.93	4.93	4.93	4.93	4.93	4.93
Reactors heating (MW)	148.34	148.34	148.34	148.34	148.34	148.34	148.34
Air blower (MW)	1.34	1.49	1.46	1.48	1.49	1.44	1.45
Carbon capture							
Flue gas blower (MW)	N/A	2.09	2.03	2.07	2.09	2.01	2.03
Solvent pump (MW)	N/A	0.18	0.077	0.072	0.039	0.055	0.052
Solvent regeneration (MW)	N/A	89.30	66.50	80.50	88.60	56.22	64.99
Total energy consumption (MW)	154.61	246.33	223.33	237.39	245.49	212.99	221.79
Energy penalty (%)	N/A	59.32	44.45	53.54	58.78	37.76	43.45

4.7.2 Economic evaluation results

The DEC obtained from the APEA is presented in Table 4.8. The SMR process without carbon capture was investigated as a baseline for comparison. The economic performance of the BHP process with different solvents was evaluated against the ECSB process. Table 4.9 details the CAPEX for the SMR process with and without carbon capture. For the standard SMR process with a production capacity of 200 $tonne_{H_2}$/day, the CAPEX is estimated at $111.5 million. The integration of PCC process using 30 wt.% MEA results in a substantial increase in CAPEX, rising by 59.9 %. This significant increase highlights the economic impact of adding carbon capture process, particularly when using MEA as the solvent.

Compared to the BHP process using 30 wt.% MEA, adopting 30-44 wt.% PZ decreases the CAPEX by 3.8 %-10.5 %. This reduction is due to the higher CO_2 absorption capacity of PZ compared to MEA, enabling PZ to achieve 90 % CO_2 capture with a lower solvent circulation rate. This reduces the required size of the absorber and stripper.

The ECSB process further decreases the CAPEX by approximately 16 %, achieved through a reduction in the DEC of the stripper. This improvement is due to the replacement of the standard stripper with an AFS. In the standard configuration, the hot CO_2 vapour is cooled by a condenser at the top of the column, while the CO_2-rich solvent is heated by a reboiler at the bottom. The AFS configuration recovers wasted exergy from the hot CO_2 vapour to heat the cold rich bypass. Therefore, AFS requires a smaller size of condenser than the standard stripper. Additionally, the wasted exergy recovery from flue gas is used to heat the CO_2-rich solvent, allowing a smaller steam heater to replace the standard reboiler. These design improvements lower the stripper cost by 33.8 %.

Table 4.10 summarizes the TAC, levelized cost of H_2 (LCH) and CO_2 avoidance cost (CAC). For the standard SMR process without carbon capture, the TAC is $ 73.43 million per year, and the LCH is approximately 1126 $/$tonne_{H_2}$. These findings align with current cost of hydrogen production from natural gas (1000-3000 $/$tonne_{H_2}$) (Massarweh et al., 2023).

The economic performance of 44 wt.% PZ is less favourable, as it results in the highest TAC, levelized cost of blue hydrogen (LCBH) and CAC. Although 44 wt.% PZ demonstrates better

energy performance compared to 30 wt.% MEA, the variable O&M costs for 44 wt.% PZ are slightly higher than that for 30 wt.% MEA. Simulation results indicate that the variable O&M increase is primarily due to the high PZ loss at high concentration.

For the BHP process using 30 wt.% MEA, the LCBH and CAC are 1725 \$/tonne$_{H_2}$ and 56 \$/tonne$_{CO_2}$, respectively. These outcomes align closely with previous studies reported by Khan et al. (2021) and Roussanaly et al. (2020). Khan et al. estimated the LCBH for an SMR plant (200 tonne$_{H_2}$/day capacity) integrated with an MEA-based PCC plant to range between 1411-1917 \$/tonne$_{H_2}$. Similarly, Roussanaly et al. simulated an SMR plant (450 tonne$_{H_2}$/day capacity) integrated with an MEA-based PCC plant, reporting the LCBH of 1884 \$/tonne$_{H_2}$ and CAC of 67 \$/tonne$_{CO_2}$.

The ECSB process using 30 wt.% PZ achieves the best economic results, with the lowest LCBH at approximately 1389 \$/tonne$_{H_2}$ and lowest CAC at approximately 33 \$/tonne$_{H_2}$. Compared to the BHP process using 30 wt.% MEA, it reduces LCBH and CAC by 19.7 % and 47.9 %, respectively.

Figure 4.8 presents the TAC of commercial-scale BHP with different solvents and configurations. The use of 30 wt.% PZ solvents and ECSB configuration demonstrates significant benefits by reducing TAC, thereby lowering both LCBH and CAC. The primary factor driving variations of TAC is the changes in the annual O&M costs. Among them, variable O&M costs is the main contributor to annual O&M costs changes. Table 4.11 lists the composition of variable O&M costs in detail. It can be seen that cost of natural gas and electricity are the two most important factors affecting variable O&M costs. They contribute more than 90 % of variable O&M costs.

The natural gas cost account for 52-72 % in different configurations, with the cost of natural gas used to produce feedstock being six times that of natural gas used as fuel. Electricity costs account for 24-37 % in different configurations. Among them, the energy and cost-saving configuration significantly reduces the electricity cost in the BHP process. This is because the configuration greatly improves the thermal efficiency of the system and the electricity cost for solvent regeneration is greatly reduced.

Furthermore, since the simulation assumes that hydrogen production and carbon capture

levels remain constant, it is foreseeable that changes in natural gas and electricity prices will affect the TAC, LCBH and CAC in a linear manner. However, the extent of the impact varies in different configurations, mainly because the proportion of natural gas cost and electricity cost in variable O&M costs varies in different configurations. Using the ECSB process with 30 % PZ as an example, a 10 % increase in natural gas prices results in a 7.1 % rise in TAC, LCBH, and CAC. In contrast, a 10 % increase in electricity prices leads to a more moderate 2.4 % increase in these costs.

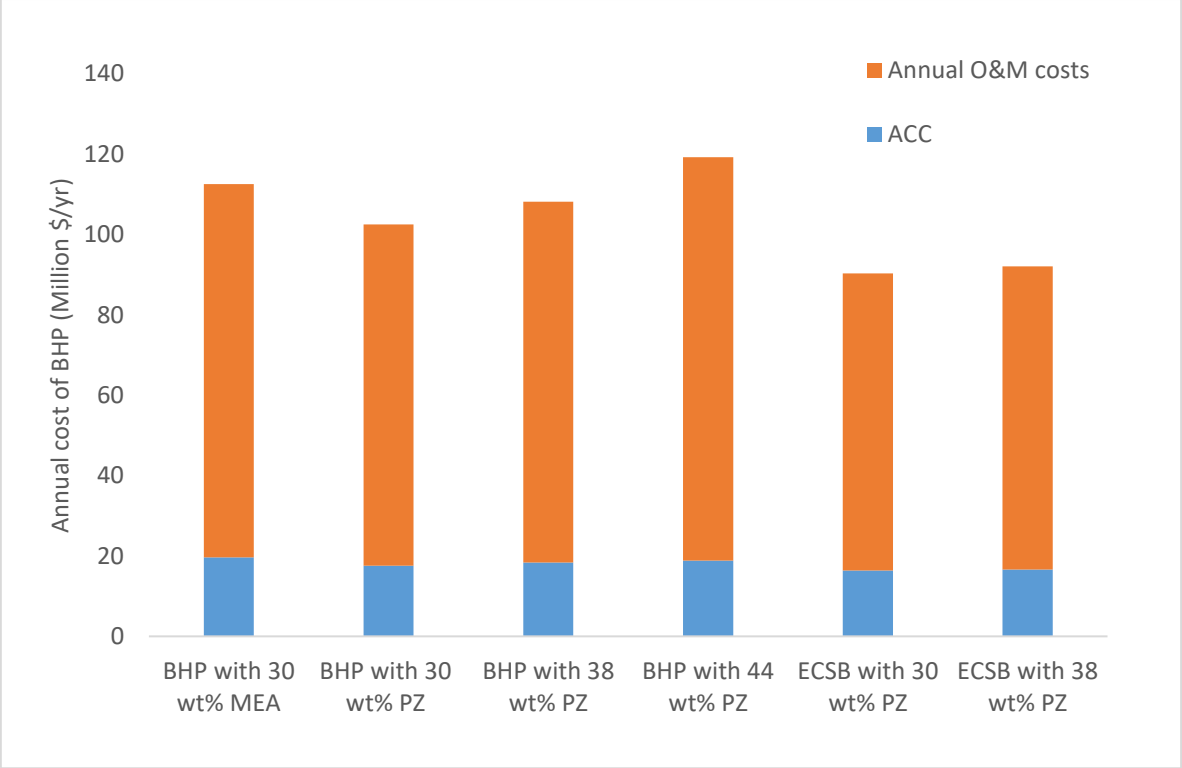

Figure 4.8 TAC of commercial-scale BHP with different solvents and configurations.

Table 4.8 The DEC of commercial-scale BHP process with different solvents and configurations.

	SMR without carbon capture	BHP with 30 wt.% MEA	BHP with 30 wt.% PZ	BHP with 38 wt.% PZ	BHP with 44 wt.% PZ	ECSB with 30 wt.% PZ	ECSB with 38 wt.% PZ
Reactors (Million $)	5.06	5.06	5.06	5.06	5.06	5.06	5.06
PSA (Million $)	0.22	0.22	0.22	0.22	0.22	0.22	0.22
Furnace (Million $)	23.74	28.62	27.38	28.14	28.54	26.82	27.29
Heat exchangers (Million $)	0.37	4.43	3.47	2.79	1.46	1.82	1.74
Coolers (Million $)	0.40	1.70	1.09	1.05	1.05	0.96	1.05
Compressors (Million $)	14.52	17.50	16.74	17.21	17.46	16.40	16.69
Pumps (Million $)	N/A	0.76	0.48	0.45	0.27	0.47	0.44
Columns (Million $)	N/A	12.55	8.99	11.36	14.10	7.31	7.42
DEC (Million $)	44.30	70.82	63.42	66.27	68.15	59.04	59.92

Table 4.9 The CAPEX of commercial-scale BHP process using different solvents and configurations.

	SMR without carbon capture (Million $)	BHP with 30 wt.% MEA (Million $)	BHP with 30 wt.% PZ (Million $)	BHP with 38 wt.% PZ (Million $)	BHP with 44 wt.% PZ (Million $)	ECSB with 30 wt.% PZ (Million $)	ECSB with 38 wt.% PZ (Million $)
DEC	44.30	70.82	63.42	66.27	68.15	59.04	59.92
Total indirect cost (TIC)	8.86	14.16	12.68	13.25	13.63	11.81	11.98
Direct field cost (DFC)	53.16	84.99	76.10	79.53	81.78	70.85	71.90
Engineering procurement and construction (EPC)	67.51	107.94	96.65	101.00	103.86	89.98	91.32
Additional costs (AC)	13.29	21.25	19.02	19.88	20.45	17.71	17.98
Installation cost (IC)	80.80	129.18	115.67	120.88	124.31	107.69	109.29
Project contingency (PC)	16.16	25.84	23.13	24.18	24.86	21.54	21.86
Total plant cost (TPC)	96.96	155.02	138.80	145.06	149.17	129.23	131.15
Owner's cost (OC)	14.54	23.25	20.82	21.76	22.38	19.39	19.67
CAPEX	111.50	178.27	159.63	166.82	171.55	148.62	150.82

Table 4.10 The economic performance of commercial-scale BHP process using different solvents and configurations.

	SMR without carbon capture	BHP with 30 wt.% MEA	BHP with 30 wt.% PZ	BHP with 38 wt.% PZ	BHP with 44 wt.% PZ	ECSB with 30 wt.% PZ	ECSB with 38 wt.% PZ
CAPEX (Million $)	111.50	178.27	159.63	166.82	171.55	148.62	150.82
ACC (Million $/yr)	12.28	19.64	17.59	18.38	18.90	16.37	16.62
Fixed O&M costs (Million $/yr)	7.55	3.99	2.86	3.24	3.51	2.15	2.23
Variable O&M costs (Million $/yr)	53.60	88.92	82.10	86.54	96.82	71.81	73.20
OPEX (Million $/yr)	61.15	92.91	84.96	89.78	100.33	73.96	75.43
TAC (Million $/yr)	73.43	112.55	102.55	108.16	119.23	90.34	92.04
LCH ($/tonne$H_2$)	1125.15	1724.62	1571.32	1657.35	1826.97	1384.28	1410.32
CAC ($/tonne$CO_2$)	N/A	55.67	40.92	47.49	62.12	29.00	31.34

Table 4.111 Contribution of consumables and utilities to variable O&M costs in commercial-scale BHP process using different solvents and configurations.

	SMR without carbon capture	BHP with 30 wt.% MEA	BHP with 30 wt.% PZ	BHP with 38 wt.% PZ	BHP with 44 wt.% PZ	ECSB with 30 wt.% PZ	ECSB with 38 wt.% PZ
Natural gas feed	43.85	43.85	43.85	43.85	43.85	43.85	43.85
Natural gas fuel	7.24	7.24	7.24	7.24	7.24	7.24	7.24
Catalyst	0.32	0.32	0.32	0.32	0.32	0.32	0.32
Water	2.19	2.36	2.66	3.09	3.26	2.25	2.36
Solvent	N/A	2.81	0.67	2.11	11.51	0.56	1.62
Electricity	N/A	32.33	27.36	29.93	30.63	17.59	17.81
Variable O&M costs (Million $/yr)	53.60	88.92	82.10	86.54	96.82	71.81	73.20
Natural gas ratio (%)	95.32	57.46	62.23	59.04	52.77	71.15	69.80
Electricity ratio (%)	0.00	36.36	33.33	34.58	31.64	24.49	24.33

4.8 Conclusions

As global hydrogen demand rises rapidly, deploying commercial-scale BHP systems is becoming increasingly critical for curbing carbon emissions associated with hydrogen production. In this chapter, steady-state models for the SMR and PCC processes were developed using Aspen plus® V11. The commercial-scale SMR model was validated with data from the IEA report, with model predictions aligning well. The differences between model predictions and IEA data are generally within 5 %. The development, validation and scale-up of PCC models were described in Chapter 3. The energy and cost-saving configuration was proposed to minimize the energy penalty associated with solvent regeneration in the PCC process. The technical and economic analyses of BHP with new configurations was carried out through modelling and simulation. The key findings from this chapter are summarized as follows:

- Technical assessment of energy performance revealed that the BHP using 30 wt.% MEA had highest energy penalty of 59.3 %. The ECSB process using 30 wt.% PZ demonstrated the lowest total energy consumption at 213 MW, reducing the energy penalty by 36.35 % compared with BHP process with 30 wt.% MEA.
- The total energy demand of the SMR process without carbon capture is 154.61 MW, with 95.9 % used for reactors heating. The use of PZ solvent and ECSB configuration significantly decreases the energy penalty of the PCC process but has minimal effect on the SMR process.
- An economic analysis was conducted with APEA. The results illustrated that the SMR process without carbon capture has a CAPEX of $ 111.5 million and a TAC of $ 73.4 million/yr. The BHP process using 30 wt.% MEA exhibited the largest increases, with CAPEX rising by 60 % and TAC by 53 %. The ECSB process using 30 wt.% PZ demonstrated the smallest increases, with CAPEX and TAC rising by 33 % and 23 %, respectively.
- The use of 30-44 wt.% PZ results in a CAPEX reduction of 3.8 %-10.5 %. The ECSB process achieves an additional 16 % CAPEX reduction, primarily due to a decrease in the DEC of

stripper. Variations in annual O&M costs were the main contributors to TAC changes.

- Although 44 wt.% PZ has better performance than 30 wt.% MEA in energy requirements, its economic performance was less favourable due to higher variable O&M costs, primarily caused by increased PZ loss at high concentrations.
- The ECSB process using 30 wt.% PZ achieves the best economic performance with the lowest LCBH at approximately 1389 \$/tonne$_{H_2}$ and the lowest CAC at approximately 33 \$/tonne$_{H_2}$. Compared to the BHP process using 30 wt.% MEA, these values represent reductions of 19.7 % in LCBH and 47.9 % in CAC.

Chapter 5. Integrated safety and economic assessment of BHP through modelling and simulation

5.1 Overview

This chapter introduces an integrated model to investigate the relationship between potential process safety improvements and economic benefits. It also proposes a new risk assessment method that is suitable for assessing the overall process risk of BHP and other configurations of reforming processes. The integrated model and its use herein can be summarised in the following steps: (I) the interaction between the process, economic and safety variables was investigated through modelling and simulation, (II) a new risk assessment method for evaluating the overall process risk was proposed based on the index approach and (III) the impact of operating parameters on process risk and economic benefits was investigated.

Section 5.2 presents the descriptions of the methodology. A brief description of the process synthesis sub-model is given in Section 5.3. Section 5.4 proposes a new index-based risk assessment method. The results were compared with a widely used index-based risk assessment method (Dow's fire and explosion index). In addition, some examples are given to help illustrate the application of this new method. Section 5.5 presents the economic analysis sub-model. The results and discussion are given in Section 5.6. Section 5.7 introduces some applications and limitations of the integrated model. The chapter conclusions are described in Section 5.8.

5.2 Methodology

This study proposes the weighted risk index (WRI) method to evaluate the overall process risk of commercial-scale BHP. In addition, an integrated model was developed to investigate the relationship between potential process safety improvements and economic benefits.

This integrated model consists of three sub-models (process synthesis sub-model, safety assessment sub-model and economic analysis sub-model). The process synthesis sub-model was used to determine the process variables involved in the BHP process through sensitivity analysis. The safety assessment sub-model was used to discover hazards and evaluate the overall risk. The economic analysis sub-model was used to estimate the economic viability of the BHP process according to the simulation results.

5.3 Process synthesis sub-model

The base design of BHP process adopted the energy and cost saving configuration that is described in Section 4.5. This configuration has been proven to decrease energy consumption and costs and is characterized by: (I) the application of PZ as a solvent in PCC process, known for its high CO_2 absorption efficiency; (II) an optimized heat exchange system that recovers the waste exergy from flue gas; and (III) the adoption of AFS which simplifies the stripper design and reduces capital cost.

The model development and validation of the ECSB process have been investigated and discussed in Chapter 4. The designed blue hydrogen plant has a production capacity of 200 tonnes per day. The performance of commercial-scale ECSB process is shown in Table 5.1. Figure 5.1 shows the flowsheet of commercial-scale ECSB model.

Table 5.1 The performance of ECSB plant at commercial scale.

Parameters	Value
Natural gas feedstock mass flowrate (kg/s)	7.29
Natural gas fuel mass flowrate (kg/s)	1.68
CH_4 conversion rate (%)	86.5
Syngas mass flow rate (kg/s)	28.23
H_2 production (kg/s)	2.45
Operating temperature of main reformer (^oC)	900
Operating pressure of main reformer (bar)	28
Solvent circulation rate (kg/s)	475
Capture level (%)	90
PZ concentration (wt%)	30
Absorber pressure (bar)	1.1
Absorber column diameter (m)	7.8
Stripper pressure (bar)	1.8

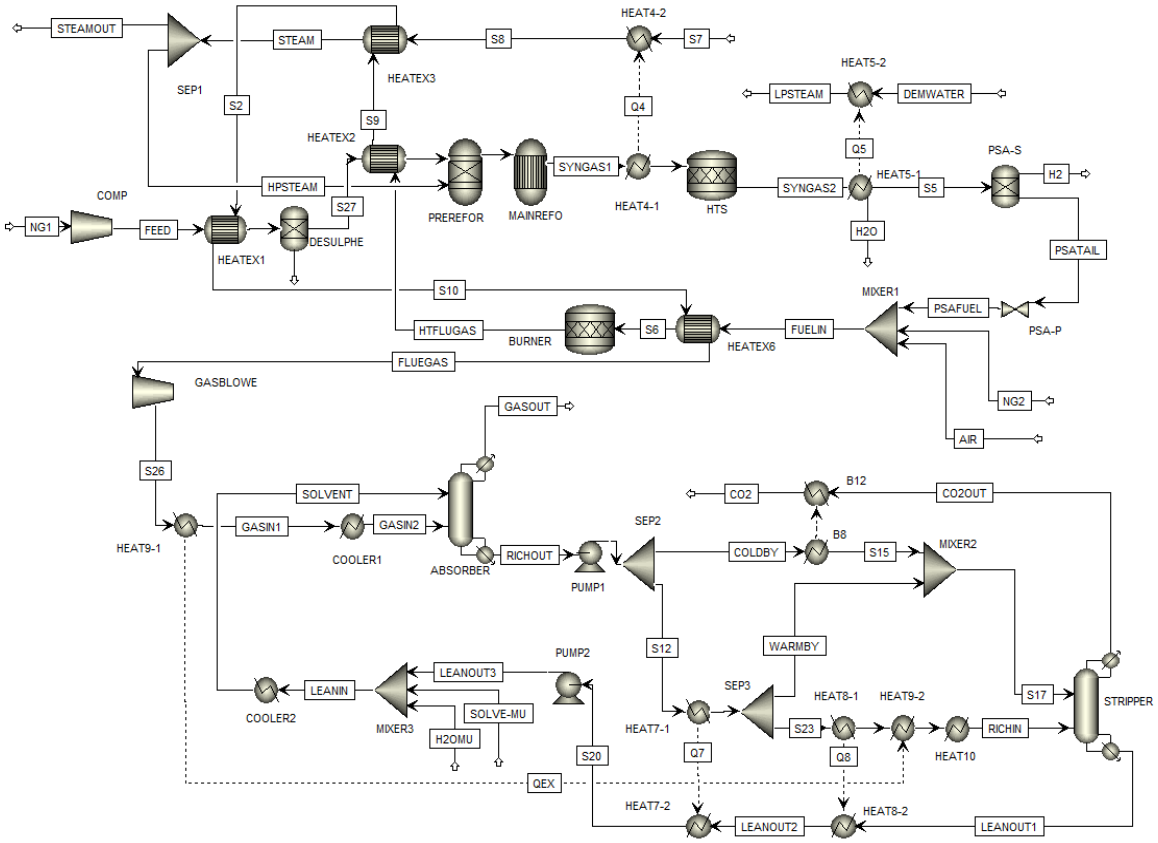

Figure 5.1 The flowsheet of commercial-scale ECSB model in Aspen Plus® V11.

5.4 Safety assessment sub-model

An index-based risk assessment method, the WRI, was developed to assess the overall process risk for commercial-scale BHP. This method is made up of three steps and considers the impact of changes in operating temperature and pressure on overall process risk. Human reliability was not taken into account in this method in order to avoid subjectivity as much as possible. Some examples are given to help illustrate the application of the WRI method.

5.4.1 Step 1: consequence identification and classification

The overall process risk is defined as a function of the severity and likelihood of the consequences. Potential hazards need to be identified, and the severity of the consequences should be estimated reasonably. This study draws on previous risk assessment research on SMR and PCC processes (JAFARI et al., 2013, Chau et al., 2022b, Wang et al., 2023a) to identify the most common hazardous scenarios in BHP process. A total of 16 scenarios were

identified, considering factors such as process control, extreme conditions, affected areas, and potential consequences. These scenarios were then classified into 4 nodes based on the process flow diagram of BHP plant. There are shown in Table 5.2.

To estimate the severity of the consequences for each scenario, a corresponding ranking system is developed. The severity of consequences for each scenario are divided into 3 levels and are defined with a range of values, according to the adverse impact on production as well as potential risks to personnel safety. This three-level classification was chosen because using more levels would increase the complexity of risk analysis, making it less practical for real-world application. On the other hand, using fewer than three levels would reduce the precision of the risk assessment, decreasing the sensitivity in identifying potential hazards. The ranking hierarchy was described as follows:

- Minor consequence (value of 1): This level indicates a relatively safe scenario, posing no significant threat to personnel. It is unlikely to result in production losses.
- Medium consequence (value of 2): This level requires caution and attention. If unaddressed, it may lead to equipment damage and minor production losses, though personnel safety remains largely unaffected. However, close monitoring is necessary to prevent escalation.
- Serious consequence (value of 3): This level represents a dangerous scenario with a high probability for equipment damage, explosion, or fire, resulting in major production losses. The risks to personnel safety are substantial, and immediate corrective action is essential to mitigate harm to workers and prevent catastrophic consequences.

Table 5.2 The scenarios identification and classification.

Nodes	Code	Scenarios	Code
Pre-treatment of natural gas and boiler feed water	N1	Failure or poor performance of natural gas inlet valve	S1-1
		Excess steam input from the boiler to de-aerator	S1-2
		A pipeline puncture at compressor transducer	S1-3
		Failure or poor performance of pre-reformer control valve	S1-4
		High temperature in compressor gas	S1-5
Steam reforming process	N2	The blockage of natural gas flow in reformer furnace tubes	S2-1
		Gas leakage of main-reformer control valve	S2-2
		The catalyst deactivation due to coke formation	S2-3
		Failure of reformer furnace torches	S2-4
Hydrogen purification unit	N3	The blockage of purge gas buffer	S3-1
		Gas leakage in PSA units	S3-2
Carbon capture process	N4	Solvent leakage from the flange or shell of heat exchanger	S4-1
		High pressure in absorber column	S4-2
		High pressure in stripper column	S4-3
		Failure of cooling tower recycle pump	S4-4
		Failure of solvent pump	S4-5

5.4.2 Step 2: calculation of weight and average frequency

The severity of the consequences for the nodes considered is expressed using the weight values of the scenarios within the nodes. This risk assessment method uses nodes as the basic unit, but the number of scenarios contained in each node is different. To avoid the impact of the difference in the number of scenarios on the risk of nodes, the severity of consequences for the nodes is estimated by calculating the average value.

First, the severity of the consequences for the 16 scenarios is estimated according to the ranking system. Then, the weight of each node is calculated based on the average severity of the consequences for scenarios, as shown in the Eq. (5.1).

$$w_i = \frac{\Sigma C_i^j}{n} \tag{5.1}$$

Where

w_i is the weight for node *i.*

C_i^j is the severity of the consequences for scenario *j* that classified in node *i.*

n is the number of C_i^j.

The node N2 is used below, as an example, to show how to calculate the weight. First, the severity of the consequences for scenarios S2-1 to S2-4 were estimated according to the ranking system. Then, the weight of node N2 was calculated by Eq. (5.1). The Table 5.3 shows the severity of the consequences for scenario S2-1 to S2-4.

Table 5.3 The severity of the consequences for scenario S2-1 to S2-4.

Code of scenarios	Severity of the consequences
S2-1	2
S2-2	2
S2-3	2
S2-4	3

The weight of node N2 was calculated by Eq. (1), which was w_2=2.25. The weight value for all nodes were calculated by same method. The calculation results are listed in Table 5.4.

Table 5.4 Nodes corresponding to the weight values.

Nodes	Weight values
Pre-treatment of natural gas and boiler feed water	1.4
Steam reforming process	2.25
Hydrogen purification unit	2
Carbon capture process	1.8

The frequency of each node is determined by calculating the average frequency of scenarios. Since this risk assessment method uses nodes as the basic unit and the number of scenarios within each node varies, the frequency of each node is estimated by calculating the average value to avoid the impact of the difference in the number of scenarios on the risk of nodes.

First, the frequency of each scenario was obtained from the previously published studies (AICE 2015, Chau et al., 2022b, JAFARI et al., 2013, Li et al., 2020). Considering that the values of these frequencies are difference in literatures, the frequency of each scenario is expressed as a range. Then, the frequency of each node was calculated by the Eq. (5.2).

$$f_i = \frac{\Sigma f_i^j}{n} \tag{5.2}$$

Where

f_i is the frequency for node *i.*

f_i^j is the frequency for the scenario *j* that classified in node *i.*

n is the number of f_i^j.

The node N2 was used as an example to show how to calculate the average frequency. First, the frequency of scenario S2-1 to S2-4 were obtained from previous studies, as shown in Table 5.5. Then, the frequency of node N2 was calculated by Eq. (5.2).

It is important to note that the frequency of each scenario is typically represented as a range. To ensure a conservative estimation, the maximum value within each range was used in the calculations, representing the worst-case scenario. Accordingly, the frequency of node N2 was calculated using Equation (5.2) as: $f_2 = (1 + 0.1 + 0.01 + 0.01) / 4 = 0.28$. The frequencies of all nodes are summarized in Table 5.6.

Table 5.5 The frequency of scenario S2-1 to S2-4 (AICE 2015, Chau et al., 2022b, JAFARI et al., 2013, Li et al., 2020).

Code of scenarios	Frequency of the scenarios (per year)
S2-1	1 to 1×10^{-1}
S2-2	1×10^{-1} to 1×10^{-2}
S2-3	1×10^{-2} to 1×10^{-3}
S2-4	1×10^{-2} to 1×10^{-3}

Table 5.6 Nodes corresponding to the frequency.

Nodes	Frequency (per year)
Pre-treatment of natural gas and boiler feed water	0.4402
Steam reforming process	0.28
Hydrogen purification unit	0.055
Carbon capture process	0.46

5.4.3 Step 3: estimation of overall process risk

Since the risk of each node contributes to the overall process risk, the overall process risk is defined as the sum of risk of each node. Although this approach makes the absolute value of the WRI heavily dependent on the number of nodes, the WRI results are still comparable for processes with the same number of nodes. The limitations of this risk assessment method are discussed in detail in Section 5.7.

The impact of operating temperature and pressure on overall process risk was considered in this study. Since it was different that the sensitivity of each unit to the change of operating parameters in BHP process, the operating parameters of the main reformer are used to refer to the operating conditions of the entire system. The effect of operating temperature changes from 700 °C to 1100 °C on overall process risk when the operating pressure is 20, 30, and 40 bar was investigated.

The correction factors of operating parameters were used to describe the impact of operating temperature and pressure on the risk of node. The estimation of the correction factors was based on the process risk index (PRI) method proposed by Chau et al. (Chau et al., 2022b). It is a heuristic-based approach to map risks and explore the impact of process deviations on process safety. This correction factor is similar to the penalty factors in F&EI, which are based on expert experience and analysis. Thus, this correction factor has a certain degree of subjectivity. To address this limitation, this study combines the results of the WRI with simulation results, aiming to minimize subjectivity.

The correction factors of temperature and pressure are given in Figure 5.2. In Figure 5.2 b1,

b2, a3, b3 and a4, increases of operating temperature and pressure were positively correlated with increases of overall process risk. This is because extreme operating temperatures and pressures increase the likelihood of hydrogen leakage and jet-fire. In Figure 5.2 a1, operating temperatures below 800 °C led to an increased overall process risk due to inhibited methane conversion at lower reforming temperatures. Consequently, excessive unconverted methane enters the furnace via the PSA tail gas, causing a sudden increase in furnace temperature. This increases the risk of pipeline rupture in equipment such as heat exchangers in Node N1. Similarly, in Figure 5.2 a2, low operating temperatures may cause blockage of the main reformer, which may result in severe production losses. In Figure 5.2 b4, the increase in operating pressure led to a decrease in the flue gas flowrate according to simulation results. This resulted in a lower required solvent circulation rate and therefore a lower risk of solvent leakage, flooding, and corrosion.

The risk of node corresponding to an operating parameter was calculated with Eq. (5.3). The overall risk of BHP process was calculated using Eq. (5.4).

$$risk = \alpha_T \alpha_P \cdot f_i \cdot w_i \tag{5.3}$$

Where

α_T is temperature correction factor for the risk of nodes.

α_P is pressure correction factor for the risk of nodes.

f_i is the frequency for node *i.*

w_i is the weight for node *i.*

$$WRI = \sum risk_{node} \tag{5.4}$$

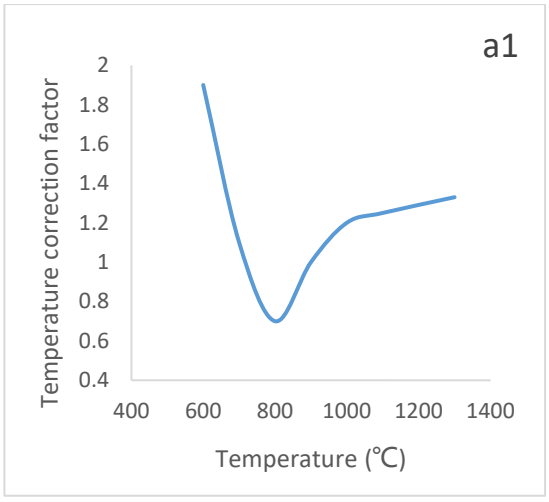
a1
Temperature correction factor
2
1.8
1.6
1.4
1.2
1
0.8
0.6
0.4
400
600
800
1000
1200
1400
Temperature (℃)

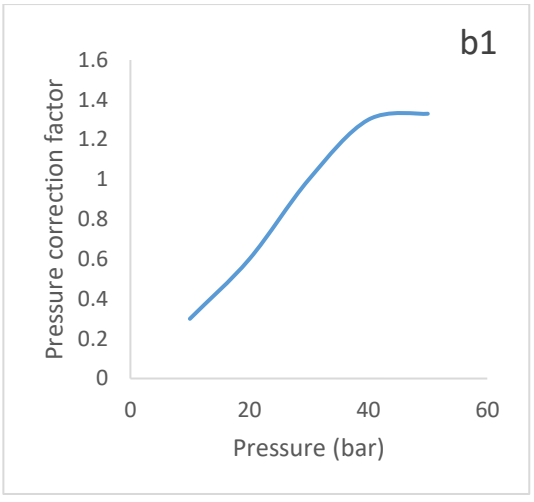
b1
Pressure correction factor
1.6
1.4
1.2
1
0.8
0.6
0.4
0.2
0
0
20
40
60
Pressure (bar)

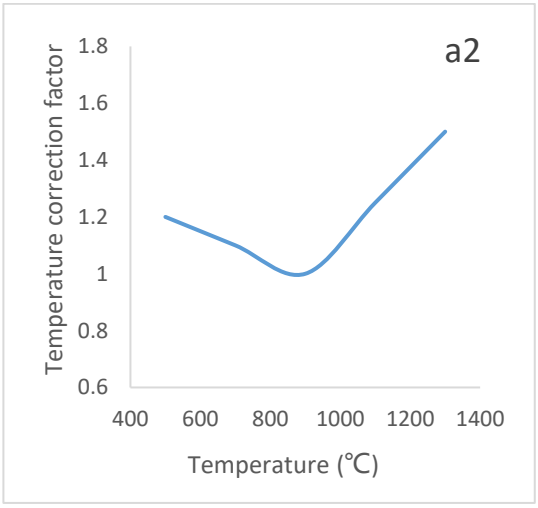
a2
Temperature correction factor
1.8
1.6
1.4
1.2
1
0.8
0.6
400
600
800
1000
1200
1400
Temperature (℃)

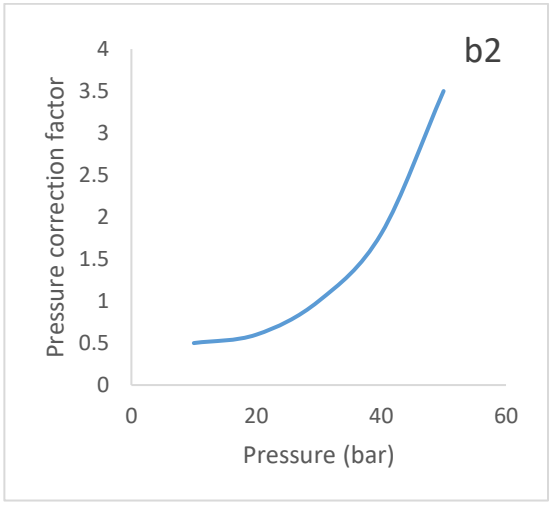
b2
Pressure correction factor
4
3.5
3
2.5
2
1.5
1
0.5
0
0
20
40
60
Pressure (bar)

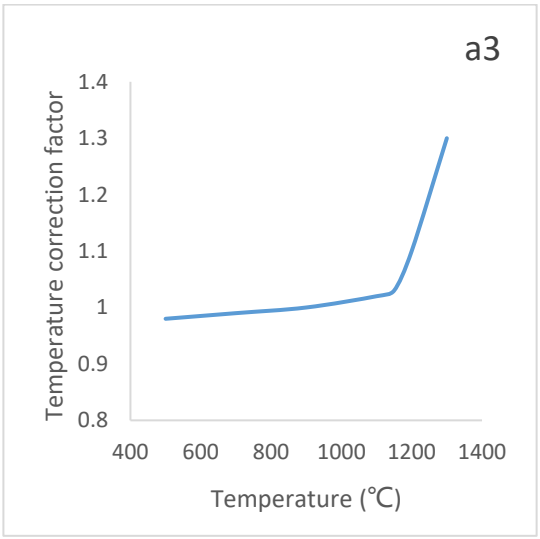
a3
Temperature correction factor
1.4
1.3
1.2
1.1
1
0.9
0.8
400
600
800
1000
1200
1400
Temperature (℃)

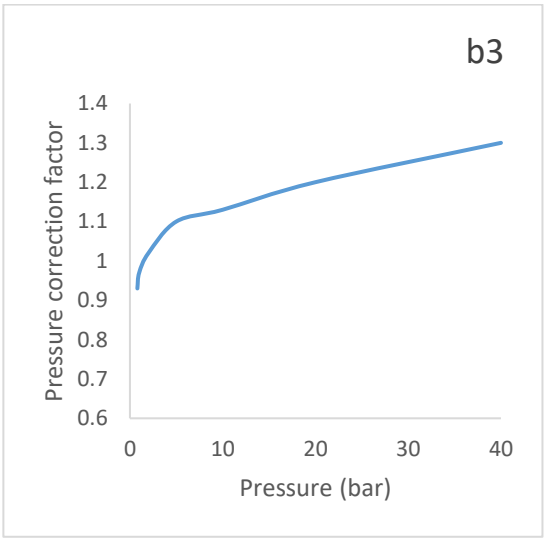
b3
Pressure correction factor
1.4
1.3
1.2
1.1
1
0.9
0.8
0.7
0.6
0
10
20
30
40
Pressure (bar)

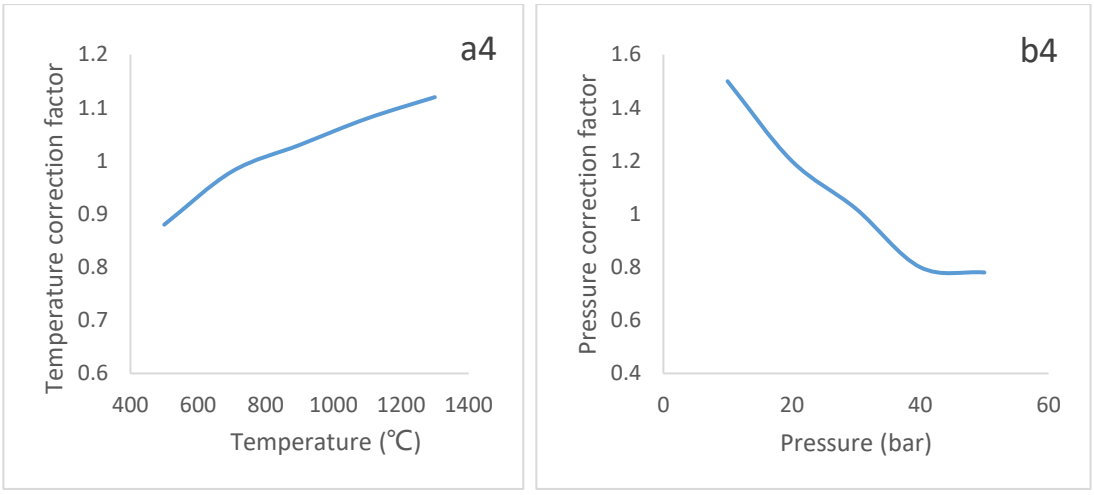

Figure 5.2 Correction factor operating parameters for different nodes. (a1) Temperature correction factor for node N1. (b1) Pressure correction factor for node N1. (a2) Temperature correction factor for node N2. (b2) Pressure correction factor for node N2. (a3) Temperature correction factor for node N3. (b3) Pressure correction factor for node N3. (a4) Temperature correction factor for node N4. (b4) Pressure correction factor for node N4.

A simple case with 900 °C and 30 bar was used as an example to show how to calculate the overall process risk. First, the risk of each node was calculated by Eq. (5.3). The correction factors for each node are obtained from Figure 5.2. The calculation results are listed in Table 5.7. Then, the overall process risk was calculated by Eq. (5.4), which was WRI=0.432+0.654+0.136+0.836=2.248.

The results of the WRI calculations under various operating conditions are presented in Section 5.6.1.1, along with a discussion of these findings. Additionally, Section 5.6.1.2 compares the WRI results with those of the F&EI, demonstrating the advantages of the WRI in assessing the overall process risks with the BHP process.

Table 5.7 The calculation results of nodes risk for the simple case.

Nodes	α_T	α_p	w_i	f_i	Risk
N1	0.700	1.000	1.400	0.440	0.432
N2	1.050	0.990	2.250	0.280	0.654
N3	0.990	1.240	2.000	0.056	0.136
N4	0.990	1.020	1.800	0.460	0.836

5.5 Economic analysis sub-model

The economic feasibility of the process was evaluated using the economic analysis sub-model that calculates the five-year net present value (NPV). The economic assessment for the BHP was conducted with the APEA, based on the detailed process flowsheet presented in Table 5.8. The developed models were transferred to APEA, where each equipment was sized and costed according to relevant design standards. The process stream pipes and splitters were not included as project components in cost estimation.

The CAPEX is estimated using the DEC. The OPEX comprised both fixed and variable annual O&M costs. The fixed O&M costs were assumed as 3 % of the CAPEX (Luo, 2016), covered items such as operating labour costs, maintenance cost, overhead charges etc. The variable O&M costs accounted for consumables and utilities, including natural gas, steam, solvent consumption, and utility costs. The solvent loss value was assumed as 0.05 kg/tonne$_{CO_2}$ (Manzolini et al., 2015). Detailed pricing information for consumables and utilities is provided in Table 5.8.

Table 5.8 The reference prices of consumables and utilities in February 2023 (IEA, 2023, TE, 2023, Li et al., 2024).

Item	value
Natural gas price ($/mmbtu)	3.64
Electricity price ($/kW)	0.406
Make-up water cost ($/tonne)	3
Make-up solvent cost ($/tonne)	8000

The annual net cash flow (CF) is calculated by Eq. (5.5), where *Q* is the annual production of hydrogen and S_{H_2} is selling price of hydrogen. The selling price of hydrogen is influenced by various factors, including production costs and regional variations. Currently, the production cost of hydrogen ranges from 1,000 to 3,000 $/tonne. Based on this, the S_{H_2} is assumed as 5000 $/tonne. The NPV is calculated by Eq. (5.6), where the t is the time of the cash flow and r is the discount factor. The time of the cash flow is assumed as 5 year and the discount factor is assumed as 10 %.

$$CF = Q \cdot S_{H2} - OPEX \tag{5.5}$$

$$NPV = \sum_{1}^{n} \frac{CF_n}{(1+r_d)^n} - CAPEX \tag{5.6}$$

5.6 Results and discussion

5.6.1 The results of risk assessment

This section presents a risk assessment of the BHP process using the WRI method introduced in the previous section. The results are compared with those of F&EI method, which has long been regarded as the widely used index-based risk assessment method. By comparing the two methods, this section highlights the differences in their sensitivity to changes in operating conditions.

5.6.1.1 Risk assessment by WRI

To investigate the impact of changes in operating parameters on overall system risk, synergies between units need to be carefully considered. In this study, key parameters such as the natural gas feedstock for reforming, the air-fuel ratio in the furnace, the CO_2 lean loading of PZ solvent, etc. are kept constant to avoid the impact of irrelevant variables on system risks. Parameters such as solvent circulation rate, heat duty, etc. are adjusted according to changes in flue gas characteristics to ensure that downstream units remain unaffected. The operating condition of 30 bar and 900 °C was investigated as the baseline, serving as the reference point for risk tolerance. The baseline condition is considered to be the upper limit of the acceptable risk for the system. If the overall process risk is lower than the baseline value, the system is considered to be within an acceptable safety level. Otherwise, the system is considered to be dangerous. Table 5.9 summarizes the results of WRI based on process simulation, with the WRI value for the baseline condition is 2.248. Therefore, the risk tolerance value for this system is 2.248.

Table 5.9 Summary of the WRI results based on process simulation.

Operating condition	WRI	Risk tolerance	Units at risk level
20 bar, 700 °C	1.857	Acceptable	All units
20 bar, 800 °C	1.703	Acceptable	All units
20 bar, 900 °C	1.841	Acceptable	All units
20 bar, 1000 °C	1.964	Acceptable	All units
20 bar, 1100 °C	2.063	Acceptable	All units
30 bar, 700 °C	2.327	Danger	Reformer
30 bar, 800 °C	2.057	Acceptable	All units
30 bar, 900 °C	2.248	Acceptable	All units
30 bar, 1000 °C	2.458	Acceptable	All units
30 bar, 1100 °C	2.601	Danger	Reformer
40 bar, 700 °C	2.904	Danger	Desulfurization, Reformer
40 bar, 800 °C	2.535	Danger	Desulfurization, Reformer, WGS
40 bar, 900 °C	2.749	Danger	Desulfurization, Reformer, WGS
40 bar, 1000 °C	3.056	Danger	Desulfurization, Reformer, WGS
40 bar, 1100 °C	3.263	Danger	Desulfurization, Reformer, WGS

The increase in reformer temperature is the most important source of hazards. Extreme temperatures and pressures increase the likelihood of reformer leaks and explosions. Since the reforming reaction is volume expansion reaction, the likelihood of hazards occurring may be higher than estimated. In addition, high temperatures may damage the catalyst, leading to failure of reformer. This may result in production losses and unpredictable hazards. The risk of desulfurization and WGS mainly comes from the increase in pressure. High operating pressure can lead to punctures in the desulfurizer and WGS. Because the PCC process operates at relatively low temperatures and pressures, the process contributes little risk to

the whole system.

Figure 5.3 summarizes the effect of changes in operating parameters on the overall process risk. The blue line in the figure represents risk tolerance. When the WRI value is higher than the risk tolerance, the system is considered dangerous, otherwise, the system is considered safe. The changes in WRI value indicate that increase in operating pressure and temperature has a primary contribution to the increase in system risk. However, when the operating temperature is less than 800 °C, the system risk increases as the temperature decreases. The primary contribution to this increased risk comes from the furnace. The conversion of methane is inhibited due to the low reforming temperature. Therefore, the PSA tail gas containing a large amount of combustible gas is sent into the furnace, causing the temperature of the furnace to rise suddenly. The extreme temperatures result in the increase of system risk.

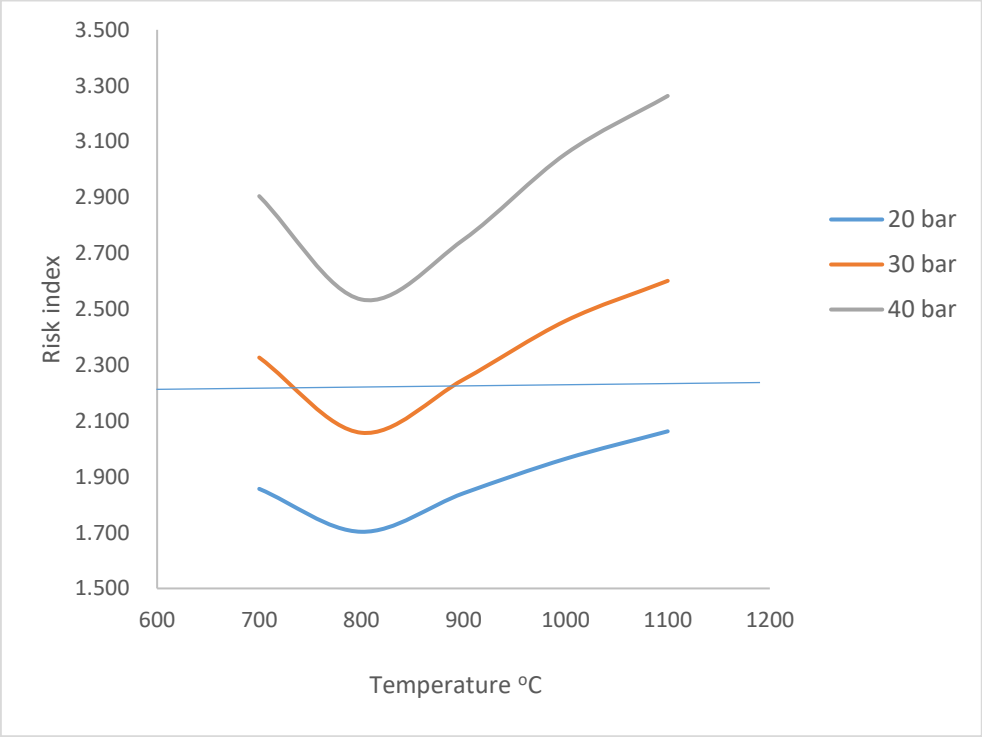

Figure 5.3 Impact of changes in operating parameters on overall process risks.

5.6.1.2 Comparison of F&EI and WRI

The WRI was benchmarked with F&EI. As mentioned earlier, F&EI is the most widely used

index-based risk assessment method (AICHE, 1994). The calculation of F&EI is determined by two key factors:

- Material Factor (MF): Represents the intrinsic hazards of the chemical substances being handled (e.g., flammability, explosiveness).
- Penalty Factors: Represent process-specific conditions that increase the likelihood of fire or explosion. These include: (a) General Process Hazards: Factors like operating pressure, temperature, and inventory size; (b) Special Process Hazards: Conditions such as exothermic reactions, presence of flammable vapours, or reactive chemicals.

The F&EI was calculated by the Eq. (5.7) and (5.8).

$$F\&EI = MF \times \text{Unit Hazard Factor (UHF)} \quad (5.7)$$

$$UHF = (1+\text{General Process Hazards}) \times (1+\text{Special Process Hazards}) \quad (5.8)$$

The value of MF and UHF are obtained and calculated with Dow's Standard Tables, which include: material factor table, general process hazard factor table, special process hazard factor table and risk classification table (AICHE, 1994).

Material factors, general process hazard factors and special process hazard factors involved in BHP are given in Table 5.10, Table 5.11 and Table 5.12.

Table 5.10 Material factors involved in BHP process.

Material	MF
Hydrogen	30
Methane	21
Propane	20
CO	16

The value of MF is determined by the most hazardous substance. In the BHP process, high concentration of hydrogen is the most dangerous substance, so MF=30.

Table 5.11 General process hazard factors involved in BHP process.

Process conditions	Penalty factor
Temperature (°C)	
≤ 100	0
100 - 300	0.3
300 - 600	0.6
600 - 800	0.8
800 - 1000	1
1000 - 1100	1.1
1100 - 1300	1.2
Pressure (bar)	
≤1	0
1 - 10	0.3
10 - 20	0.6
20 - 30	0.8
30 - 40	1

The impact of operating conditions on system risk is considered, so the general process hazard factor is not a fixed value. Taking the main reformer running under baseline conditions (900 °C and 30 bar) as an example, the value of general process hazard factor = 1+0.8 = 1.8.

Table 5.12 Some special process hazard factors.

Conditions	Penalty factor
Explosion potential	1
Toxic release	0.3
Exothermic reactions	0.4
Fast reaction (unable to control reaction rate)	0.4

The special process hazard in the BHP is the explosion potential caused by high concentrations of flammable gases. Thus, the special process hazard factors = 1.

According to the values obtained from Table 5.10-5.12, the UHF and F&EI of the main reformer running under baseline conditions (900 °C and 30 bar) are as follows.

UHF = (1+1.8) × (1+1.0) = 5.6

F&EI = MF×UHF = 30×5.6 = 168

The degree of hazard for the main reformer is classified according to the F&EI score. The Dow's risk classification is given in Table 5.13.

Table 5.13 Risk classification standard table.

F&EI Index Range	Degree of hazard
< 60	Light risk
61 - 96	Moderate risk
97 - 127	Intermediate risk
128 – 158	Heavy risk
> 159	Severe risk

With an F&EI of 168, the main reformer running under baseline conditions (900 °C and 30 bar)

falls into the Severe risk category. The results of risk assessment for BHP process using F&EI method are presented in Table 5.14, 5.15 and 5.16. The results are compared with the WRI results in Table 5.9.

The F&EI results show that the BHP process has a heavy risk under all operating conditions. Additionally, the reformer is classified as a severe risk in more than half of the cases. This contrasts with the results of WRI, which consider the system to be safe at temperatures less than 1000 °C and pressures less than 30 bar. The main reason for this difference is that F&EI is highly sensitive to the flammable gas material. The degree of hazard is significantly increased due to the presence of a large amount of high-concentration hydrogen in the BHP process.

Another finding is that F&EI and WRI reached consistent conclusions on the sources of system risk. The reformer, desulfurization and WGS are considered the most hazardous units in the BHP process. In addition, the F&EI results show that the burner has a heavy risk under certain extreme operating conditions due to the presence of a large amount of flammable gas in this unit.

Compared with the WRI, F&EI is less sensitive to variations in operating conditions. Its results show minimal changes in the degree of hazard, with only the classification of reformer being updated from heavy risk to severe risk. This is because the F&EI heavily depends on material factors for risk classification, making it less influenced by changes in operating conditions. When operating conditions deviate, F&EI may not be able to successfully identify hazards. In contrast, the risk level of the reformer, desulfurization and WGS in WRI changes with vary in operating conditions. The reason for this difference is that WRI balances the influence of different risk factors. In addition, the WRI can detect the associated impacts caused by improper operations by observing changes in overall process risk.

Table 5.14 Summary of the F&EI results based on process simulation at 20 bar.

Operating condition	F&EI	Degree of hazard	Units at hazard	Risk tolerance of WRI	Units at risk level
20 bar, 700 °C	144	Heavy risk	Heavy risk: Desulfurization, Reformer, WGS	Acceptable	Acceptable: All units
20 bar, 800 °C	144	Heavy risk	Heavy risk: Desulfurization, Reformer, WGS	Acceptable	Acceptable: All units
20 bar, 900 °C	156	Heavy risk	Heavy risk: Desulfurization, Reformer, WGS	Acceptable	Acceptable: All units
20 bar, 1000 °C	156	Heavy risk	Heavy risk: Desulfurization, Reformer, WGS	Acceptable	Acceptable: All units
20 bar, 1100 °C	162	Severe risk	Severe risk: Reformer Heavy risk: Desulfurization, burner, WGS	Acceptable	Acceptable: All units

Table 5.15 Summary of the F&EI results based on process simulation at 30 bar.

Operating condition	F&EI	Degree of hazard	Units at hazard	Risk tolerance of WRI	Units at risk level
30 bar, 700 °C	156	Heavy risk	Heavy risk: Desulfurization, Reformer, burner, WGS	Danger	Danger: Reformer
30 bar, 800 °C	156	Heavy risk	Heavy risk: Desulfurization, Reformer, WGS	Acceptable	Acceptable: All units
30 bar, 900 °C	168	Severe risk	Severe risk: Reformer Heavy risk: Desulfurization, WGS	Acceptable	Acceptable: All units
30 bar, 1000 °C	168	Severe risk	Severe risk: Reformer Heavy risk: Desulfurization, WGS	Acceptable	Acceptable: All units
30 bar, 1100 °C	174	Severe risk	Severe risk: Reformer Heavy risk: Desulfurization, burner, WGS	Danger	Danger: Reformer

Table 5.16 Summary of the F&EI results based on process simulation at 40 bar.

Operating condition	F&EI	Degree of hazard	Units at hazard	Risk tolerance of WRI	Units at risk level
40 bar, 700 °C	168	Severe risk	Severe risk: Reformer Heavy risk: Desulfurization, burner, WGS	Danger	Danger: Desulfurization, Reformer
40 bar, 800 °C	168	Severe risk	Severe risk: Reformer Heavy risk: Desulfurization, WGS	Danger	Danger: Desulfurization, Reformer, WGS
40 bar, 900 °C	180	Severe risk	Severe risk: Reformer Heavy risk: Desulfurization, WGS	Danger	Danger: Desulfurization, Reformer, WGS
40 bar, 1000 °C	180	Sever risk	Severe risk: Reformer Heavy risk: Desulfurization, WGS	Danger	Danger: Desulfurization, Reformer, WGS
40 bar, 1100 °C	186	Sever risk	Severe risk: Reformer Heavy risk: Desulfurization, burner, WGS	Danger	Danger: Desulfurization, Reformer, WGS

5.6.2 The results of economic assessment

The results of CAPEX, OPEX and five-year NPV at different operating conditions are presented in Table 5.17, 5.18 and 5.19. The highest CAPEX of $ 169 million is achieved by the operating conditions with 20 bar and 1100 °C. The lowest CAPEX of $ 141 million is achieved by the operating conditions with 40 bar and 800 °C. The highest OPEX of 128 million $/yr is achieved by the operating conditions with 40 bar and 1100 °C. The lowest OPEX of 98 million $/yr is achieved by the operating conditions with 20 bar and 700 °C. The highest NPV of $ 920 million is achieved by the operating conditions with 20 bar and 1000 °C. The lowest NPV of $ -1.6 million is achieved by the operating conditions with 40 bar and 700 °C.

The results of CAPEX are summarised in Figure 5.4. The increase in operating temperature leads to an increase in CAPEX. The reason is that maintaining high temperatures in the reformer requires burning a large amount of natural gas fuel, resulting in increased flue gas flowrate. Thus, a larger air blower, absorber and stripper are required in the PCC process. However, the operating condition of 700 °C is a special case. In the simulation, a low methane conversion rate is found at the operating temperature of 700 °C. Because the low temperature inhibits the conversion of methane into hydrogen, the PSA tail gas contains a large amount of combustible gas. In this case, the temperature of the furnace reaches up to 1000 °C and natural gas fuel is no longer needed. More air is required to maintain the air-fuel ratio. This results in an increase in flue gas flowrate and an increase in CAPEX from the PCC process.

Pressure variations influence CAPEX through multiple factors. Among these, the most significant contributor is the change in the cost of heat exchangers. Additionally, variations in the costs of other equipment, such as adsorber, stripper, pumps and air blower, also play an important role. In the temperature range of 800–1000 °C, a clear trend of decreasing capital cost with increasing pressure is observed. This is primarily due to the rise in gas density at higher pressures, which enhances heat transfer performance and reduces the required heat exchange area, thereby significantly lowering the cost of heat exchangers.

However, this trend may not be realized in practical applications. Higher pressure necessitates greater mechanical strength, requiring thicker materials for components such

as exchanger shells, pipes, and flanges—ultimately increasing manufacturing costs. Since the simulation does not account for material-related factors, it only reflects the reduction in heat exchanger size at high pressure, leading to the reduction on CAPEX.

In addition, two anomalous trends were observed at 700 and 1100 °C. At 700 °C, the methane conversion rate was already lower than 30 %. Under this condition, the PSA tail gas contained a large amount of combustible gas. As pressure increased, the methane conversion rate further decreased, resulting in even more combustible gas being fed into the furnace. Consequently, the flue gas flow rate rose significantly, leading to a sharp increase in the cost of the air blower. This divergence in cost behaviour between the air blower and the heat exchanger under rising pressure conditions accounts for the non-linear trend observed at 700 °C, where CAPEX first increases and then declines.

At 1100 °C, the extremely high flue gas temperature enhances heat exchange efficiency during solvent regeneration, leading to a reduction in stripper costs. However, at 40 bar, the lower methane conversion results in a greater amount of unconverted combustible gases being directed to the furnace, thereby increasing flue gas flowrate. This, in turn, raises the cost of the absorber, causing the CAPEX at 40 bar to be slightly higher than that at 30 bar.

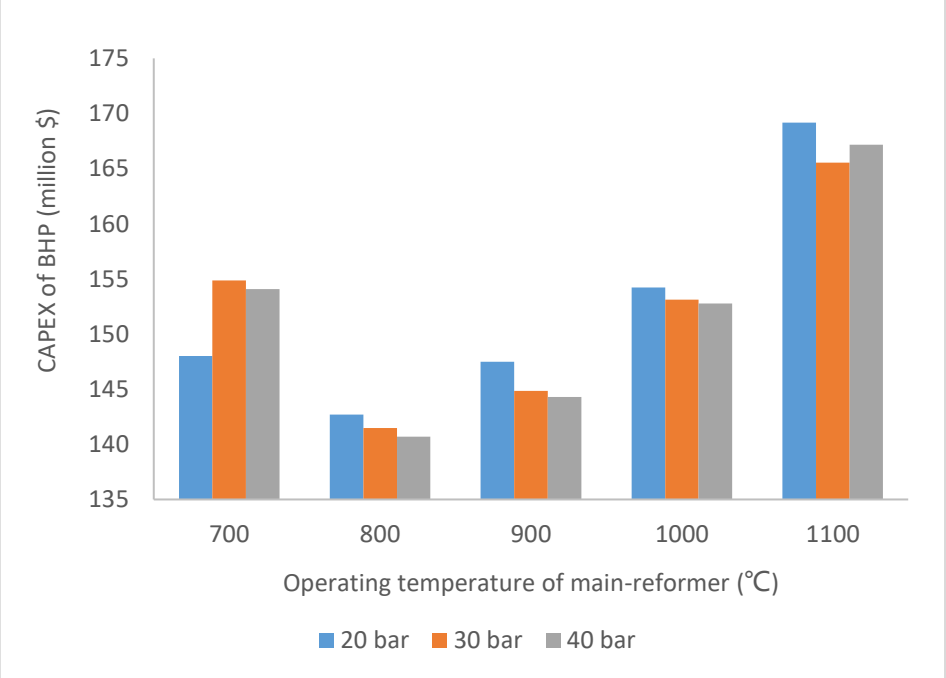

Figure 5.4 CAPEX of commercial-scale BHP process at different operating conditions.

Figure 5.5 summaries the results of OPEX. The increases in operating temperature and pressure are positively correlated with increases in OPEX. As mentioned above, large amounts of natural gas fuel are required to maintain the high operating temperature, which results in increased OPEX. In addition, the high operating temperature led to increased flue gas flowrate. Therefore, a higher solvent circulation rate is required to capture CO_2, which further increases OPEX. Increased flowrate of natural gas fuel and circulation rate of solvent are the major contributors to increased OPEX when the operating temperature rises. However, when the operating pressure rises, the main contribution to increased OPEX is different. As operating pressure increases, the electrical duty required to compress natural gas feed increases, which is the major contributor to increased OPEX.

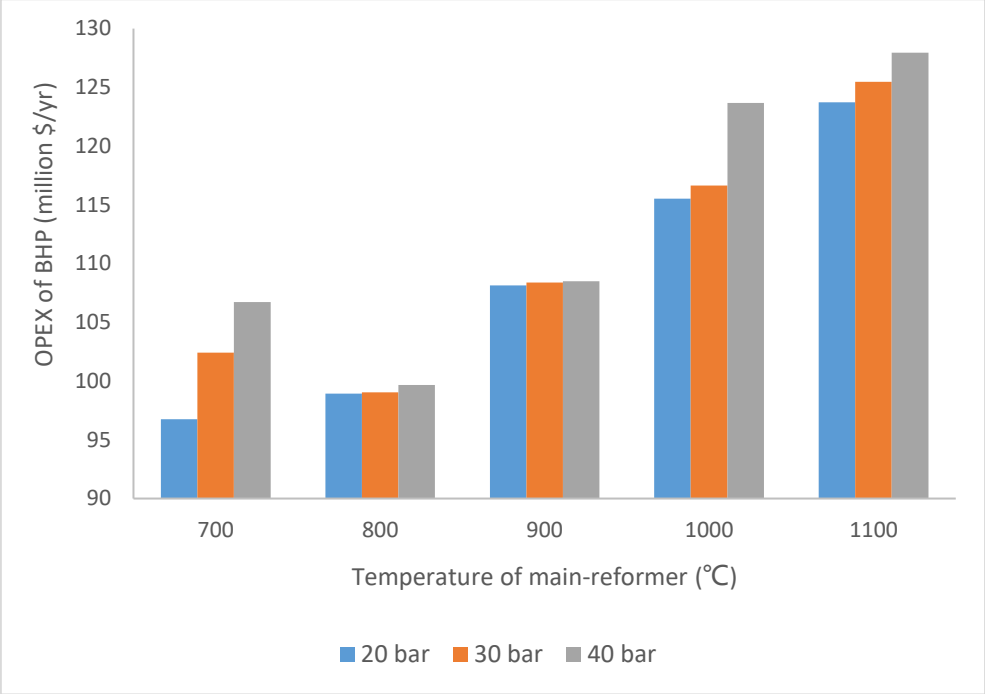

Figure 5.5 OPEX of commercial-scale BHP process at different operating conditions.

Figures 5.6, 5.7 and 5.8 show the results of annual hydrogen production and five-year NPV at different operating conditions. There is a strong correlation between the increase in NPV and the increase in annual hydrogen production. This illustrates that the main factor affecting the economic performance of commercial-scale BHP is not CAPEX and OPEX but the production and selling price of hydrogen.

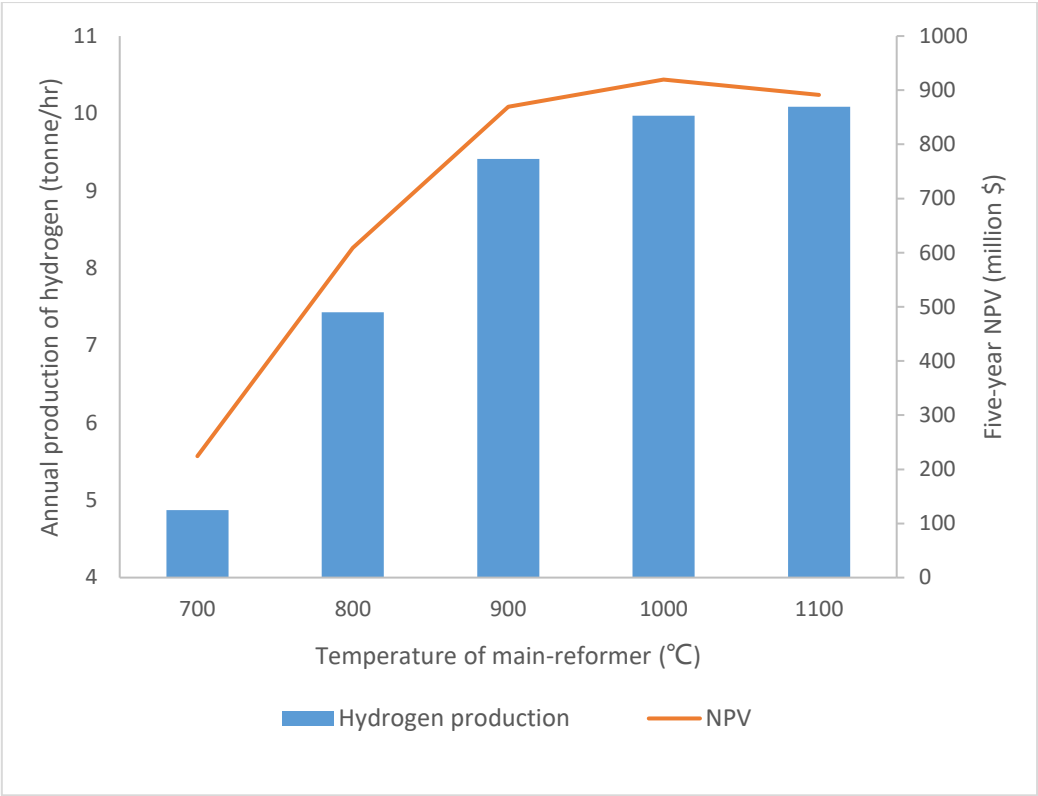

Figure 5.6 The results of annual hydrogen production and five-year NPV at 20 bar.

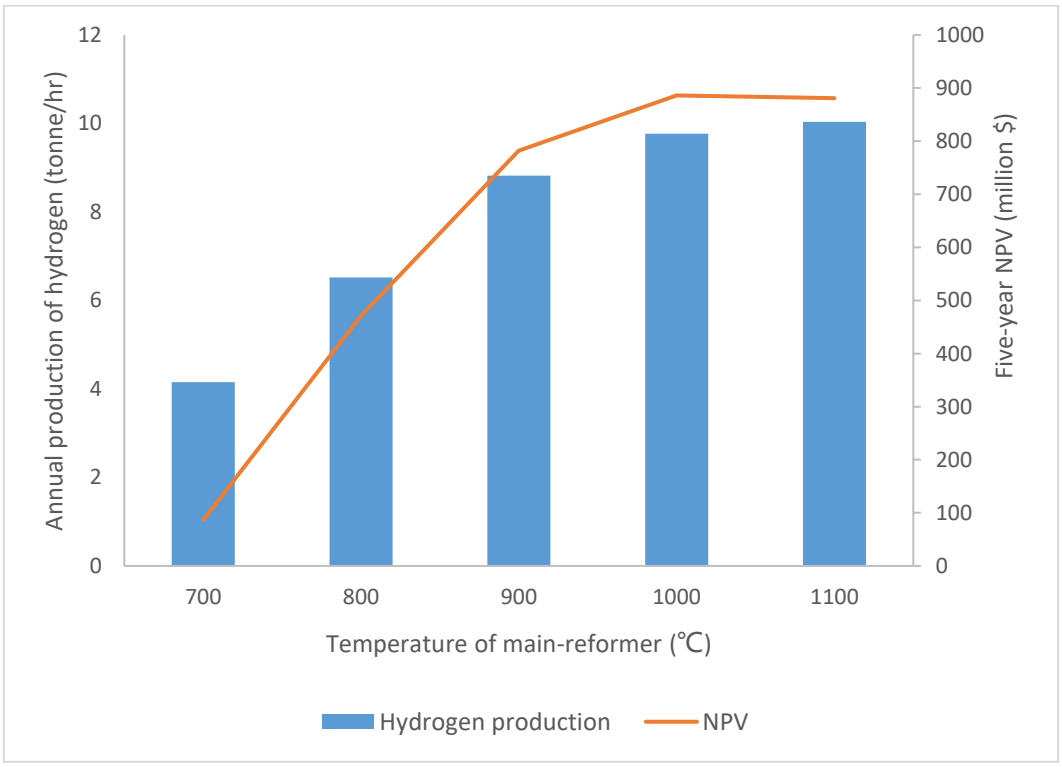

Figure 5.7 The results of annual hydrogen production and five-year NPV at 30 bar.

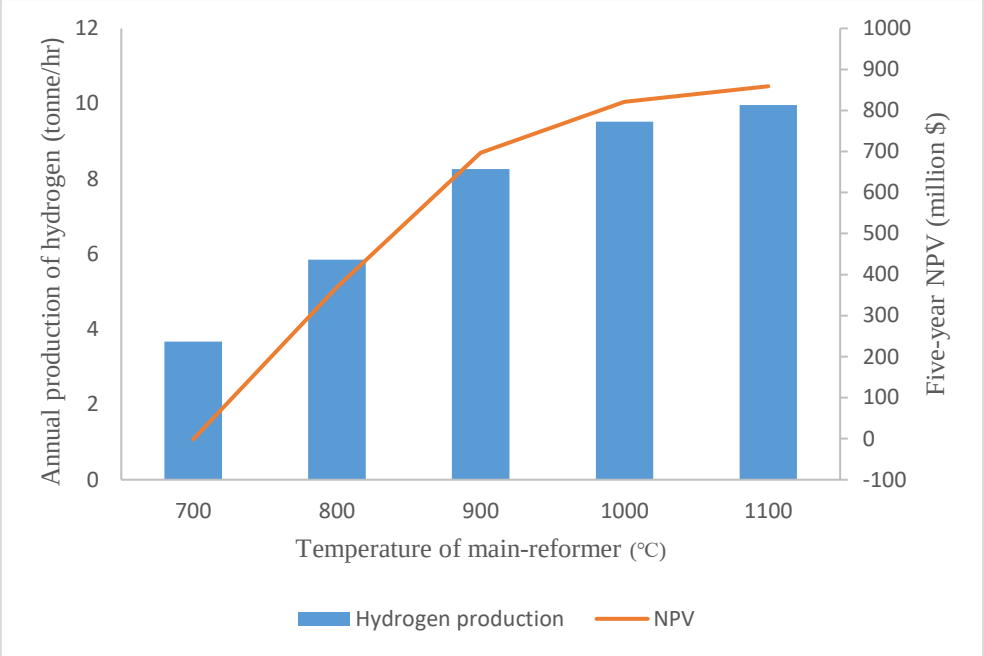

Figure 5.8 The results of annual hydrogen production and five-year NPV at 40 bar.

Figure 5.9 summarizes the results of five-year NPV at different operating conditions. The increase in operating temperature and the decrease in operating pressure have made a significant contribution to the increase in NPV. This is because the reforming reaction is an exothermic and volume expansion process. Therefore, high temperature and low pressure are beneficial to the conversion of methane into hydrogen. The increase in hydrogen production results in an increase of the NPV.

It is worth noting that when the operating temperature is 1000 °C, the NPV achieves the maximum value. This is because the methane conversion rate is close to 98% at this operating temperature. It is difficult to increase hydrogen production with further heating, but it significantly increases the CAPEX and OPEX. Therefore, the NPV at the temperature of 1100 °C is less than that at 1000 °C. In addition, a significant negative value of $ -1.6 million is achieved when the operating conditions are at 40 bar and 700°C. In this case, low temperature and high pressure severely inhibit the conversion of methane, resulting in a significant decrease in hydrogen production.

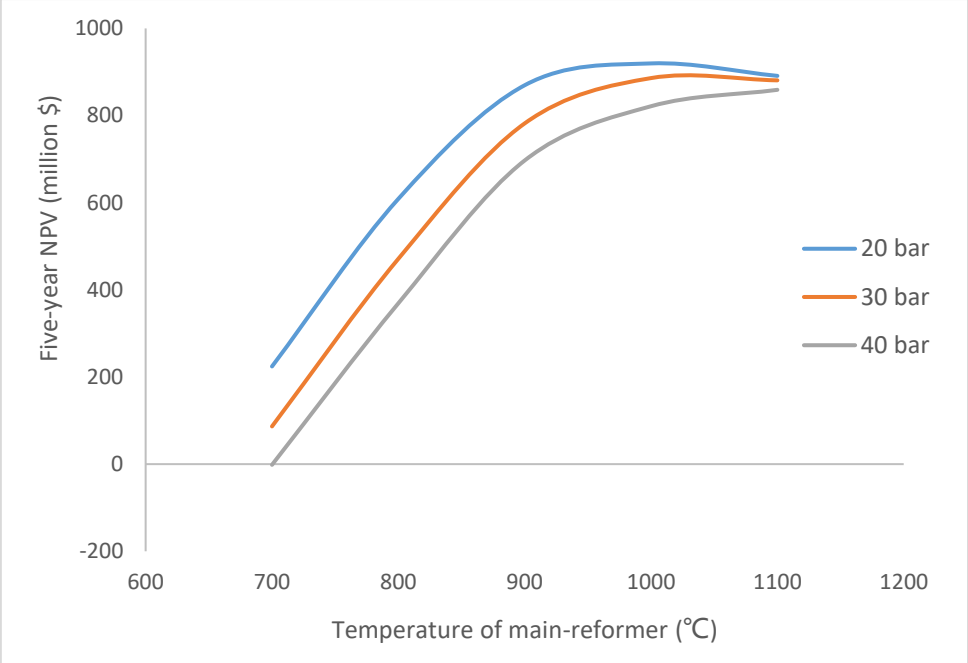

Figure 5.9 The results of five-year NPV at different operating conditions.

Table 5.17 The economic performance of commercial-scale BHP process with different operating temperature at 20 bar.

	700 °C	**800 °C**	**900 °C**	**1000 °C**	**1100 °C**
DEC (Million $)	58.80	56.69	58.60	61.27	67.20
CAPEX (Million $)	148.02	142.70	147.50	154.23	169.16
Fixed O&M costs (Million $/yr)	4.44	4.28	4.42	4.63	5.07
variable O&M costs (Million $/yr)	92.30	94.64	103.71	110.89	118.65
OPEX (Million $)	96.74	98.92	108.14	115.52	123.72
Hydrogen production (tonne/hr)	4.87	7.43	9.41	9.97	10.09
CF (Million $)	98.20	198.23	268.30	283.29	279.68
Five-year NPV (Million $)	224.24	608.74	869.57	919.65	891.06

Table 5.18 The economic performance of commercial-scale BHP process with different operating temperature at 30 bar.

	700 °C	**800 °C**	**900 °C**	**1000 °C**	**1100 °C**
DEC (Million $)	61.52	56.20	57.54	60.83	65.77
CAPEX (Million $)	154.85	141.47	144.84	153.11	165.55
Fixed O&M costs (Million $/yr)	4.65	4.24	4.35	4.59	4.97
variable O&M costs (Million $/yr)	97.78	94.80	104.04	112.06	120.51
OPEX (Million $)	102.43	99.04	108.39	116.65	125.48
Hydrogen production (tonne/hr)	4.15	6.52	8.82	9.77	10.04
CF (Million $)	63.69	161.62	244.50	274.12	276.03
Five-year NPV (Million $)	86.58	471.20	782.02	886.00	880.82

Table 5.19 The economic performance of commercial-scale BHP process with different operating temperature at 40 bar.

	700 °C	**800 °C**	**900 °C**	**1000 °C**	**1100 °C**
DEC (Million $)	61.21	55.89	57.33	60.69	66.41
CAPEX (Million $)	154.06	140.69	144.30	152.77	167.17
Fixed O&M costs (Million $/yr)	4.62	4.22	4.33	4.58	5.01
variable O&M costs (Million $/yr)	102.11	95.45	104.15	119.08	122.94
OPEX (Million $)	106.73	99.67	108.48	123.67	127.96
Hydrogen production (tonne/hr)	3.67	5.85	8.26	9.52	9.97
CF (Million $)	40.22	134.48	221.92	256.99	270.72
Five-year NPV (Million $)	-1.59	369.08	696.94	821.42	859.06

5.6.3 Integrating risk and economics analysis

This study investigates the relationship between safety improvements and economic benefits of commercial-scale BHP with a capacity of 200 tonne$_{H_2}$/day. As shown in Figures 5.3 and 5.9, significant impacts on the economic and risk performance of the commercial-scale BHP process can be observed when operating temperature and pressure are varied. Since the steam reforming reaction is an endothermic and volume expansion reaction, low temperature and high pressure limit the conversion of methane and reduce economic benefits. The low methane conversion rate leads to a significant accumulation of combustible gas in the PSA tail gas. It will result in the temperature increase in furnace, thereby increasing the risk of equipment damage. In addition, high operating pressure increase the likelihood of the blockage of natural gas flow in the reformer tubes. This may lead to an increase in pressure from desulphurization to pre-reformer, which may end up with main-reformer explosion. Therefore, operating temperatures below 800 °C and operating pressures above 30 bar are scenarios that should be avoided in commercial-scale BHP process.

Although the high operating temperature improve the economic benefits, it also increases the likelihood of damage to reformers, heat exchangers and other equipment. It is worth noting that when the operating temperature is 1000 °C, the methane conversion rate is close to 98%. Further increasing the temperature can hardly improve economic benefits, but greatly increase the likelihood of equipment damage and production loss. Therefore, the recommended operating temperature should be less than 1000 °C. In addition, an additional cooling unit located between the main-reformer and the WGS helps improve process safety by avoiding hazards caused by high operating temperatures.

In simulations, economic performance of BHP process benefits from low operating pressures. This is because low operating pressure shifts the reaction equilibrium toward the production of more hydrogen. Increased hydrogen production is the main reason for the increase in NPV. In addition, system risk is reduced when operating pressure is reduced. However, low operating pressure results in a reduction in the reaction rate of the steam reforming, which increases the residence time in the reformer. The low operating pressure may increase the

CAPEX because a lager reformer is required to meet the increase in residence time. Therefore, the low operating pressure may have unexpected negative impacts on economic performance of commercial-scale BHP.

5.7 Applications and limitations of the integrated model

This study develops an integrated model specifically adapted to the commercial-scale BHP process. This model effectively captures the interaction between process, economic and safety variables. The engineering decisions based on safety-economy trade-offs can be made by analysing these interactions. The proposed WRI method can also be applied to other configurations of reforming processes, such as ATR, dry methane reforming (DMR), etc.

However, when WRI is used in other configurations, the results are not directly comparable. The reason is that the results of WRI are closely related to the number of nodes investigated. Thus, when the WRI is used in different configurations, the results are comparable only if the number of nodes investigated is consistent. In addition, another problem with this risk assessment method is that human reliability is not considered. Due to the lack of relevant data, WRI method does not include consideration of human reliability. However, a study by Mirza et al. (Mirza et al., 2011) showed that approximately 70% of hydrogen fires and explosion incidents between 1992 and 2008 were related to human and organizational factors. Therefore, it is important to consider human reliability aspects into the risk assessment to get a holistic view of the overall process risk in the commercial-scale BHP process.

One of the drawbacks of the integrated model is uncertainty of the results at low operating pressures. Because it is difficult for steady-state models to simulate changes in residence time, a dynamic model is needed to further investigate the economic performance of commercial-scale BHP at low operating pressures.

5.8 Conclusions

In this chapter, an integrated model was developed to investigate the relationship between safety improvements and economic benefits of BHP. The characteristics of the integrated

model are: (a) The interaction between the process, economic and safety variables is investigated through modelling and simulation, (b) A new risk assessment method for evaluating the overall process risk was proposed based on the index approach and (c) The impact of operating parameters on process risk and economic benefits was investigated. The following are the key findings of this chapter:

- The results of risk assessment showed that the increase in reformer temperature is the most important source of hazards. Desulfurization and WGS are also the common sources of unsafe conditions. the PCC process is generally safe because it operates at relatively low temperatures and pressures. Some potential risks, such as solvent leakage and flooding, are less harmful to the whole system.
- Compared with the widely used index-based risk assessment method (F&EI), WRI is more sensitive to changes in operating conditions because it balances the influence of different risk factors.
- The highest NPV of $ 920 million is achieved by the operating conditions with 20 bar and 1000 °C. The lowest NPV of $ -1.6 million is achieved by the operating conditions with 40 bar and 700 °C. The results of economic assessment showed that there is a strong correlation between the increase in NPV and the increase in annual hydrogen production.
- The increase in operating temperature significantly increases the CAPEX and OPEX of BHP process. The highest CAPEX of $ 169 million is achieved by the operating conditions with 20 bar and 1100 °C. The lowest CAPEX of $ 141 million is achieved by the operating conditions with 40 bar and 800 °C. The highest OPEX of 128 million $/yr is achieved by the operating conditions with 40 bar and 1100 °C. The lowest OPEX of 98 million $/yr is achieved by the operating conditions with 20 bar and 700 °C.
- The results of integrating risk and economics analysis showed that the recommended operating temperature should be between 800-1000 °C. The operating pressures above 30 bar is a scenario that should be avoided. In addition, an additional cooling unit located between the main-reformer and the WGS helps avoid hazards caused by high operating temperatures.

Chapter 6. Conclusions and recommendations for future research

6.1 Conclusions

This thesis investigates the energy, economic and safety evaluation of commercial-scale BHP process through modelling and simulation. The performance of different configurations is evaluated and compared with standard BHP process.

6.1.1 Modelling, simulation and performance assessment of large-scale PCC process using PZ and AFS configuration

In chapter 3, a steady-state model of a solvent-based PCC process with MEA and PZ was developed in Aspen Plus® V11. The models were validated using experimental data from a pilot plant. The model results were in good agreement with the experimental data and the model predictions were within ±10 % of the experimental data. The validated pilot-scale PCC process model was scaled up to capture 90 % of CO_2 from the commercial-scale SMR plant. The energy performance of the commercial-scale PCC process using PZ and AFS configuration was evaluated and compared with a commercial-scale PCC process using 30 wt.% MEA and standard configuration.

The energy performance of different solvents evaluation showed that PZ has a clear advantage in energy performance compared with MEA. The regeneration energy of the standard PCC process can be decreased from 4.29 GJ/tonne$_{CO_2}$ using 30 wt.% MEA to 3.78 GJ/tonne$_{CO_2}$ using 30 wt.% PZ. Sensitivity analysis showed that the energy consumption of the standard PCC process decreases as the CO_2 lean loading increases. The energy consumption of standard PCC process using 30 wt.% PZ attained a minimum when the lean loading around 0.2 mol$_{CO_2}$/mol$_{solvent}$. In addition, increasing stripper pressure and column height are both beneficial to reducing energy consumption. However, higher stripper pressure and column height may result in additional capital and operating costs.

Parametric studies showed that the CO_2 lean loading have a major effect on the energy performance. Therefore, it is a main subject in the optimisation of solvent processes. The results of process optimisation showed that the lowest energy consumption of 3.19 GJ/tonne$_{CO_2}$ was achieved by the optimal process using 30 wt.% PZ and AFS configuration, which is a significant reduction compared to 4.17 GJ/tonne$_{CO_2}$ in the baseline case.

6.1.2 Technical and economic performance assessment of BHP using new configuration through modelling and simulation

In chapter 4, the technical and economic performance of BHP process was evaluated through modelling and simulation. The steady-state models for the SMR and PCC processes were developed in Aspen plus® V11. The SMR process was validated at commercial scale with data from the IEA. The PCC model was validated at pilot scale against experimental data from the literature and then scaled up to capture CO_2 from the flue gas of SMR plant.

Technical analysis was performed to investigate the energy performance of commercial-scale BHP process. The findings revealed that BHP process with 30 wt.% MEA resulted in the highest energy penalty of 59.32%. The ECSB process using 30 wt.% PZ achieved the lowest total energy consumption of 213 MW, reducing the energy penalty by 36.35 % compared to the BHP process using 30 wt.% MEA.

The economic analysis was conducted in APEA. The results indicated that the SMR process without carbon capture had a CAPEX of $ 111.5 million and a TAC of $ 73.4 million per year. The BHP process using 30 wt.% MEA showed the highest cost increases, with a 60 % rise in CAPEX and a 53 % increase in TAC. In contrast, the ECSB process using 30 wt.% PZ demonstrated the lowest cost increases, with a 33 % rise in CAPEX and a 23 % increase in TAC.

6.1.3 Integrated safety and economic assessment of blue hydrogen production through modelling and simulation

In chapter 5, an integrated model was developed to investigate the relationship between safety improvements and economic benefits of BHP. A new risk assessment method (WRI) was proposed to assess the potential hazards for multiple accident scenarios in BHP, which

can also be applied to other similar configurations of reforming processes. Compared with the widely used index-based risk assessment method (F&EI), WRI is more sensitive to changes in operating conditions because it balances the influence of different risk factors.

The results of risk assessment illustrated that the increase in reformer temperature is the most important source of hazards. Desulfurization and WGS are also the common sources of unsafe conditions. the PCC process is generally safe because it operates at relatively low temperatures and pressures. Some potential risks, such as solvent leakage and flooding, are less harmful to the whole system. Compared with the widely used index-based risk assessment method (F&EI), WRI is more sensitive to changes in operating conditions because it balances the influence of different risk factors.

The results of economic assessment showed that there is a strong correlation between the increase in NPV and the increase in annual hydrogen production. In addition, the increase in operating temperature significantly increases the CAPEX and OPEX of BHP process. The results of integrating risk and economics analysis showed that the recommended operating temperature should be between 800-1000 °C. The operating pressures above 30 bar is a scenario that should be avoided. In addition, an additional cooling unit located between the main-reformer and the WGS helps avoid hazards caused by high operating temperatures.

6.1.4 General conclusions

This study comprehensively evaluates and optimizes commercial-scale BHP process through modelling, simulation, and performance evaluation. Energy consumption, operating costs, and capital costs are significantly reduced by using new solvents and configurations. The optimized process enhances the feasibility of BHP as a clean energy solution. The energy and cost-saving configurations developed in this work improve the economic feasibility and scalability of PCC process, making it suitable for high-emission industries such as power generation, cement, and steel production. These advances may promote global decarbonization efforts, help achieve net-zero emissions targets and mitigate environmental impacts.

In addition, the introduction of WRI improves the identification of key hazards (such as high reformer temperature and pressure), thereby enhancing process safety in commercial

deployments. This study lays a solid foundation for safer industrial practices.

This work bridges the gap between technological innovation and practical application, providing a feasible solution for industrial decarbonization and accelerating energy transformation. By combining energy evaluation, economic evaluation, and risk assessment, this study establishes the foundation for the deployment of commercial-scale BHP process. The results of this study have significant implications for industrial decarbonization, energy system transformation, and global sustainable development goals.

6.2 Recommendations for future research

The following areas are recommended for further research on the BHP process.

6.2.1 Investigation of other configurations and solvents in BHP process

This thesis develops a commercial-scale BHP process based on SMR and PCC technology. In addition, the energy, economic and safety performance of using ECSB configuration and different concentrations of PZ are investigated. However, there are still many techniques, configurations and solvents that can be selected in BHP process. For instance, ATR and POX can be used as alternatives to SMR for hydrogen production. In terms of carbon capture, membrane separation and cryogenic distillation could be considered instead of chemical absorption. From the solvent perspective, amine blends and emerging ionic liquids are being widely studied.

In addition to the most widely used SMR process, ATR is considered to be the most suitable hydrogen production technology for commercial-scale BHP. Some studies have explored the possibility of using ATR in BHP (Faheem et al., 2021, Oni et al., 2022, Minutillo et al., 2020, Cho et al., 2024, Noh et al., 2024). Although ATR technology has certain advantages in methane conversion rate and energy consumption, its high capital cost may be an important obstacle. In addition, membrane separation technology is receiving more and more attention in the field of carbon capture. This technology has been widely studied in the in-situ CO_2 capture of SMR (Shirasaki et al., 2009, Lu and Xie, 2016, Voldsund et al., 2016, Chompupun et al., 2018). For the solvent-based PCC process, the research on new

configurations (Rezazadeh et al., 2017, Gao and Rochelle, 2019, Canepa et al., 2013, Otitoju et al., 2021) and new solvents (Liang et al., 2015, Rabensteiner et al., 2015a, Hosseini-Ardali et al., 2020, Sen et al., 2020) provides the possibility of further reducing energy consumption and costs.

Investigation of different technologies, configurations, and solvents will reveal technology combinations that may further reduce energy consumption and costs. Process optimization based on the best technology combination will help find the operating conditions with the lowest energy consumption and cost.

6.2.2 Study on coke and solid formation in BHP process using PZ solvent

In this thesis, coke formation and PZ precipitation are two issues that have been neglected. The former can lead to catalyst deactivation and reduce methane conversion. The latter affects the absorption of CO_2 by the solvent. Since coke form slowly at high S/C ratio, the effects of coke formation can be addressed by periodic cleaning. Solids precipitate from lean PZ solvent streams only at temperatures below 20 °C. Therefore, these two issues are usually overlooked in commercial-scale BHP studies. However, this is undoubtedly a challenge for BHP plants using PZ located in cold regions such as Europe and North America, which want to reduce maintenance frequency. Therefore, studies on coke and solid formation and their impact on the design and operation of BHP processes using PZ solvent must be carefully evaluated. This will help design engineers and operators understand the areas in the plant where coke and solid formation may occur and the steps that need to be taken to avoid coke and solid formation.

In addition, a life cycle analysis (LCA) was not performed for the BHP process developed in this thesis. Therefore, it is recommended that future development and analysis of BHP process should include a cradle-to-grave assessment to quantify its environmental impacts.

6.2.3 Development of node assessment system and consideration of human reliability aspects

In this thesis, an index-based risk assessment method was developed. The proposed WRI

method can also be applied to other reforming process configurations. However, when WRI is used in other configurations, the results are not directly comparable. The reason is that the results of WRI are closely related to the number of nodes investigated. Thus, when the WRI is used in different configurations, the results are comparable only if the number of nodes investigated is consistent. Therefore, a unified node assessment system needs to be established to make it possible to compare the risks of different configurations.

In addition, another problem with this risk assessment method is that human reliability is not considered. Due to the lack of relevant data, WRI method does not include consideration of human reliability. However, a study by Mirza et al. (Mirza et al., 2011) showed that approximately 70 % of hydrogen fires and explosion incidents between 1992 and 2008 were related to human and organizational factors. Therefore, it is important to consider human reliability aspects into the risk assessment to get a holistic view of the overall process risk in the commercial-scale BHP process.

6.2.4 The technical and economic performance of commercial-scale BHP at low operating pressures through dynamic modelling

In this thesis, an integrated model specifically adapted to the commercial-scale BHP process was developed. This model effectively captures the interaction between process, economic and safety variables. The engineering decisions based on safety-economy trade-offs can be made by analysing these interactions. However, one of the drawbacks for the integrated model is uncertainty of the results at low operating pressures. Because it is difficult for steady-state models to simulate changes in residence time, a dynamic model is needed to further investigate the energy and economic performance of commercial-scale BHP at low operating pressures.

References

ABIDIN, M. Z., RUSLI, R., KHAN, F. & SHARIFF, A. M. 2018. Development of inherent safety benefits index to analyse the impact of inherent safety implementation. *Process Safety and Environmental Protection,* 117**,** 454-472.

ABU-ZAHRA, M. R., SCHNEIDERS, L. H., NIEDERER, J. P., FERON, P. H. & VERSTEEG, G. F. 2007. CO2 capture from power plants: Part I. A parametric study of the technical performance based on monoethanolamine. *International Journal of Greenhouse gas control,* 1**,** 37-46.

ADE, N., ALSUHAIBANI, A., EL-HALWAGI, M. M., GOYETTE, H. & WILHITE, B. 2022. Integrating safety and economics in designing a steam methane reforming process. *International Journal of Hydrogen Energy,* 47**,** 6404-6414.

AGBONGHAE, E., HUGHES, K., INGHAM, D., MA, L. & POURKASHANIAN, M. 2014. Optimal process design of commercial-scale amine-based CO2 capture plants. *Industrial & Engineering Chemistry Research,* 53**,** 14815-14829.

AICE 2015. *American Institute of Chemical Engineers. Center for Chemical Process Safety. Guidelines for Initiating Events and Independent Protection Layers in Layer of Protection Analysis*, Hoboken, New Jersey: John Wiley & Sons.

AICHE 1994. Explosion Index Hazard Classification Guide. *AICHE New York*.

AIMIKHE, V.J. & EYANKWARE, O.E., 2023. Recent advances in white hydrogen exploration and production: a mini review. *Journal of Energy Research and Reviews*, 13(4), 64-79.

ANTONINI, C., PéREZ-CALVO, J.-F., VAN DER SPEK, M. & MAZZOTTI, M. 2021a. Optimal design of an MDEA CO2 capture plant for low-carbon hydrogen production—A rigorous process optimization approach. *Separation and Purification Technology,* 279**,** 119715.

ANTONINI, C., PEREZ-CALVO, J. F., VAN DER SPEK, M. & MAZZOTTI, M. 2021b. Optimal design of an MDEA CO2 capture plant for low-carbon hydrogen production - A rigorous process optimization approach. *Separation and Purification Technology,* 279.

ANTONINI, C., TREYER, K., STREB, A., VAN DER SPEK, M., BAUER, C. & MAZZOTTI, M. 2020. Hydrogen production from natural gas and biomethane with carbon capture and storage–A techno-environmental analysis. *Sustainable Energy & Fuels,* 4**,** 2967-2986.

ARTANTO, Y., JANSEN, J., PEARSON, P., DO, T., COTTRELL, A., MEULEMAN, E. & FERON, P. 2012. Performance of MEA and amine-blends in the CSIRO PCC pilot plant at Loy Yang Power in Australia. *Fuel,* 101**,** 264-275.

ASPEN 2008. Rate Based model of the CO2 capture process by MEA using Aspen Plus. *Aspen Technology Inc, Cambridge, MA, USA*.

ASPENTECH. 2022. *The Leading Process Simulation Software in the Chemical Industry* [Online]. https://www.aspentech.com/en/products/engineering/aspen-plus: Aspentech. [Accessed 13 Jan 2022].

AUSTGEN, D. M., ROCHELLE, G. T., PENG, X. & CHEN, C. C. 1989. Model of vapor-liquid equilibria for aqueous acid gas-alkanolamine systems using the electrolyte-NRTL equation. *Industrial & engineering chemistry research,* 28**,** 1060-1073.

BAADE, W., FARNAND, S., HUTCHISON, R. & WELCH, K. 2012. CO2 capture from SMRs: A demonstration project: REFINING DEVELOPMENTS. *Hydrocarbon processing (International ed.),* 91**,** 63-68.

BIRD, R., STEWART, W. & LIGHTFOOT, E. 2007. Transport Phenomena, 2nd Edn. New York, NY: John Wilwe & Sons. Inc.

BISHNOI, S. & ROCHELLE, G. T. 2000. Absorption of carbon dioxide into aqueous piperazine: reaction kinetics, mass transfer and solubility. *Chemical engineering science,* 55**,** 5531-5543.

BISHNOI, S. & ROCHELLE, G. T. 2002. Absorption of carbon dioxide in aqueous piperazine/methyldiethanolamine. *AIChE journal,* 48**,** 2788-2799.
BOURNE, S., CROUCH, S. & SMITH, M. 2014. A risk-based framework for measurement, monitoring and verification of the Quest CCS Project, Alberta, Canada. *International Journal of Greenhouse Gas Control,* 26**,** 109-126.
BOYANO, A., BLANCO-MARIGORTA, A., MOROSUK, T. & TSATSARONIS, G. 2011. Exergoenvironmental analysis of a steam methane reforming process for hydrogen production. *Energy,* 36**,** 2202-2214.
BRANDL, P., BUI, M., HALLETT, J. P. & MAC DOWELL, N. 2021. Beyond 90% capture: Possible, but at what cost? *International Journal of Greenhouse Gas Control,* 105**,** 103239.
BRAVO, J. L., PATWARDHAN, A. A. & EDGAR, T. F. 1992. Influence of effective interfacial areas in the operation and control of packed distillation columns. *Industrial & engineering chemistry research,* 31**,** 604-608.
BRAVO, J. L., ROCHA, J. A. & FAIR, J. 1985. Mass transfer in gauze packings. *Hydrocarbon processing (International ed.),* 64**,** 91-95.
CAMMERAAT, E., DECHEZLEPRêTRE, A. & LALANNE, G. 2022. Innovation and industrial policies for green hydrogen.
CANEPA, R., WANG, M., BILIYOK, C. & SATTA, A. 2013. Thermodynamic analysis of combined cycle gas turbine power plant with post-combustion CO2 capture and exhaust gas recirculation. *Proceedings of the Institution of Mechanical Engineers, Part E: Journal of Process Mechanical Engineering,* 227**,** 89-105.
CAPOCELLI, M., LUBERTI, M., INNO, S., D'ANTONIO, F., DI NATALE, F. & LANCIA, A. 2019. Post-combustion CO2 capture by RVPSA in a large-scale steam reforming plant. *Journal of Co2 Utilization,* 32**,** 53-65.
CHAU, K., DJIRE, A. & KHAN, F. 2022a. Review and analysis of the hydrogen production technologies from a safety perspective. *International Journal of Hydrogen Energy,* 47**,** 13990-14007.
CHAU, K., DJIRE, A., VADDIRAJU, S. & KHAN, F. 2022b. Process Risk Index (PRI)–A methodology to analyze the design and operational hazards in the processing facility. *Process Safety and Environmental Protection,* 165**,** 623-632.
CHEN, B., LIAO, Z., WANG, J., YU, H. & YANG, Y. 2012. Exergy analysis and CO2 emission evaluation for steam methane reforming. *International journal of hydrogen energy,* 37**,** 3191-3200.
CHEN, C.-H., YU, C.-T. & CHEN, W.-H. 2021. Improvement of steam methane reforming via in-situ CO2 sorption over a nickel-calcium composite catalyst. *International Journal of Hydrogen Energy,* 46**,** 16655-16666.
CHEN, C. C. & EVANS, L. B. 1986. A local composition model for the excess Gibbs energy of aqueous electrolyte systems. *AIChE journal,* 32**,** 444-454.
CHEN, E., ZHANG, Y., LIN, Y., NIELSENB, P. & ROCHELLE, G. 2017. Review of recent pilot plant activities with concentrated piperazine. *Energy Procedia,* 114**,** 1110-1127.
CHERBAŃSKI, R. & MOLGA, E. 2018. Sorption-enhanced steam methane reforming (SE-SMR)–A review: Reactor types, catalyst and sorbent characterization, process modeling. *Chemical and Process Engineering,* 39.
CHILTON, T. H. & COLBURN, A. P. 1934. Mass transfer (absorption) coefficients prediction from data on heat transfer and fluid friction. *Industrial & engineering chemistry,* 26**,** 1183-1187.
CHO, S., NOH, W. & LEE, I. 2024. Hybrid systems design for blue and green hydrogen co-production: Integration of autothermal reforming with solid oxide electrolysis. *Energy Conversion and Management,* 300**,** 117969.
CHOMPUPUN, T., LIMTRAKUL, S., VATANATHAM, T., KANHARI, C. & RAMACHANDRAN, P. A. 2018. Experiments, modeling and scaling-up of membrane reactors for hydrogen production via steam methane reforming. *Chemical Engineering and Processing-Process Intensification,* 134**,** 124-140.

CLOSMANN, F., NGUYEN, T. & ROCHELLE, G. T. 2009. MDEA/Piperazine as a solvent for CO2 capture. *Energy Procedia,* 1**,** 1351-1357.

COLLINS, L. 2023. *Hydrogen explosion in Austria, Hydrogen insight, Austria* https://www.hydrogeninsight.com/industrial/hydrogen-explosion-in-austria-i-live-more-than-3km-away-and-the-blast-made-my-windows-shake/2-1-1498784 [Online]. [Accessed].

COLLODI, G., AZZARO, G., FERRARI, N., SANTOS, S., BROWN, J., COTTON, B. & LODGE, S. 2017. Techno-economic evaluation of SMR based standalone (merchant) hydrogen plant with CCS. *IT Report, Editor*.

DAWOOD, F., ANDA, M. & SHAFIULLAH, G. M. 2020. Hydrogen production for energy: An overview. *International Journal of Hydrogen Energy,* 45**,** 3847-3869.

DERKS, P., KLEINGELD, T., VAN AKEN, C., HOGENDOORN, J. & VERSTEEG, G. 2006. Kinetics of absorption of carbon dioxide in aqueous piperazine solutions. *Chemical Engineering Science,* 61**,** 6837-6854.

DIAB, J., FULCHERI, L., HESSEL, V., ROHANI, V. & FRENKLACH, M. 2022. Why turquoise hydrogen will Be a game changer for the energy transition. *International Journal of Hydrogen Energy,* 47**,** 25831-25848.

DIEGO, M. E., BELLAS, J.-M. & POURKASHANIAN, M. 2018. Techno-economic analysis of a hybrid CO2 capture system for natural gas combined cycles with selective exhaust gas recirculation. *Applied energy,* 215**,** 778-791.

DING, Y. & ALPAY, E. 2000. Adsorption-enhanced steam–methane reforming. *Chemical Engineering Science,* 55**,** 3929-3940.

EDALI, M., ABOUDHEIR, A. & IDEM, R. 2009. Kinetics of carbon dioxide absorption into mixed aqueous solutions of MDEA and MEA using a laminar jet apparatus and a numerically solved 2D absorption rate/kinetics model. *International Journal of Greenhouse Gas Control,* 3**,** 550-560.

ERMATCHKOV, V., KAMPS, Á. P.-S. & MAURER, G. 2003. Chemical equilibrium constants for the formation of carbamates in (carbon dioxide+ piperazine+ water) from 1H-NMR-spectroscopy. *The Journal of Chemical Thermodynamics,* 35**,** 1277-1289.

ERMATCHKOV, V., PéREZ-SALADO KAMPS, Á., SPEYER, D. & MAURER, G. 2006. Solubility of carbon dioxide in aqueous solutions of piperazine in the low gas loading region. *Journal of Chemical & Engineering Data,* 51**,** 1788-1796.

FAHEEM, H. H., TANVEER, H. U., ABBAS, S. Z. & MAQBOOL, F. 2021. Comparative study of conventional steam-methane-reforming (SMR) and auto-thermal-reforming (ATR) with their hybrid sorption enhanced (SE-SMR & SE-ATR) and environmentally benign process models for the hydrogen production. *Fuel,* 297**,** 120769.

FATIGATI, F., DI GIULIANO, A., CARAPELLUCCI, R., GALLUCCI, K. & CIPOLLONE, R. 2021. Experimental Characterization and Energy Performance Assessment of a Sorption-Enhanced Steam–Methane Reforming System. *Processes,* 9**,** 1440.

FREEMAN, S. A., DUGAS, R., VAN WAGENER, D. H., NGUYEN, T. & ROCHELLE, G. T. 2010. Carbon dioxide capture with concentrated, aqueous piperazine. *International Journal of Greenhouse Gas Control,* 4**,** 119-124.

GALLUCCI, F. & VAN ANNALAND, M. S. Novel membrane reactor concepts for hydrogen production. 5th World Hydrogen Technologies Convention (WHTC2013); September 25-28, 2013, Shanghai, China, 2013.

GAO, T. & ROCHELLE, G. T. 2019. CO2 absorption from gas turbine flue gas by aqueous piperazine with intercooling. *Industrial & Engineering Chemistry Research,* 59**,** 7174-7181.

GAO, T., SELINGER, J. L. & ROCHELLE, G. T. 2019. Demonstration of 99% CO2 removal from coal flue gas by amine scrubbing. *International Journal of Greenhouse Gas Control,* 83**,** 236-244.

GAO, X., RAMAN, A. A. A., HIZADDIN, H. F., BELLO, M. M. & BUTHIYAPPAN, A. 2021. Review on the inherently safer design for chemical processes: past, present and future. *Journal of Cleaner*

Production, 305**,** 127154.
GASPAR, J., VON SOLMS, N., THOMSEN, K. & FOSBøL, P. L. 2016. Multivariable optimization of the piperazine CO2 post-combustion process. *Energy Procedia,* 86**,** 229-238.
GHUNGRUD, S. A., DEWOOLKAR, K. D. & VAIDYA, P. D. 2019. Cerium-promoted bi-functional hybrid materials made of Ni, Co and hydrotalcite for sorption-enhanced steam methane reforming (SESMR). *International Journal of Hydrogen Energy,* 44**,** 694-706.
GPP 2023. GlobalPetrolPrices, https://zh.globalpetrolprices.com/United-Kingdom/electricity_prices/.
GUR, T. M. 2021. Perspective—Electrochemical Gasification: Revisiting an Old Reaction in New Perspective and Turning "Black" Hydrogen to "Blue." *Journal of the Electrochemical Society*, 168(11), 114516.
HALABI, M., DE CROON, M., VAN DER SCHAAF, J., COBDEN, P. & SCHOUTEN, J. 2012a. Kinetic and structural requirements for a CO2 adsorbent in sorption enhanced catalytic reforming of methane–Part I: Reaction kinetics and sorbent capacity. *Fuel,* 99**,** 154-164.
HALABI, M., DE CROON, M., VAN DER SCHAAF, J., COBDEN, P. & SCHOUTEN, J. 2012b. A novel catalyst–sorbent system for an efficient H2 production with in-situ CO2 capture. *International journal of hydrogen energy,* 37**,** 4987-4996.
HEAL, K. & KEMP, T. 2013. North West Sturgeon Refinery Project Overview-Carbon Capture Through Innovative Commercial Structuring in the Canadian Oil Sands. *Energy Procedia,* 37**,** 7046-7055.
HEIKKILä, A.-M. 1999. *Inherent safety in process plant design: an index-based approach*, VTT Technical Research Centre of Finland.
HERCE, C., CORTES, C. & STENDARDO, S. 2017. Computationally efficient CFD model for scale-up of bubbling fluidized bed reactors applied to sorption-enhanced steam methane reforming. *Fuel Processing Technology,* 167**,** 747-761.
HETZER, H. B., ROBINSON, R. & BATES, R. G. 1968. Dissociation constants of piperazinium ion and related thermodynamic quantities from 0 to 50. deg. *The Journal of Physical Chemistry,* 72**,** 2081-2086.
HORVATH, A. L. 1985. *Handbook of aqueous electrolyte solutions*, Halsted Press.
HOSSEINI-ARDALI, S. M., HAZRATI-KALBIBAKI, M., FATTAHI, M. & LEZSOVITS, F. 2020. Multi-objective optimization of post combustion CO2 capture using methyldiethanolamine (MDEA) and piperazine (PZ) bi-solvent. *Energy,* 211**,** 119035.
HOWARTH, R. W. & JACOBSON, M. Z. 2021. How green is blue hydrogen? *Energy Science & Engineering,* 9**,** 1676-1687.
IEA 2021. Hydrogen, IEA, Paris https://www.iea.org/reports/hydrogen.
IEA 2022. Electrolyzers: Tracking Clean Energy Progress, *IEA* , Pairs https://www.iea.org/energy-system/low-emission-fuels/electrolysers.
IEA 2023. *Global Hydrogen Review 2023, IEA, Paris https://www.iea.org/reports/global-hydrogen-review-2023* [Online]. [Accessed].
IEAGHG 2017. Techno - Economic Evaluation of SMR Based Standalone (Merchant) Hydrogen Plant with CCS. IEA Greenhouse Gas R&D Programme.
IPCC 2019. 2019 Refinement to the 2006 IPCC Guidelines for National Greenhouse Gas Inventories. Intergovernmental Panel on Climate Change.
IRURETAGOYENA, D., HELLGARDT, K. & CHADWICK, D. 2018. Towards autothermal hydrogen production by sorption-enhanced water gas shift and methanol reforming: a thermodynamic analysis. *International Journal of Hydrogen Energy,* 43**,** 4211-4222.
JAFARI, M. J., LAJEVARDI, S. & MOHAMMADFAM, I. 2013. Semi quantitative risk assessment of a Hydrogen production unit. *International Journal of Occupational Hygiene,* 5**,** 101-108.
JAFARI, M. J., MOHAMMADI, H., RENIERS, G., POUYAKIAN, M., NOURAI, F., TORABI, S. A. & MIANDASHTI, M. R. 2018. Exploring inherent process safety indicators and approaches for their estimation: A systematic review. *Journal of Loss Prevention in the Process Industries,* 52**,** 66-80.

JAFARI, M. J., ZAREI, E. & BADRI, N. 2012. The quantitative risk assessment of a hydrogen generation unit. *international journal of hydrogen energy,* 37**,** 19241-19249.
JANSEN, D., GAZZANI, M., MANZOLINI, G., VAN DIJK, E. & CARBO, M. 2015. Pre-combustion CO2 capture. *International Journal of Greenhouse Gas Control,* 40**,** 167-187.
KARIMI, M., HILLESTAD, M. & SVENDSEN, H. F. 2011. Capital costs and energy considerations of different alternative stripper configurations for post combustion CO2 capture. *Chemical engineering research and design,* 89**,** 1229-1236.
KATEBAH, M. & LINKE, P. 2022. Analysis of hydrogen production costs in Steam-Methane Reforming considering integration with electrolysis and CO2 capture. *Cleaner Engineering and Technology,* 10**,** 100552.
KHAN, F. I. & ABBASI, S. 1997. OptHAZOP—an effective and optimum approach for HAZOP study. *Journal of Loss Prevention in the Process Industries,* 10**,** 191-204.
KHAN, F. I. & ABBASI, S. 1998. Multivariate hazard identification and ranking system. *Process Safety Progress,* 17**,** 157-170.
KHAN, F. I. & AMYOTTE, P. R. 2004. Integrated inherent safety index (I2SI): a tool for inherent safety evaluation. *Process safety progress,* 23**,** 136-148.
KHAN, M. H. A., DAIYAN, R., NEAL, P., HAQUE, N., MACGILL, I. & AMAL, R. 2021. A framework for assessing economics of blue hydrogen production from steam methane reforming using carbon capture storage & utilisation. *International Journal of Hydrogen Energy,* 46**,** 22685-22706.
KIDAM, K., SAHAK, H. A., HASSIM, M. H., SHAHLAN, S. S. & HURME, M. 2016. Inherently safer design review and their timing during chemical process development and design. *Journal of Loss Prevention in the Process Industries,* 42**,** 47-58.
KVAMSDAL, H. M., JAKOBSEN, J. P. & HOFF, K. A. 2009. Dynamic modeling and simulation of a CO2 absorber column for post-combustion CO2 capture. *Chemical Engineering and Processing: Process Intensification,* 48**,** 135-144.
LAWAL, A., WANG, M., STEPHENSON, P. & YEUNG, H. 2009. Dynamic modelling of CO2 absorption for post combustion capture in coal-fired power plants. *Fuel,* 88**,** 2455-2462.
LAWRENCE, D. 1996. *Quantifying inherent safety of chemical process routes.* Loughborough University.
LEE, D. K., BAEK, I. H. & YOON, W. L. 2004. Modeling and simulation for the methane steam reforming enhanced by in situ CO2 removal utilizing the CaO carbonation for H2 production. *Chemical Engineering Science,* 59**,** 931-942.
LEPAUMIER, H., DA SILVA, E. F., EINBU, A., GRIMSTVEDT, A., KNUDSEN, J. N., ZAHLSEN, K. & SVENDSEN, H. F. 2011. Comparison of MEA degradation in pilot-scale with lab-scale experiments. *Energy Procedia,* 4**,** 1652-1659.
LI, A., LIM, C. J. & GRACE, J. R. 2008. Staged-separation membrane reactor for steam methane reforming. *Chemical Engineering Journal,* 138**,** 452-459.
LI, K., COUSINS, A., YU, H., FERON, P., TADE, M., LUO, W. & CHEN, J. 2016. Systematic study of aqueous monoethanolamine-based CO2 capture process: model development and process improvement. *Energy Science & Engineering,* 4**,** 23-39.
LI, L., KING, D. L., NIE, Z., LI, X. S. & HOWARD, C. 2010. MgAl2O4 spinel-stabilized calcium oxide absorbents with improved durability for high-temperature CO2 capture. *Energy & fuels,* 24**,** 3698-3703.
LI, X., HAN, Z., ZHANG, R., ZHANG, Y. & ZHANG, L. 2020. Risk assessment of hydrogen generation unit considering dependencies using integrated DEMATEL and TOPSIS approach. *International Journal of Hydrogen Energy,* 45**,** 29630-29642.
LI, Y., REN, J., MA, H. & CAMPBELL, A. N. 2024. Technical and economic performance assessment of blue hydrogen production using new configuration through modelling and simulation. *International Journal of Greenhouse Gas Control,* 134**,** 104112.

LIANG, Z. H., RONGWONG, W., LIU, H., FU, K., GAO, H., CAO, F., ZHANG, R., SEMA, T., HENNI, A. & SUMON, K. 2015. Recent progress and new developments in post-combustion carbon-capture technology with amine based solvents. *International Journal of Greenhouse Gas Control,* 40**,** 26-54.

LITTEL, R., VAN SWAAIJ, W. P. M. & VERSTEEG, G. F. 1990. Kinetics of carbon dioxide with tertiary amines in aqueous solution. *AIChE journal,* 36**,** 1633-1640.

LIU, K., SONG, C. & SUBRAMANI, V. 2010a. *Hydrogen and syngas production and purification technologies*, John Wiley & Sons.

LIU, W., LOW, N. W., FENG, B., WANG, G. & DINIZ DA COSTA, J. C. 2010b. Calcium precursors for the production of CaO sorbents for multicycle CO2 capture. *Environmental science & technology,* 44**,** 841-847.

LU, N. & XIE, D. 2016. Novel membrane reactor concepts for hydrogen production from hydrocarbons: a review. *International Journal of Chemical Reactor Engineering,* 14**,** 1-31.

LUO, X. 2016. *Process modelling, simulation and optimisation of natural gas combined cycle power plant integrated with carbon capture, compression and transport.* University of Hull.

MA, C. B., ZHANG, W. Z., ZHENG, Y. & AN, A. M. 2021. Economic Model Predictive Control for Post-Combustion CO2 Capture System Based on MEA. *Energies,* 14.

MAHECHA-BOTERO, A., GRACE, J. R., LIM, C. J., ELNASHAIE, S., BOYD, T. & GULAMHUSEIN, A. 2009. Pure hydrogen generation in a fluidized bed membrane reactor: application of the generalized comprehensive reactor model. *Chemical engineering science,* 64**,** 3826-3846.

MANDAL, B. & BANDYOPADHYAY, S. 2005. Simultaneous absorption of carbon dioxide and hydrogen sulfide into aqueous blends of 2-amino-2-methyl-1-propanol and diethanolamine. *Chemical Engineering Science,* 60**,** 6438-6451.

MANZOLINI, G., FERNANDEZ, E. S., REZVANI, S., MACCHI, E., GOETHEER, E. & VLUGT, T. 2015. Economic assessment of novel amine based CO2 capture technologies integrated in power plants based on European Benchmarking Task Force methodology. *Applied Energy,* 138**,** 546-558.

MASSARWEH, O., AL-KHUZAEI, M., AL-SHAFI, M., BICER, Y. & ABUSHAIKHA, A. S. 2023. Blue hydrogen production from natural gas reservoirs: A review of application and feasibility. *Journal of CO2 Utilization,* 70**,** 102438.

MINUTILLO, M., PERNA, A. & SORCE, A. 2020. Green hydrogen production plants via biogas steam and autothermal reforming processes: energy and exergy analyses. *Applied Energy,* 277**,** 115452.

MIRZA, N. R., DEGENKOLBE, S. & WITT, W. 2011. Analysis of hydrogen incidents to support risk assessment. *International journal of hydrogen energy,* 36**,** 12068-12077.

MOHAMMADFAM, I. & ZAREI, E. 2015. Safety risk modeling and major accidents analysis of hydrogen and natural gas releases: A comprehensive risk analysis framework. *International journal of hydrogen energy,* 40**,** 13653-13663.

MOIOLI, S., GIUFFRIDA, A., ROMANO, M. C., PELLEGRINI, L. A. & LOZZA, G. 2016. Assessment of MDEA absorption process for sequential H2S removal and CO2 capture in air-blown IGCC plants. *Applied Energy,* 183**,** 1452-1470.

MOSTAFAVI, E., ASHRAFI, O. & NAVARRI, P. 2021. Assessment of process modifications for amine-based post-combustion carbon capture processes. *Cleaner Engineering and Technology,* 4**,** 100249.

NIELSEN, P. T., LI, L. & ROCHELLE, G. T. 2013. Piperazine degradation in pilot plants. *Energy Procedia,* 37**,** 1912-1923.

NOH, W., PARK, S., KIM, Y., LEE, J., KIM, J. & LEE, I. 2024. Systems design and techno-economic analysis of a novel cryogenic carbon capture process integrated with an air separation unit for autothermal reforming blue hydrogen production system. *Journal of Cleaner Production,* 457**,** 142341.

OCHOA-FERNáNDEZ, E., LACALLE-VILA, C., CHRISTENSEN, K. O., WALMSLEY, J. C., RøNNING, M., HOLMEN, A. & CHEN, D. 2007. Ni catalysts for sorption enhanced steam methane reforming. *Topics in Catalysis,* 45**,** 3-8.

OKONKWO, E. C., AL-BREIKI, M., BICER, Y. & AL-ANSARI, T. 2021. Sustainable hydrogen roadmap: A holistic review and decision-making methodology for production, utilisation and exportation using Qatar as a case study. *International Journal of Hydrogen Energy,* 46**,** 35525-35549.

ONI, A., ANAYA, K., GIWA, T., DI LULLO, G. & KUMAR, A. 2022. Comparative assessment of blue hydrogen from steam methane reforming, autothermal reforming, and natural gas decomposition technologies for natural gas-producing regions. *Energy Conversion and Management,* 254**,** 115245.

OTITOJU, O., OKO, E. & WANG, M. 2021. Technical and economic performance assessment of post-combustion carbon capture using piperazine for large scale natural gas combined cycle power plants through process simulation. *Applied Energy,* 292**,** 116893.

PALANIAPPAN, C., SRINIVASAN, R. & TAN, R. 2004. Selection of inherently safer process routes: a case study. *Chemical Engineering and Processing: Process Intensification,* 43**,** 641-647.

PAPALAS, T., ANTZARAS, A. N. & LEMONIDOU, A. A. 2020. Intensified steam methane reforming coupled with Ca-Ni looping in a dual fluidized bed reactor system: A conceptual design. *Chemical Engineering Journal,* 382**,** 122993.

PARK, S., XU, S., ROGERS, W., PASMAN, H. & EL-HALWAGI, M. M. 2020. Incorporating inherent safety during the conceptual process design stage: A literature review. *Journal of Loss Prevention in the Process Industries,* 63**,** 104040.

PELLEGRINI, L. A., DE GUIDO, G. & MOIOLI, S. 2020. Design of the CO2 removal section for PSA tail gas treatment in a hydrogen production plant. *Frontiers in Energy Research,* 8**,** 77.

PENG, D.-Y. & ROBINSON, D. B. 1976. A new two-constant equation of state. *Industrial & Engineering Chemistry Fundamentals,* 15**,** 59-64.

PéREZ-BOTELLA, E., VALENCIA, S. & REY, F. 2022. Zeolites in adsorption processes: State of the art and future prospects. *Chemical Reviews,* 122**,** 17647-17695.

PICHOT, D., GRANADOS, L., MOREL, T., SCHULLER, A., DUBETTIER, R. & LOCKWOOD, F. 2017. Start-up of Port-Jérôme CRYOCAP™ Plant: Optimized Cryogenic CO2 Capture from H2 Plants. *Energy Procedia,* 114**,** 2682-2689.

PINSENT, B., PEARSON, L. & ROUGHTON, F. 1956. The kinetics of combination of carbon dioxide with hydroxide ions. *Transactions of the Faraday Society,* 52**,** 1512-1520.

PLAZA, J. M. & ROCHELLE, G. T. 2011. Modeling pilot plant results for CO2 capture by aqueous piperazine. *Energy Procedia,* 4**,** 1593-1600.

PNNL. 2023. *Hydrogen Tools Portal, EERE, the U.S.* https://h2tools.org/lessons?search_api_fulltext= [Online]. [Accessed].

POSEY, M. L. & ROCHELLE, G. T. 1997. A thermodynamic model of Methyldiethanolamine– CO2–H2S– Water. *Industrial & engineering chemistry research,* 36**,** 3944-3953.

POWER, G., BUSSE, A. & MACMURRAY, J. 2018. Demonstration of Carbon Capture and Sequestration of Steam Methane Reforming Process Gas Used for Large-Scale Hydrogen Production. Air Products and Chemicals, Inc., Allentown, PA (United States).

PRESTON, C. IEAGHG Summary Report of the Shell Quest Carbon Capture and Storage Project. 14th Greenhouse Gas Control Technologies Conference Melbourne, 2018. 21-26.

RABENSTEINER, M., KINGER, G., KOLLER, M., GRONALD, G. & HOCHENAUER, C. 2015a. Investigation of carbon dioxide capture with aqueous piperazine on a post combustion pilot plant - Part II: Parameter study and emission measurement. *International Journal of Greenhouse Gas Control,* 37**,** 471-480.

RABENSTEINER, M., KINGER, G., KOLLER, M. & HOCHENAUER, C. 2015b. PCC pilot plant studies with aqueous potassium glycinate. *International Journal of Greenhouse Gas Control,* 42**,** 562-570.

RADFARNIA, H. R. & ILIUTA, M. C. 2012. Development of zirconium-stabilized calcium oxide absorbent for cyclic high-temperature CO2 capture. *Industrial & engineering chemistry research,* 51**,** 10390-10398.

RADFARNIA, H. R. & ILIUTA, M. C. 2014. Development of Al-stabilized CaO–nickel hybrid sorbent–catalyst for sorption-enhanced steam methane reforming. *Chemical Engineering Science,* 109**,** 212-219.

RAHMAN, Z. U., AHMAD, I., KANO, M. & MUSTAFA, J. 2019. Model development and exergy analysis of a microreactor for the steam methane reforming process in a cfd environment. *Entropy,* 21**,** 399.

RAKIB, M. A., GRACE, J. R., LIM, C. J. & ELNASHAIE, S. S. 2011. Modeling of a fluidized bed membrane reactor for hydrogen production by steam reforming of hydrocarbons. *Industrial & engineering chemistry research,* 50**,** 3110-3129.

RAKIB, M. A., GRACE, J. R., LIM, C. J., ELNASHAIE, S. S. E. H. & GHIASI, B. 2010. Steam reforming of propane in a fluidized bed membrane reactor for hydrogen production. *International Journal of Hydrogen Energy,* 35**,** 6276-6290.

RAO, A. B. & RUBIN, E. S. 2002. A technical, economic, and environmental assessment of amine-based CO2 capture technology for power plant greenhouse gas control. *Environmental Science & Technology,* 36**,** 4467-4475.

RATHNAYAKA, S., KHAN, F. & AMYOTTE, P. 2011a. SHIPP methodology: Predictive accident modeling approach. Part I: Methodology and model description. *Process safety and environmental protection,* 89**,** 151-164.

RATHNAYAKA, S., KHAN, F. & AMYOTTE, P. 2011b. SHIPP methodology: Predictive accident modeling approach. Part II. Validation with case study. *Process safety and environmental protection,* 89**,** 75-88.

RAYER, A. V., SUMON, K. Z., SEMA, T., HENNI, A., IDEM, R. O. & TONTIWACHWUTHIKUL, P. 2012. Part 5c: solvent chemistry: solubility of CO2 in reactive solvents for post-combustion CO2. *Carbon Management,* 3**,** 467-484.

RAZI, N., SVENDSEN, H. F. & BOLLAND, O. 2013. Validation of mass transfer correlations for CO2 absorption with MEA using pilot data. *International Journal of Greenhouse Gas Control,* 19**,** 478-491.

REDLICH, O. & KWONG, J. N. 1949. On the thermodynamics of solutions. V. An equation of state. Fugacities of gaseous solutions. *Chemical reviews,* 44**,** 233-244.

REZAZADEH, F., GALE, W. F., ROCHELLE, G. T. & SACHDE, D. 2017. Effectiveness of absorber intercooling for CO2 absorption from natural gas fired flue gases using monoethanolamine solvent. *International Journal of Greenhouse Gas Control,* 58**,** 246-255.

RINKER, E. B., ASHOUR, S. S. & SANDALL, O. C. 1996. Kinetics and modeling of carbon dioxide absorption into aqueous solutions of diethanolamine. *Industrial & engineering chemistry research,* 35**,** 1107-1114.

ROCHELLE, G., CHEN, E., FREEMAN, S., VAN WAGENER, D., XU, Q. & VOICE, A. 2011. Aqueous piperazine as the new standard for CO2 capture technology. *Chemical engineering journal,* 171**,** 725-733.

ROCHELLE, G. T., WU, Y., CHEN, E., AKINPELUMI, K., FISCHER, K. B., GAO, T., LIU, C.-T. & SELINGER, J. L. 2019. Pilot plant demonstration of piperazine with the advanced flash stripper. *International Journal of Greenhouse Gas Control,* 84**,** 72-81.

ROMANO, M. C., ANTONINI, C., BARDOW, A., BERTSCH, V., BRANDON, N. P., BROUWER, J., CAMPANARI, S., CREMA, L., DODDS, P. E. & GARDARSDOTTIR, S. 2022. Comment on "How green is blue hydrogen?". *Energy Science & Engineering*.

ROUSSANALY, S., ANANTHARAMAN, R. & FU, C. 2020. Low-carbon footprint hydrogen production from natural gas: A techno-economic analysis of carbon capture and storage from steam-methane reforming.

RUIJTERS, E. & STOELINGA, M. 2015. Fault tree analysis: A survey of the state-of-the-art in modeling, analysis and tools. *Computer science review,* 15**,** 29-62.
SALKUYEH, Y. K., SAVILLE, B. A. & MACLEAN, H. L. 2017. Techno-economic analysis and life cycle assessment of hydrogen production from natural gas using current and emerging technologies. *International Journal of Hydrogen Energy,* 42**,** 18894-18909.
SANTOS, D. M., SEQUEIRA, C. A. & FIGUEIREDO, J. L. 2013. Hydrogen production by alkaline water electrolysis. *Química Nova,* 36**,** 1176-1193.
SAWADA, Y., TANAKA, J., SUZUKI, C., TANASE, D. & TANAKA, Y. 2018. Tomakomai CCS demonstration project of Japan, CO2 injection in progress. *Energy Procedia,* 154**,** 3-8.
SEN, R., KOCH, C. J., GOEPPERT, A. & PRAKASH, G. S. 2020. Tertiary amine-ethylene glycol based tandem CO2 capture and hydrogenation to methanol: direct utilization of post-combustion CO2. *ChemSusChem,* 13**,** 6318-6322.
SHAHID, M. Z. & KIM, J.-K. 2023. Design and economic evaluation of a novel amine-based CO2 capture process for SMR-based hydrogen production plants. *Journal of Cleaner Production,* 402**,** 136704.
SHARIFF, A. M., LEONG, C. T. & ZAINI, D. 2012. Using process stream index (PSI) to assess inherent safety level during preliminary design stage. *Safety science,* 50**,** 1098-1103.
SHIRASAKI, Y., TSUNEKI, T., OTA, Y., YASUDA, I., TACHIBANA, S., NAKAJIMA, H. & KOBAYASHI, K. 2009. Development of membrane reformer system for highly efficient hydrogen production from natural gas. *International Journal of Hydrogen Energy,* 34**,** 4482-4487.
SHIRIZADEH, B. & QUIRION, P. 2023. Long-term optimization of the hydrogen-electricity nexus in France: Green, blue, or pink hydrogen? *Energy Policy*, 181, 113702.
SINNOTT, R. 2005. *Chemical Engineering Design: Chemical Engineering Volume 6*, Elsevier.
SJARDIN, M., DAMEN, K. & FAAIJ, A. 2006. Techno-economic prospects of small-scale membrane reactors in a future hydrogen-fuelled transportation sector. *Energy,* 31**,** 2523-2555.
SOLTANI, R., ROSEN, M. & DINCER, I. 2014. Assessment of CO2 capture options from various points in steam methane reforming for hydrogen production. *International journal of hydrogen energy,* 39**,** 20266-20275.
SONG, C., LIU, Q., DENG, S., LI, H. & KITAMURA, Y. 2019. Cryogenic-based CO2 capture technologies: State-of-the-art developments and current challenges. *Renewable and sustainable energy reviews,* 101**,** 265-278.
SUBRAVETI, S. G., ROUSSANALY, S., ANANTHARAMAN, R., RIBOLDI, L. & RAJENDRAN, A. 2021a. Techno-economic assessment of optimised vacuum swing adsorption for post-combustion CO2 capture from steam-methane reformer flue gas. *Separation and Purification Technology,* 256**,** 117832.
SUBRAVETI, S. G., ROUSSANALY, S., ANANTHARAMAN, R., RIBOLDI, L. & RAJENDRAN, A. 2021b. Techno-economic assessment of optimised vacuum swing adsorption for post-combustion CO2 capture from steam-methane reformer flue gas. *Separation and Purification Technology,* 256.
SULTANA, S. & HAUGEN, S. 2022. Development of an inherent system safety index (ISSI) for ranking of chemical processes at the concept development stage. *Journal of Hazardous Materials,* 421**,** 126590.
SUN, H. & DING, H. 2014. Plant simulation and operation optimisation of SMR plant with different adjustment methods under part-load conditions. *Computers & Chemical Engineering,* 68**,** 107-113.
TANAKA, Y., SAWADA, Y., TANASE, D., TANAKA, J., SHIOMI, S. & KASUKAWA, T. 2017. Tomakomai CCS demonstration project of Japan, CO2 injection in process. *Energy Procedia,* 114**,** 5836-5846.
TE. 2023. *TRADING ECONOMICS: US natural gas price* [Online]. https://tradingeconomics.com/commodity/natural-gas. [Accessed February 2023].

TERRIEN, P., LOCKWOOD, F., GRANADOS, L. & MOREL, T. 2014. CO2 capture from H2 plants: Implementation for EOR. *Energy Procedia,* 63**,** 7861-7866.

TWH. 2021. *"What is hydrogen and how is it made?" The World of Hydrogen* [Online]. Available: https://www.theworldofhydrogen.com/gasunie/what-is-hydrogen/. [Accessed 2024].

VAN-DE-GRAAF, T., OVERLAND, I., SCHOLTEN, D. & WESTPHAL, K. 2020. The new oil? The geopolitics and international governance of hydrogen. *Energy Research & Social Science,* 70**,** 101667.

VAN WAGENER, D. H. 2011. *Stripper modeling for CO_2 removal using monoethanolamine and piperazine solvents.*

VAN WAGENER, D. H., ROCHELLE, G. T. & CHEN, E. 2013. Modeling of pilot stripper results for CO2 capture by aqueous piperazine. *International Journal of Greenhouse Gas Control,* 12**,** 280-287.

VIGNEAULT, A. & GRACE, J. R. 2015. Hydrogen production in multi-channel membrane reactor via steam methane reforming and methane catalytic combustion. *International Journal of Hydrogen Energy,* 40**,** 233-243.

VO, N. D., KANG, J.-H., OH, M. & LEE, C.-H. 2021. Dynamic model and performance of an integrated sorption-enhanced steam methane reforming process with separators for the simultaneous blue H2 production and CO2 capture. *Chemical Engineering Journal,* 423**,** 130044.

VOLDSUND, M., JORDAL, K. & ANANTHARAMAN, R. 2016. Hydrogen production with CO2 capture. *International Journal of Hydrogen Energy,* 41**,** 4969-4992.

WANG, F., CAO, J., ZHANG, Y., AVISO, K. B., TAN, R. R., LI, Z. & JIA, X. 2023a. Safety risk assessment of the large-scale carbon capture, utilization, and storage demonstration project in Dongying, China. *Journal of Cleaner Production***,** 137699.

WANG, M., LAWAL, A., STEPHENSON, P., SIDDERS, J. & RAMSHAW, C. 2011. Post-combustion CO2 capture with chemical absorption: A state-of-the-art review. *Chemical Engineering Research & Design,* 89**,** 1609-1624.

WANG, S., NABAVI, S. A. & CLOUGH, P. T. 2023b. A review on bi/polymetallic catalysts for steam methane reforming. *international journal of hydrogen energy*.

WILKE, C. & CHANG, P. 1955. Correlation of diffusion coefficients in dilute solutions. *AIChE journal,* 1**,** 264-270.

ZHANG, Q., SHEN, C., ZHANG, S. & WU, Y. 2016. Steam methane reforming reaction enhanced by a novel K2CO3-Doped Li4SiO4 sorbent: Investigations on the sorbent and catalyst coupling behaviors and sorbent regeneration strategy. *International Journal of Hydrogen Energy,* 41**,** 4831-4842.

ZHANG, X., ZHANG, C.-F. & LIU, Y. 2002. Kinetics of absorption of CO2 into aqueous solution of MDEA blended with DEA. *Industrial & engineering chemistry research,* 41**,** 1135-1141.

ZHANG, Y., CHEN, H., CHEN, C.-C., PLAZA, J. M., DUGAS, R. & ROCHELLE, G. T. 2009. Rate-based process modeling study of CO2 capture with aqueous monoethanolamine solution. *Industrial & engineering chemistry research,* 48**,** 9233-9246.

ŽIVKOVIĆ, L. A., POHAR, A., LIKOZAR, B. & NIKAČEVIĆ, N. M. 2016. Kinetics and reactor modeling for CaO sorption-enhanced high-temperature water–gas shift (SE–WGS) reaction for hydrogen production. *Applied Energy,* 178**,** 844-855.